Blood platelet behaviour and platelet-von Willebrand Factor interaction under force

Dissertation
Mathematisch-Naturwissenschaftliche Fakultät
Universität Augsburg

Jennifer Ivonne Angerer
2011

1. Korrektor: Prof. Dr. Achim Wixforth
2. Korrektor: Prof. Dr. Armin Reininger

Tag der Abgabe: 06.05.2011

Tag der mündlichen Prüfung: 24.06.2011

Content

Abstract

Platelet integrity and dynamics are crucial in hemostasis and thrombosis. During these processes, circulating disc shaped platelets are recruited from the blood stream to sites of vascular injuries. The initial platelet and plasma protein, von Willebrand factor (vWF), interaction occurs platelet activation independent. Depending on the combination of laminar blood flow shear stress and the platelet-vWF interplay, the unactivated platelets either adhere or form tethers by pulling membrane pieces from the moving platelets. The irreversible attachment step of activated platelets to vWF induces spreading and in contrast, to collagen, which is exposed after endothelial injury, aggregation.

The major aim of this interdisciplinary thesis was to bridge the gap between in vitro measurements and the understanding of factors influencing the platelet-vWF interaction. Specific focus was given on individual phenomena as well as collective phenomena. The single investigations involved variations in the platelet mechanical properties as well as in the vWF. To explore the role of cortical tension of the platelet envelope, their cytoskeleton was disrupted. Variations in the cholesterol concentration, which is a component of the plasma membrane, were quantified to measure the impact on the investigated platelet functions as platelet adhesion and tether formation. Altering the size distribution of the vWF multimer and mutations in the vWF protein were investigated to clarify the role of the vWF functionality on the platelet-vWF interplay. The formation of platelet-vWF aggregates was characterised to study the conditions of stenosis and atherosclerotic occlusions.

The multi step experiments discuss variations in the hematocrit (HCT), especially the impact of platelet-red blood cell collisions and the flattening of the flow profile by higher HCTs. The platelet-tumor cells interactions were studied to clarify the role of tumor cells in platelet activation, aggregation and receptor transfer.

The results of the individual phenomena showed that disrupting platelet F-actin with cytochalasin D decreased the platelet adhesion to vWF, the membrane tight adhesion area and the tether length compared to untreated platelets. On the contrary, breaking up the microtubular system with nocodazole had the inverse effect. These results indicate that the membrane tension is reduced after cytochalasin D treatment and increased after nocodazole treatment. Consequently, the membrane undulations would be enlarged after F-actin disruption and reduced after microtuble breakage. The platelet cholesterol loading as well as the depletion decreased the platelet adhesion and the tether length slightly. However, both cholesterol concentrations increased minimal the weak platelet adhesion area compared to

control platelets. The cholesterol concentration is assumed to minimal enhance the membrane-cytoskeleton adhesion. To clarify the role of vWF on the platelet-vWF interplay, first the investigated various commercially available vWF products showed comparable results in platelet adhesion to vWF or collagen and in tether formation to vWF. In contrast, the subfractions of one product, Haemate, depicted the differences in the multimer distribution. The large multimers were most pronounced at the beginning of the aggregate formation to collagen as well as at high shear rates as high as 10,000s^{-1}. However, the smaller multimers were comparable with the larger ones after 2min of flow exposure at 1,500s^{-1}. Second, the vWF loss of function mutant (lofm) decreased the platelet adhesion, increased the rolling velocity and left the tether length constant compared to the vWF wild type (WT). Third, above a critical threshold of 10,000s^{-1} to 15,000s^{-1} reversible platelet-vWF aggregates were formed, although platelets were not activated. Platelet-vWF conglomerates were constantly rolling in flow direction, grew in size with increasing shear rate, but were unaffected by flow time exposure increase. These aggregates assembled in whole blood and in washed blood cell suspensions reconstituted with various vWF proteins. Recombinant full-length vWF generated larger vWF networks than a commercial vWF preparation from pooled human plasma. In contrast, platelet-sugar free vWF rolling aggregates formation was hindered. Perfusion of collagen coated surfaces caused shear dependent assembly of vWF networks anchored to the collagen fibrils and capture of activation-blocked platelets within them. The von Willebrand disease (vWD) type 2B mutant, a gain of function mutation, rendered the rolling platelet-vWF conglomerate formation at a shear rate as low as 1,500s^{-1}.

The multi component experiments showed that variations in the HCT did not affect the adhesion area and the tether formation, but the adhered platelet number was strongly influenced. These variations are proposed to be mainly due to concentration changes of the platelets near the vessel wall. This higher concentration leads to an increased adhesion probability. Small cell lung carcinoma cells (SCLC) and maligne melanoma cells (MV3) and their supernatants induced platelet aggregation and secretion of adenosine triphosphate (ATP). Over vWF, SCLC or MV3 cell blood suspensions caused no tumor cell adhesion or platelet interaction. By flow cytometer measurements no transfer of tumor cells receptors to platelets or vice versa could be observed. Metastasizing SCLC cells entering the blood stream might induce platelet aggregation due to induced ATP secretion of platelets. The impact of platelet microparticle incubation of tumor cells remained the interaction pattern and the receptor transfer unchanged.

1. Introduction

In haemostasis and thrombosis platelet integrity and dynamics are of central importance. At sites of vascular injuries circulating platelets are recruited from the blood stream to initiate wound closure (Reininger 2008 b)). Little is known on the impact of individual and collective phenomena on the actual biophysical mechanism of platelet recruitment. The complex behaviour and interaction of cellular objects like platelets and the plasma protein, von Willebrand factor (vWF), is investigated under blood flow conditions. Finally, the platelet-tumor cell interaction is analysed. Due to the complexity of this interdisciplinary project each result chapter of the performed experiments will be introduced by a specific introduction concerning the scientific topic, in order to aid the readability and understandability of this thesis.

The following general introduction will cover the basics of haemostasis and thrombosis as well as the involved physical and biological processes.

1.1 Haemostasis and thrombosis

At sites of vascular injury platelets aggregate and form thrombi, which results in a bleeding stop. However, in some cases these platelet aggregates occlude atherosclerotic arteries causing cardiac and cerebrovascular diseases (Reininger 2009; Andrews and Berndt 2008; Reininger 2008 a); Reininger 2008 b); Reininger 2006; Ruggeri et al., 2006; Lopez and Dong 2005; Andrews and Berndt 2004; Bernardo et al., 2004; Shrimpton et al., 2002). After vascular injury collagen of various types (e.g. type I, III) is exposed to the blood flow (fig. 1). Collagen is the major component of the subendothelium. The negatively charged endothelial cell layer lining the inner walls of the blood vessel provides a channel for the delivery of nutrients, hormones and oxygen, whilst also acts as a barrier against toxins, drugs and infective viruses (Pötzsch and Madlener 2009). A further function of this layer is to prevent the adhesion of circulating cells from the blood flow to the vessel wall (fig. 1) (Reininger 2006; Savage et al., 1999). Platelet adhesion, their aggregation and thrombus formation occur in distinct steps. In arterial flow platelets circulate in the blood stream as disc shaped objects, which can withstand high dynamical shear stress and their shape is important to their function in haemostasis (White and Jennings 1999; White and Rao 1998; Cramer et al., 1991; White 1987).

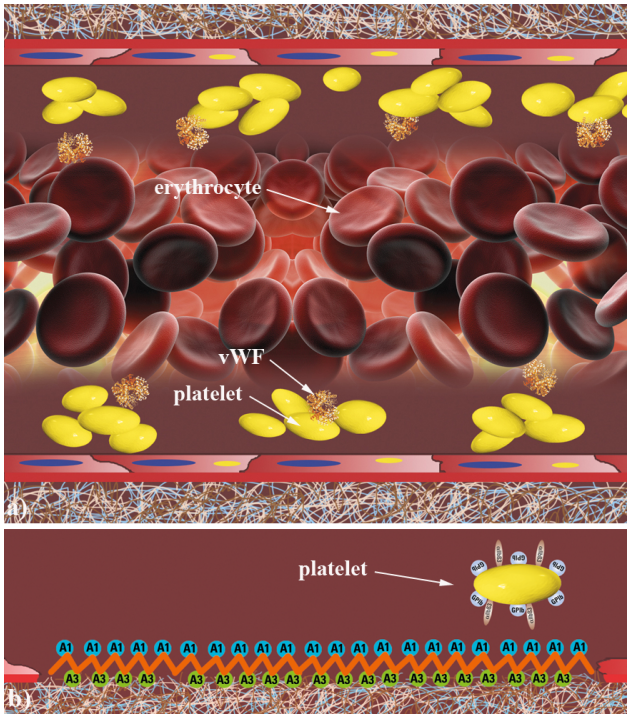

Figure 1: Scheme of arterial blood flow in distinct steps. In a) the bulk of erythrocytes is lifted towards the centre of the vessel wall (axial migration), thus creating a platelet rich fluid boundary layer near the vessel wall (plasma skimming). This separation is due to the Fahraeus Lindqvist effect. Soluble vWF is shown in its globular form. Above a critical shear rate the vWF molecule is stretched. In b) a sketch of shear induced vWF immobilization and unfolding on subendothelial collagen type I and III during blood flow is depicted. The platelet GPIbα interacts with the vWF A1 domain. Additionally, vWF is released from Weibel-Palade bodies and from the α-granules of the platelets (modified and adapted from Reininger 2008 a)).

To respond to vascular injury, platelets adhere to endothelial damage, become activated, undergo shape change, which is combined with a platelet cytoskeletal contraction, and spread in an attempt to seal the vascular leakage (Kuznetsova et al., 2007; Barkalow et al., 2003; Grgurevich et al., 2002; Gaffet et al., 1995; Fritz et al., 1994; Holmsen 1994; Cramer et al., 1991; Wurzinger 1990). This change in the morphology of the platelets leads to a secretion of platelet ingredients and to variations in the membrane composition. The activation is mainly responsible for the formation of filamentous pseudopods, which connect the platelets among each other. In particular, coagulation factors, vascoactive agents and platelet activating agents such as adenosine triphosphate (ATP) are secreted. Due to the release of these mediators, more thrombocytes get activated and consequently, the blood clotting is accelerated (Pötzsch and Madlener 2009). In this activation mechanism the glycoprotein GPIbα is believed to play an essential role by serving as the surface receptor that attaches platelets to the surface (Cramer et al., 1991; Chesterman and Berndt 1986; George et al., 1984). This interaction is mediated by the vWF that binds to the subendothelial structures under blood flow (fig. 1) (Reininger 2009; Andrews and Berndt 2008; Reininger 2008 a); Yago et al., 2008; Reininger et al., 2006; Lopez and Dong 2005; Bernardo et al., 2004; Shrimpton et al., 2002; Cramer et

al., 1991; Chesterman and Berndt 1986; George et al., 1984). The interplay of the vWF A1 domain with the GPIbα receptor has a short half-life time and by itself cannot provide irreversible adhesion. Through the binding site for actin binding proteins, the GPIb anchors directly to the membrane skeleton (Van Lier et al., 2005; Kasirer-Friede et al., 2004). This interaction is the first introductory step for the thrombus formation. Until no permanent adhesion, which leads to aggregation and spreading, is mediated by the glycoprotein VI or the integrin αIIbβ3, the platelets translocate and form tethers (fig. 2), as a consequence of the torque induced by the blood flow (White and Rao 1998; Tablin and Castro 1992; Casella et al., 1981; Jung et al., 1981). Furthermore, it was also observed that the main platelet body could detach from the tether and the surface, yielding in a single tube-shaped platelet fragment (fig. 2). These fragments translocate independently or detach completely from the surface and form ruptured tethers as observed by various groups (fig. 2) (Reininger et al., 2006; Casella et al., 1981). Tethers are clearly distinct from filopodia, which are actively formed due to intracellular actin polymerisation following platelet stimulation. Morphological, filopodia are twice as thick and form seven times slower than tethers (Reininger et al., 2006). The GPIbα domain on tethers is clustered in distinct subdomains and F-actin is detected in tether ends (Reininger et al., 2006), whereas no microtubules are detected in the tether (White and Rao 1998; Tablin and Castro 1992; Casella et al., 1981; Jung et al., 1981).

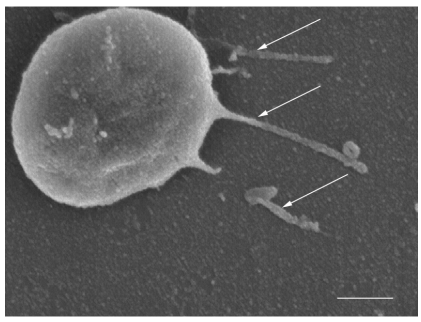

Figure 2: Scanning electron micrograph of the platelet tether formation under blood flow due to interaction with the vWF A1 domain. The white arrows show tethers on the platelet body and additionally ruptured tethers (scale bar: 500nm) (taken from Reininger et al., 2006).

Above a critical shear rate of approximately 1,500s^{-1} platelet attachment to thrombogenic surfaces depends on the platelet GPIbα receptor and its interaction with the vWF A1 domain (Reininger 2009; Bergmeier et al., 2006; Reininger et al., 2006). Soluble vWF binds via its A3 domain to collagen and therefore, allows platelet arrest. The crucial task of the GPIbα and the vWF A1 domain is to enhance binding, while shear forces increase and thus, the unfavourable condition for adhesion (Reininger 2009; Reininger 2008 a); Ruggeri et al., 2006; Savage et al., 1999). This platelet-vWF interaction requires no prior platelet activation and is

only transient. The GPIbα receptor is present in the membrane as the complex GP Ib-IX-V. Platelets can permanently bind to vWF by engagement of their integrin αIIbβ3 receptors with the Arg-Gly-Asp sequence in the vWF C1 domain. This complex receptor ligand interplay is summarized in a model sketch in figure 3 (Reininger 2009; Reininger 2008 a); Goto et al., 1995; Ruggeri et al., 1983).

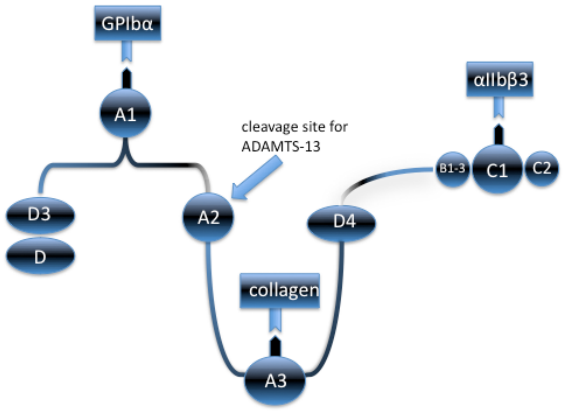

Figure 3: Scheme of the vWF binding sites and cleavage site for ADAMTS 13 (adapted from Reininger 2008 a)).

This adhesion step is dependent on the platelet activation and calcium intracellular signalling. After activation the platelets change their shape, spread and attract further platelets from the flowing blood (Pötzsch and Madlener 2009; Reininger 2009; Reininger 2008 a); Reininger 2006; Goto et al., 1995; Ruggeri et al., 1983). Newly arriving platelets at the vascular injury site require more vWF to bridge not only the platelets to exposed collagen, but also to each other by being sandwiched between the multiple platelet layers of a haemostatic plug (Pötzsch, Madlener 2009; Reininger 2009; Reininger 2007; Reininger 2006). Primary haemostasis characterizes the concerted action of all these processes: initial platelet arrest, platelet adhesion, and platelet aggregation. These activated platelets exhibit a phosphatidylserine rich membrane surface, which is an acceleration factor for blood coagulation and can not be found in resting platelets (Butenas et al., 2001). Platelet activation is a stringent condition for assembly and activation of tissue factor, factor VII, the tenase complex and the prothrombinase complex and thus, mediate secondary haemostasis. The final platelet clot is a fibrin-stabilized platelet aggregate that occludes the vessel injury and prevents deleterious leakage of blood (Pötzsch and Madlener 2009; Bruhn et al., 2007; Reininger 2006). The prothrombotic response is simultaneously limited to the region of leakage closure by potent antithrombotic and anticoagulatory counter-regulation (Reininger 2008 a)).

1.2 Cellular components of the blood

Max Schultze reported in 1865 on cells in the blood, which were smaller than erythrocytes and were able to agglutinate (Schultze 1865). 17 years later Giulio Bizzozero investigated blood platelets by means of vital microscopy in amphibians and observed that platelets attach to vascular injury prior to the formation of blood clot (Bizzozero 1882). This was the first step in the field of thrombotic blood clotting research (Pötzsch and Madlener 2009). Blood in the human body is in constant motion to deliver cells and nutrients to all regions in the organism. Whole blood consists of plasma, red blood cells, platelets, and white blood cells. Plasma is a water-based solution composed mainly of proteins and electrolytes. Platelets constitute only 0.3% of the blood's volume, but erythrocytes constitute nearly half the blood volume (Crowl and Fogelson 2009; Hathcock 2006; Goldsmith 1971). The volume ratio of cellular and fluid components of the blood is described by the hematocrit (HCT) value. Normal HCT values are in the range of 41% for women and of 46% for men (Silbernagel and Despopoulous 2007). Therefore, erythrocytes are responsible for most of the viscous and elastic fluid properties (Hathcock 2006; Duke 1910). Erythrocytes act as micro mixers within the blood, as the velocity profile is parabolic. This profile causes erythrocytes to move over one another with a shear dependent rotational motion (Hathcock 2006; Goldsmith and Turitto 1986). Erythrocytes are responsible for the gas transport in the blood. Leukocytes are divided in different groups: the granulocytes, the monocytes and the lymphocytes. All of them have functions in the immune system (Koolmann and Röhm 2002). Platelets are involved in the haemostatic repair of vasculature. This challenging task seems to be displayed especially under high shear conditions (Bruhn et al., 2007). Platelets are enucleate and negatively charged cytoplasmic fragments of megakaryocytes and are released from the bone marrow into the blood (Sackmann and Merkel 2010; Pötzsch and Madlener 2009; Bruhn et al., 2007; Reininger 2006; Ogawa 1993; Golde 1991). The inactive platelet plasma membrane shows an ordered distribution of the membrane phospholipids, which is altered after activation. Due to this distribution change the clotting process is fostered and accelerated (Pötzsch and Madlener 2009). As the lipid bilayer is incompressible, the increase of the surface area of a platelet, which once activated undergoes spreading, is provided by the tiny folds on the exposed surface and by channels of the open canalicular system (Behnke 1970). Their membrane is relatively smooth compared to the leukocyte membrane and shows a fine rugose appearance, resembling the gyri and sulci on the surface of the brain (White and Escolar 1993). Small openings of the surface, which connect the open canalicular system, are randomly dispersed. The platelet membrane has a thicker exterior coat or glycocalyx than other blood cells (White

1971). Platelets contain three major components of secretory organelles, including α-granules, dense bodies and lysosomes (Heijnen et al., 1998). Their lifetime in circulating blood is 7-10 days (Reininger 2008 a); White 2007). Non-activated platelets circulate disk shaped in the blood stream with an average diameter of 2.0µm to 5.0µm and a thickness of around 0.5µm to 1µm (fig. 2) (Prötzsch and Madlener 2009; Bessis 1973; Tocantins 1938; Bizzozero 1882; Donne 1842). At high flow rates thrombocytes interact with a variety of plasma proteins, which are tightly regulated to allow on the one hand the sealing of a vascular injury, but on the other hand prevent an overshooting reaction such as lumen occlusion and thromboembolism. Intense attention will be given to the largest plasma protein in the blood flow, the vWF. The vWF functionality and properties will be discussed in chapter 1.3. VWF helps to arrest fast flowing platelets on exposed collagen of the damaged subendothelial surface (Pötzsch and Madlener 2009; Reininger 2007; Reininger 2006). Resting platelets express approximately 25,000 to 30,000 of the GPIb-IX receptors (Andrews et al., 1999) and about 80,000 GPIIb-IIIa receptors (White 1987). Both receptors are mobile and their ability to move is extremely important for their function in hemostasis. After platelet activation and spreading these receptors move spontaneously and can cluster (White et al., 1995 a); White et al., 1995 b); White et al., 1995 c); Escolar et al., 1994; White et al., 1994; White and Escolar 1990).

1.2.1 Cytoskeleton of platelets

The two basic components of the platelet membrane are the phosholipid bilayer and the underlying cytoskeleton. The platelet membrane acts as a barrier between the cytosol and the extra cellular fluid, whereas the cytoskeleton is responsible for the cell's shape, strength and motility (Hochmuth and Marcus 2002; Hochmuth et al., 1983; Hochmuth and Evans 1982). Platelets circulate in the blood stream as disc shaped objects, which can withstand high dynamical shear stress. To tolerate such forces acting on the platelet, platelets have developed a highly organized cytoskeleton. The impact of variations in the cytoskeleton will be discussed in detail in chapter 4. It consists of peripheral microtubule coils and rigid crosslinked actin filaments that fill the cytoplasmic space and are connected to a membrane skeleton composed of spectrin and its associated proteins (Pötzsch and Madlener 2009; Hartwig 2007; Barkalow et al., 2003; White and Jennings 1999; White and Rao 1998; Cramer et al., 1991; Hartwig and DeSisto 1991; Fox et al., 1988; White 1987). Shape changes require a remodelling of the resting cytoskeleton and the assembly of new cytoplasmic actin filaments

(Hartwig 2007). The platelet's discoid form is lost and it becomes round. Fingerlike structures grow from the cell periphery. Then the platelet flattens over the surface and extends broad lamellae. As the platelet flattens, the granules and organelles are squeezed into the centre of the cell. Approximately 0.5µm long actin filaments fill the lamellipodia (Fox et al., 1987). After platelet activation the platelet integrin αIIbβ3 becomes tethered to the underlying actin filaments by binding interactions between it and a still unresolved number of adhesive site proteins (Buridge et al., 1990; Burridge and Fath 1989). Additionally, dynamic disassembly and rearrangement of the microtubules occur. These microtubules have been shown to centralise and constrict, due to their association with the cortical actin shell, which also contracts upon activation (Tablin and Castro 1992; Jung et al., 1981; Nachmias 1980).

Microtubules show a cylindrical structure, in which the tubulin heterodimers are packed around a central core. α- and β-tubulin form α-, β-heterodimers, which polymerize to protofilaments. Thirteen linear protofilaments compose a ringlike complex, which accumulates through a further polymerisation to a long tube of several microns (100µm). Only one microtubuli coil is responsible for the platelets discoid shape and its cytoskeletal support system (Prötzsch and Madlener 2009; Escolar et al., 1986; Kenney and Linck 1985). The coil is not a bundle or microtubules bound together. It is a single microtubule wound up many times to fit inside the resting platelets (White and Sauk 1984). Microtubules assemble from the centrosome and grow outward into the cell cortex. From this point they turn and run in parallel with the cell edges (Patel et al., 2005). The microtubule bundle lies close to the cell wall, but never appears to contact it (Pipeleers et al., 1977). Microtubules are dynamic and polar structures. It is possible to distinguish between a fast-growing end, the plus end, and a slow growing, the minus end, which tends to loose subunits, if not stabilized. Embedding them in a structure, called the centrosome, stabilizes the minus ends of microtubules, and the rapidly growing ends are then free to add tubulin molecules. These plus ends can shorten as well as lengthen: after growing outward for many minutes by adding subunits, its plus end may undergo a sudden transition that causes it to loose subunits, so that the microtubule shrinks rapidly inward and may disappear (Alberts et al., 2003; Koolman and Röhm 2002; Brinkley 1985). The microtubule-associated proteins crosslink to the microtubule coil to maintain its stability and to link to the underlying cytoskeleton (Tablin and Castro 1992; Tablin et al., 1990; Kenney et al., 1988; Tablin et al., 1988; White et al., 1986; Kenney and Linck 1985).

The cell cortex is formed by actin filaments lying just beneath the plasma membrane and these filaments are cross-linked into a dynamic network by various actin-binding proteins.

These filaments are polarized structures (Huxley 1963). The cortical actin filament network determines the shape and mechanical properties of the plasma membrane as for example internal transformation, contraction of the hemostatic plug and retraction of clots (Escolar et al., 1986). Actin occurs in two different shapes, one monomolecular shaped globular actin, G-actin, and the other one as helical homopolymer filamentous actin, F-actin. G-actin is an antisymmetric molecule, which contains two domains. With increasing ionic strength the G-actin reversible assembles to F-actin. G-actin carries tight adhered ATP molecules, which are slowly hydrolysed by F-actin to adenosine diphosphate (ADP) (Kim et al., 2009; Alberts et al., 2003; Koolman and Röhm 2002; Fox et al., 1984; Flanagan and Lin 1980; Brenner and Korn 1979). As single G-actin molecules are linked in the same direction parallel, the F-actin is polar, negatively charged. It is composed of two different ends, which show variable polymerisation sites. If the ends are not stabilized by specific molecules, the plus end of the F-actin will constantly grow to a critical concentration of the G-actin, whereas the minus end will simultaneously collapse. That dynamic behaviour of growing and shrinking, without net change in filament length, is called treadmilling. This phenomenon, like dynamic instability, is a no equilibrium behaviour that requires input of energy, which is provided by the ATP hydrolysis that accompanies polymerization (Mohrdieck et al., 2007; Alberts et al., 2003; Pelletier et al., 2003; Koolman and Röhm 2002; Godette and Frieden 1986; Brenner and Korn 1979). The F-actin length can vary from less than one micrometer to several tens of micrometers. The persistence length of actin filaments, which is a parameter of their bending stiffness, is about 17μm. This is in the order of the typical contour length of actin filaments (Mohrdieck et al., 2007; Le Goff et al., 2002). Especially, the F-actin networks are involved in cell morphology, motility and adhesion processes (Pelletier et al., 2003).
Spectrin molecules bind directly to the cytoplasmatic side of the plasma membrane (Prötzsch and Madlener 2009; Kenney and Linck 1985). The cytoplasm of platelets is rich in glycogen (White and Jennings 1999).

1.2.2 Cholesterol and platelet membranes

Platelet membranes are composed of lipid bilayers. These are fluid, which enables individual molecules to diffuse rapidly. However, in the lipid bilayers cholesterol and glycolipids are organised. Especially, large amounts of cholesterol are found in the eucaryotic plasma membranes (Alberts et al., 2003). The cholesterol loading of membranes affects the permeability, transport and enzymatic activities of the membrane and the availability of

membrane surface receptors. Cholesterol is insoluble in water, but it is dissolvable in phosholipids (Cooper 1987). A unique ability of cholesterol is to increase the lipid order in fluid membranes, while maintaining fluidity and diffusion rates. Cholesterol provides low permeability barriers to lipid membranes and is the basis for large mechanical coherence. The bending modulus κ of the platelet membrane is increased by cholesterol and therefore, the repulsive undulation force is diminished. Cholesterol is considered to be important for several plasma membrane-based properties in the human body, such as raft formation, protein sorting, and cell signalling (Mouritsen and Zuckermann 2004). The influence of the cholesterol concentration on the platelet functions will be discussed in chapter 5.

1.3 Von Willebrand Factor

The von Willebrand disease (vWD) has been investigated since 1926, when Erik Adolf von Willebrand reported a severe bleeding disorder from a family living on an island of the Finland coastline (Reininger 2008 a); Haberichter and Montgomery 2006; Schneppenheim and Budde 2006). Bleeding is related with pseudohaemophilia, but in the following decades it was pinpointed to be a failure in haemostasis residing in the plasma of the patients. In 1971, Zimmerman was able to identify immunological vWF (Reininger 2008 a); Schneppenheim and Budde 2006; Zimmerman et al., 1971). The influence of vWF mutations on the platelet-vWF interaction will be focused in chapter 7. VWF is a multimeric glycoprotein of identical subunits, which are composed of 2,050 residues with multiple A-, B-, C-, and D-type domains (Reininger 2008 a); Reininger 2008 b); Yago et al., 2008; Verweij et al., 1986). The multimers are formed within the endoplasmatic reticulum by disulphide linkage of dimers of approximately 500kD and result in multimers of various sizes that may exceed 10,000kD or 1μm in length (Reininger 2008 a); Arya et al., 2002; Fowler and Fretto 1989). VWF in plasma is globular and above a critical shear rate the vWF molecule is stretched. By atomic force microscopy (AFM) stretched vWF fibres absorbed on OTS-SAM were imaged in tapping mode under aqueous conditions (Siediecki et al., 1996) and the reversible formation from globular to stretched vWF molecules under flow condition was reported by Schneider and coworkers (Schneider et al., 2007). Endothelial cells and megakaryocytes synthesize and store vWF. VWF is stored in Weibel–Palade bodies of the endothelial cells, rod-shaped organelles and presumably derived from the Golgi apparatus (Pötzsch and Madlener 2009; Reininger 2008 a); Reininger 2007; Butenas et al., 2001; Weibel and Palade 1964). VWF can be secreted from endothelial cells either (i) constitutively by molecules that are released directly

upon synthesis, or (ii) via a regulated pathway, in which stored mature vWF molecules are released after stimulation by secretagogues. The release of vWF can either be apical or luminal into the circulating blood or basolateral or abluminal into the subendothelial matrix (Reininger 2008 a); Wagner 1989; Van der Kwast et al., 1986). Generally, it is assumed that vWF stored within the Weibel–Palade bodies is composed of the largest multimeric species, i.e. ultra-large vWF, that are usually not observed in the blood of normal individuals (Reininger 2008 a); Tsai et al., 1989; Wagner and Marder 1984). The metalloproteinase ADAMTS 13 cleaves ultra-large vWF at the A2 domain and is thus, a physiological mechanism to prevent their appearance in the circulation (Reininger 2008 a); Moake et al., 1982). The second storage site for vWF is within the platelet α-granules (Reininger 2008 a); Cramer et al., 1988). This storage may contain as much as 20% of the total vWF present in blood and consists also of the ultra-large vWF multimers (Pötzsch and Madlener 2009; Reininger 2008 a)). As platelets release their granule contents only upon stimulation by agonists such as ADP, collagen and thrombin, this secures ultra-large vWF multimer availability at sites of vascular leakage. Simultaneous release of ultra-large vWF multimers from adjacent endothelial cells ensures the presence of haemostatically most effective multimers at the vessel wall and in the fluid phase in the immediate vicinity of the vascular lesion (Pötzsch and Madlener 2009; Reininger 2008 a); Nesheim et al., 1991; Koutts et al., 1978). The impact on the vWF multimer size on the platelet-vWF crosstalk will be analysed in chapter 6 and 8.

1.4 Physical properties of the blood flow

Under arterial and arteriolar flow conditions dependent on the shear rate and HCT, platelets show an enhanced concentration near the blood vessel wall (Crowl and Fogelson 2009; Woldhuis et al., 1992; Tangelder et al., 1985). More details on the influence of the HCT will be quantified in chapter 9. The peak platelet concentration was not directly at the wall. It was approximately 5µm to 10µm in distance to the vessel wall, an effect attributed to hydrodynamic lift or repulsion forces between the platelets and the wall (Hathcock 2006; Eckstein et al., 1987; Tilles and Eckstein 1987). Platelets marginate to the vessel wall from the centre. Thus, under most arterial flow conditions the platelet concentration near the wall is increased by a factor of 2 to 3 compared to the centre of the vessel dependent on both the HCT and the shear rate (Hathcock 2006; Holme et al., 1997; Takada et al., 1994; Aarts et al., 1988; Alkhamis et al., 1988; Goldsmith and Turitto 1986). However, erythrocytes concentrate

towards the high-velocity region near the centre of the vessel (Hathcock 2006; Eckstein et al., 1987; Tilles and Eckstein 1987), leaving a thin, slower-moving, cell poor layer near the wall. The near-wall platelets are influenced by inelastic collisions with red blood cells (Tokarev et al., 2011). The high-velocity movement of erythrocytes through small vessels relative to that of plasma is associated with depressed local HCT values in such vessels (Fahraeus-Lindquist effect), thereby partially explaining the local decrease in blood viscosity. Additionally, reducing the vessel diameter decreases the apparent viscosity of flowing blood. This effect is most pronounced as the vessel diameter is lowered from 100µm to 10µm. This reduction might be due to several physical factors (Hathcock 2006; Thurston 1972; Chien et al., 1966; Fahraeus and Lindquist 1931). A few microns above the vessel wall the frictional drag of the wall causes the axial flow velocity to go back to zero and Brownian motion causes the radial movement towards the reactive wall (Hathcock 2006; Goldsmith and Turitto 1986; Bird et al., 1960). Its magnitude can be estimated based on the molecule size, shape and the kinematic viscosity of the medium using the Stokes–Einstein relationship (Hathcock 2006; Bird et al., 1960). Diffusion based transport is only effective over short distances and not across the whole vessel diameter. Under steady laminar flow conditions the diffusion rate is dependent on the diffusion of the cell, on the bulk cell concentration and the length of the vessel. The number of collisions between the cell and the wall strongly influences the diffusion rate (Hathcock 2006). Platelets are too large to be significantly controlled by Brownian motion (Crowl and Fogelson 2009; Goldsmith 1971). The diffusive transport is important for proteins (Crowl and Fogelson 2009; Hathcock 2006; Bird et al., 1960). The velocity profile across the vessel is roughly parabolic and the non-uniform cell distribution depends on the fluid dynamics of blood as a heterogeneous medium (Crowl and Fogelson 2009; Hathcock 2006; Bird et al., 1960). As the flow through the vasculature is laminar, the viscous forces damp out relative momentum differences between adjacent fluid layers. These forces prevent disturbances between the layers and creating a smooth velocity profile across the vessel, approximating a parabola (Hathcock 2006; Goldsmith and Turitto 1986). Commonly, the blood movements throughout the vasculature are pressure driven across a branched network of vessels of varying contours, diameters and length scales. Arterial flow is pulsatile. The amplitude of pulsatility decreases with the distance to the heart (Hathcock 2006; Wootton and Ku 1999; Swanson et al., 1986). The blood viscosity is a rheological parameter that depends on complex interactions and deformations of suspended cells. Physical effects alter the local HCT. Additionally, radial distribution of cells across a vessel influence blood viscosity in a non-Newtonian manner (Fahraeus and Lindquist 1931). For most physiological shear rates the

viscosity of the blood is ~ 0.035P (g/cms) (Hathcock 2006; Goldsmith and Turitto 1986). The apparent blood viscosity enlarges in a non-Newtonian manner as the shear rates reduce < $100s^{-1}$, thus enhancing vascular resistance (Thurston 1972).

Generally, shear rates in arteries are higher compared to those in veins. The highest wall shear rates reached in small arterioles of 10–50μm diameters vary between $500s^{-1}$ and $5{,}000s^{-1}$. In the pathological obstructing atherosclerosis state wall shear rates of $3{,}000–10{,}000s^{-1}$ have been measured in coronary arteries with 50% stenosis (Back et al., 1977; Reininger 2008 a)) and can exceed $50{,}000s^{-1}$ at higher degrees of occlusion (Reininger 2008 a); Mailhac et al., 1994; Strony et al., 1993).

1.5 Theoretical analysis of the cells behaviour

1.5.1 Adhesion of cells

The adhesion of cells or platelets from shear flow is a dynamic process that is controlled not only by a complex interplay of specific attractive short-range lock and key forces (fig. 4) and long-range repulsion forces, but also by the elasticity of the membrane and the soft shell (Evans and Calderwood 2007; Boulbitch et al., 2001; Albersdörfer et al., 1997; Bruinsma 1995; Evans 1985; Leckband et al., 1995; Lipowsky and Seifert 1991; Seifert and Lipowsky 1990; Bell 1978). In the case of platelets and vWF the lock and key interactions are exemplary between the GPIbα and the vWF A1 domain. The most important non-specific repulsive forces are probably the undulation forces or Helfrich repulsions. These result from thermally excited bending fluctuations. The mean square of the amplitude of the oscillation $\langle u^2 \rangle$ of the a quadratic membrane piece with a length d increases with ~ d^2,

$$\left\langle u^2 \right\rangle = (k_B T / \chi)^2 d^2, \qquad (1)$$

where k_B is the Boltzmann constant, T the temperature, χ the bending modulus (Sackmann 2004; Simson and Sackmann 1998; Seifert 1995; Sackmann 1995). Aside these also unspecific interactions, electrostatic and van der Waals forces, between the platelet membrane and the vWF surface also exist (Sackmann 2004; Simson and Sackmann 1998). During adhesion the receptors start to form clusters (fig. 4), thereby enhancing the adhesion energy (Smith et al., 2008; Reininger et al., 2006; Boulbitch et al., 2001; Albersdörfer et al., 1997; Goldmann et al., 1996; Cramer et al., 1991). For platelets the bond formation during the adhesion process is believed to take place in two steps. First, the platelets adhere point wise through the interaction of single ligands at receptors of the membrane and form discrete

adhesion points (DAPs). Thereafter, clusters are formed from receptor-ligand pairs (adhesion domains, tight adhesion regions), which stabilise the adhesion. The clusters form because of a lateral phase separation of the receptors and the sugar polymers of the gylcocalyx (fig. 4), which is driven by the competition of the attractive lock and key forces and the induced repulsive force of the polymers (Sackmann 2004; Sackmann and Bruinsma 2002; Simson and Sackmann 1998).

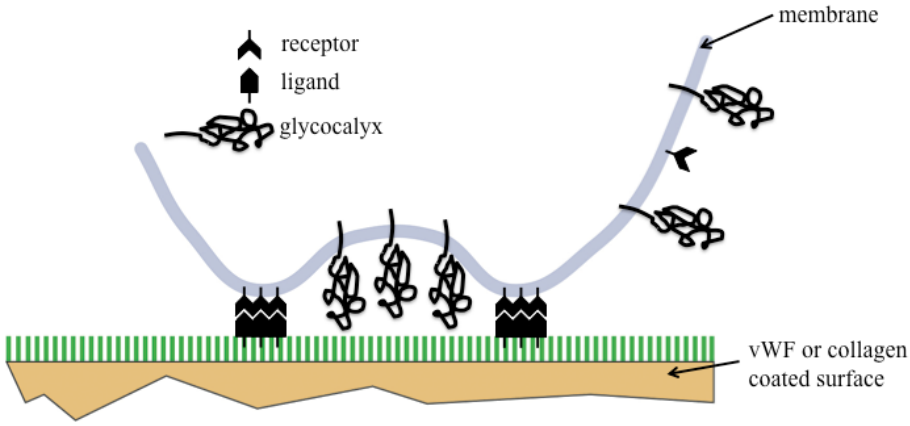

Figure 4: Schematic drawing of the lock and key interactions and the repulsive forces of the gycocalyx at a membrane. The grey line represents the model membrane (adapted from Sackmann 2004).

In the late actively regulated stage of adhesion, the actin cytoskeleton couples to the adhesion domains. These adhesion domains are in close contact (~ 7nm) strongly adhering with the non-fluctuating regions of the substrate (Smith et al., 2008; Albersdörfer et al., 1997). At homogenous tight adhesion zones the receptor-ligand pair concentration of the membrane is high (Boulbitch et al., 2001; Guttenberg et al., 2001) The clustering of the receptor during the adhesion process might be due to a reduction of the local repulsion between the cell and the substrate (Albersdörfer et al., 1997; Ammam and Lipowsky 1996). For membranes under low tension, thermally induced fluctuations of the surface are more pronounced than those of a membrane under moderate tension (Kim et al., 2009; Glassinger and Raphael 2006; Evans 1995). Helfrich derived a scaling law that tried to correlate the undulatory repulsion, the tension and the attraction through a $1/z^2$ van der Waals potential

$$\langle z \rangle_{eq}^2 = 1/\sigma \tag{2}$$

and

$$\langle g_{ad} \rangle = \sigma \tag{3}$$

where $\langle z \rangle_{eq}$ is the equilibrium mean spacing, σ the tension and g_{ad} the adhesion energy between membranes per unit area of adhesive contact (Helfrich 1995).

1.5.2 Theoretical analysis of the formation of membrane tethers

During blood flow two physical conditions are crucial for the tether formation process. First the localization of the force to a spot on the surface and second the existence of excess area in the blood platelet (Evans and Yeung 1994). Exerting a force at a point on the platelet surface led to the formation of long, thin cylindrically shaped tethers (Hochmuth and Marcus 2002; Hochmuth et al., 1983; Hochmuth and Evans 1982). As the formation of a tether involves the creation of a high curvature, the work to pull a tether is basically done against the bending energy (Harmandaris and Deserno 2006; Boek et al., 2005; Marrink and Mark 2001; Lindahl and Edholm 2000). The force required to maintain a tether at a given length depends upon both membrane elastic properties and tension (Glassinger and Raphael 2006). If yield tension is provided, tethers might be stable (Bukman et al., 1996). The membrane tension is assumed to increase, as the tether is lengthened (Glassinger and Raphael 2006; Koster et al., 2003). The tether behaviour is actually influenced by small variations in the tension of the membrane (Glassinger and Raphael 2006). The apparent surface tension is determined by the sum of the in-plane, far-field tension and the energy of adhesion between membrane and cytoskeleton (Hochmuth et al., 1996). The increase in energy of the system during tether formation arises from two sources: (i) an increase in bending energy owing to the movement of membrane with no curvature from the disk like cell body to the cylindrical tether with a constant curvature and (ii) the separation of the membrane from the cytoskeleton, where there is a chemical affinity or free energy of adhesion γ between membrane and cytoskeleton (Hochmuth et al., 1996).

2. Scope of the work

Aim of this interdisciplinary PhD thesis was to bridge the gap between soft cellular objects e.g., platelets and a dissolved plasma protein, e.g. vWF, which both change form and function in a mutual interplay that is dependent on shear. Huge effort was undertaken to show the interaction under blood flow conditions, mimicking the in vivo situation. Individual (e.g. single platelet adhesion) as well as collective phenomena (e.g. platelet adhesion in the presence of red blood cells) were studied using mainly the microfluidic flow chamber. Specific focus was given to the impact of changes in the platelet mechanics, by variations in the cytoskeleton, as well as the erythrocyte concentration, the HCT, and the role of the blood coagulation glycoprotein vWF. These goals were achieved by combining experimental and theoretical concepts.

The influence on the GPIbα and vWF A1 domain interaction by changing various parameters either of the platelets or of the vWF protein was investigated. To clarify this complex platelet-vWF crosstalk phenomenon, the thesis is divided in specific chapters, in which different impacts on the platelets and on the vWF molecule are investigated. Each chapter deals with a distinct problem. Finally, a general conclusion will be drawn. The main focus was placed on either the platelet adhesion and tether formation on vWF, which does not require any prior platelet activation, or on the platelet aggregate formation on collagen. A schematic overview of the investigated impacts on variations of the platelets and the vWF is provided in figure 5.

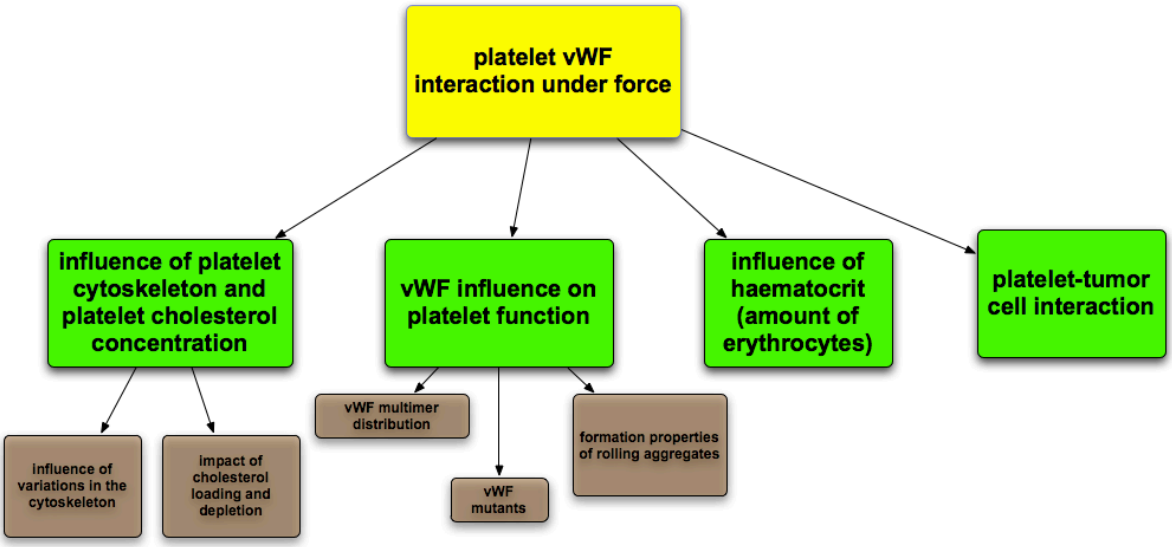

Figure 5: Schematic overview of the investigated topics of this thesis.

In the first result chapter the influence of variations in the cytoskeleton is discussed. Here, the platelets were treated with cytochalasin D, which disrupts the F-actin of the platelets, or the microtubuli breaking drug, nocodazole. In the next chapter the impact of cholesterol loading and depletion is investigated. The next three chapters deal with variations of the vWF protein. The importance of the multimer size distribution of the vWF molecule and the comparison of commercially available products is studied. The next chapter shows the impact of vWF mutations and in the last chapter concerning vWF, the characterization of rolling platelet-vWF aggregates is described. The physical influence of the platelet-vWF interplay is investigated by changes in the HCT. The work discusses in the final chapter the platelet-tumor cell interaction.

3. Materials and methods

3.1 Biological sample preparation

The biological sample preparation was mainly adapted with slight modification to the work previous published by Reininger and Ruggeri (Reininger et al., 2006; Ruggeri et al., 1983; Ruggeri et al., 1999). The entire chemicals and suppliers are listed in the appendix A.

3.1.1 Blood samples preparation with activation inhibited platelets

Venous blood from normal consented female or male donors, who had not ingested platelet relevant drugs for at least 10 days, was collected in a test tube. For the cytoskeleton (see chapter 4), cholesterol (see chapter 5) and HCT (see chapter 9) flow experiments the test tube contains the anticoagulant acid citrate dextrose (0,106M trisodium citrate), the irreversible thrombin inhibitor H-D-Phe-Pro-Arg chloromethyl ketone (PPACK; 46µM), prostaglandin E_1 (PGE_1; 0.35µl/ml), the αIIbβ3 inhibitor aggrastat concentrate (0.25µg/ml) and apyrase grade 7 (1.3 ATPase U/mL). For the combined AFM-patch clamp set-up (see chapter 4) the H-D-Phe-Pro-Arg chloromethyl ketone concentration was increased to 93µM (Reininger et al., 2006). The blood sample was centrifuged at 170g for 15min. For cytoskeleton flow experiments the platelet rich plasma (PRP) was incubated in a rolling chamber with cytochalasin D (final concentration: 4µM) dissolved in DMSO for 1h or with nocodazole (final concentration: 5µg/ml) for 2h at 37°C. For the combined AFM-patch clamp set-up the PRP was incubated at least 1h to a 4h maximum with cytochalasin D (final concentration: 8µM) or at least 2h to a 4h maximum with nocodazole (final concentration: 10µg/ml) at 37°C (Reininger et al., 2006). For cholesterol flow experiments the PRP was enriched with or depleted with cholesterol by incubation with 100mM methyl-β-cyclodextrin (MβCD) saturated in 10mM cholesterol or using 10mM MβCD not complexed with cholesterol and incubated for 30min at 37°C. The platelet count in the final suspension was adjusted to the orginal value in the blood (230,000-390,000/µl). The PRP for the HCT perfusion experiments was centrifuged at 1083g for 15min. The platelet count in the final suspension was adjusted to 200,000/µl and the HCT to around 20%, 40% and 60%.

3.1.2 Blood sample preparation with plasma free blood and activation inhibited platelets

Venous blood from normal consented donors (see chapter 3.1.1) was collected in a test tube containing 1.6mg/mL EDTA to block platelet activation and inhibit integrin receptor function (Savage et al., 2002), H-D-Phe-Pro-Arg chloromethyl ketone (PPACK; 46µM), prostaglandin E_1 (PGE_1; 0.35µl/ml), apyrase grade 7 (1.3 ATPase U/mL) and citrate dextrose solution (ACD; 200µl/ml). In modifications to Ruggeri's protocol, blood cells were washed free of plasma constituents by repeated centrifugation and resuspension in Hepes-Tyrode buffer (10mM HEPES, 140mM NaCl, 2.7mM KCl, 0.4mM NaH_2PO_4, 10mM $NaHCO_3$, and 5mM dextrose), at pH 6.5 (Ruggeri et al., 1983). The sedimented cells (including platelets and leukocytes on top of the erythrocyte cushion) were resuspended and subsequently centrifuged at 1000g for 13min. The supernatant was washed and purified 4 times with fresh buffer suspension, resulting in progressively decreasing residual amounts of plasma proteins. After the first centrifugation step apyrase grade 7 (0.65 ATPase U/mL) was added to the cell suspension. After each centrifugation step until the third one, the added concentration of apyrase grade 7 was bisected. After the final centrifugation step, the cell pellet was resuspended in modified HEPES-Tyrode buffer, pH 7.4, containing 50mg/mL of bovine serum albumin (BSA), as well as 1.0mmol/L $CaC1_2$, 0.5mmol/L $MgCl_2$ and prostaglandin E_1 (PGE_1; 0.35µl/ml) (Ruggeri et al., 1999). For the vWF products comparison perfusion experiments over collagen (see chapter 6) the multimeric vWF products (Fanhdi, Haemate, Haemoctin, Immunate, Octanate, Wilate, Haemate subfractions (E100, E140, E180, E250); final concentration: 100µg/ml or 10µg/ml) were added to the blood suspension. To rolling platelet-vWF aggregate flow experiments (see chapter 8) multimeric vWF proteins (recombinant vWF, plasma vWF, plasma derived vWF with and without sugar, Haemate, Haemate subfractions (E100, E250); final concentration: 20µg/ml), labelled with Alexa Fluor 488 or unlabelled, were added to the washed blood suspension, except for the whole blood experiments. These were carried out with the same inhibitors, but without the washing procedure.

3.1.3 Blood samples preparation with activated platelets

For the cytoskeleton (chapter 4) and tumor cell experiments (see chapter 10) venous blood from normal consented donors (see chapter 3.1.1) was collected in a test tube containing the anticoagulant acid citrate dextrose (0,106M trisodium citrate). The blood sample was centrifuged at 170g for 15min. For tumor cell experiments the blood sample was centrifuged

at 120g for 20min to obtain PRP. The PRP for cytosekeletal experiments was incubated in a rolling chamber with cytochalasin D (final concentration: 4µM) dissolved in DMSO for 1h or with nocodazole (final concentration: 5µg/ml) for 2h at 37°C (Reininger, et al., 2006). For the vWF products comparison experiments (see chapter 6) the test tube contains 1.6mg/mL EDTA, H-D-Phe-Pro-Arg chloromethyl ketone (PPACK; 46µM). For the vWF products comparison perfusion experiments over collagen (see chapter 6) the multimeric vWF products (Fanhdi, Haemate, Haemoctin, Immunate, Octanate, Wilate, Haemate subfractions (E100, E140, E180, E250); final concentration: 100µg/ml or 10µg/ml) were added to the blood suspension after a slightly modification of the washing procedure in chapter 3.1.2. No inhibitors during the washing procedure were used and the washing steps were repeated 3 times. The same blood preparation, as for the vWF products over collagen, was used for the WT and loss of function mutant (lofm) flow experiments (see chapter 7) over collagen. Multimeric vWF (WT, lofm (provided by Prof. Dr. Schneppenheim, Hamburg); final concentration: 10µg/ml) was added to the washed blood suspension.

3.1.4 Cells culture

Human small cell lung carcinoma cells (SCLC) typically grow as aggregates in solution and maligne melanoma cells (MV3) adherent. The cells were cultivated in RPMI at pH 7.0, at 37°C in a 5% CO_2 atmosphere with 95% humidity. For experimental use or further passage the non-adherent SCLC cells were cultivated 6 to 8 days and MV3 cells were adherent grown to a confluent layer in 3 to 5 days. For flow chamber, aggregation and ATP secretion experiments the cells were either kept in the tissue media or resuspended in Tyrode buffer (17mM Hepes [N-2-hydroxyethylpiperazine-N′-2-ethanesulfonic acid], 130mM NaCl, 2.7 mM KCl, 0.4mM NaH_2PO_4, and 2.8mM dextrose) to an average final concentration of 10,000 +/- 2,000 cells/µl for SCLC cells and 2,000 +/- 400 cells/µl for MV3 cells. To resuspend the SCLC cells and MV3 cells in Tyrode buffer, the cells were centrifugated 2 times at 45g for 3min. For flow cytometer measurements the cells were resuspended in Tyrode buffer (1:10 dilution).

3.2 Methods

3.2.1 Flow chamber set-up

3.2.1.1 Flow chamber

Coated glass cover slips were used as a substrate and assembled with parallel plates to form a rectangular flow chamber. These cover slips were coated for cytoskeleton (see chapter 4), HCT (see chapter 9) and tumor cell (see chapter 10) perfusion experiments with immobilized multimeric vWF (Haemate; final concentration: 100µg/ml). To provide enough binding sites on the surface for the platelets the glass slides were coated with an increased physiological vWF concentration to distinguish the alterations. For cholesterol perfusion experiments (see chapter 5) the glass cover slips were coated with immobilized multimeric vWF (WT (provided by Prof. Dr. Schneppenheim, Hamburg); final concentration 10µg/ml). The glass cover slips for the vWF product comparison experiments (see chapter 6) were coated with either the immobilized multimeric vWF products (Fanhdi, Haemate, Haemoctin, Immunate, Octanate, Wilate; final concentration: 100µg/ml or 10µg/ml) or fibrillar type I collagen equine tendon (final concentration: 1:10 of stock solution). Perfusion experiments of vWF WT and lofm (see chapter 7) were performed by using immobilized multimeric vWF (WT, lofm (provided by Prof. Dr. Schneppenheim, Hamburg); final concentration: 10µg/ml) or fibrillar type I collagen equine tendon (final concentration: 1:10 of stock solution) coated on to glass cover slips. Rolling aggregate perfusion experiments (see chapter 8) were performed with either recombinant dimeric vWF A1 (final concentration: 20µg/ml) or fibrillar type I collagen equine tendon (final concentration: 10% of stock solution) coating.

3.2.1.2 Flow champer actuation

Perfusion experiments were conducted using a syringe pump (Harvard Apparatus, Boston, MA) at 37°C. Whole blood was aspirated for the cytoskeleton impact on the adhesion and the tether formation (see chapter 4) at a flow rate of 10,000s^{-1} and on spreading at a flow rate of 800s^{-1} through the chamber. For cholesterol experiments (see chapter 5) the flow rates ranged from 5,000s^{-1} to 20,000s^{-1} and for vWF product comparison experiments (see chapter 6) from 400s^{-1} to 40,000s^{-1}. For the WT and vWF lofm mutant experiments (see chapter 7) the flow rates were adjusted in the range of 1,500s^{-1} to 20,000s^{-1}, for rolling aggregate experiments (see chapter 8) of 0s^{-1} to 50,000s^{-1} and for HCT experiments (see chapter 9) of 400s^{-1} to 20,000s^{-1}. The shear rate was set to 100s^{-1} for tumor cell flow experiments (see chapter 10).

3.2.1.3 Microscopy

Reflection interference contrast microscopy (RICM) was performed using an optical upright microscope (Axioskop 2 plus; Zeiss, Germany) with a plan neofluoar antiflex objective (63x, oil immersion, N.A.=1.6, Zeiss, Germany) equipped with a wavelength-independent quarter-wave plate and a 50-W mercury lamp for illumination. The measured visual field per frame was around 5,000µm^2. Except for the tumor cell experiments an inverted microscope (Eclipse TE2000-E; Nikon, Dusseldorf, Germany) was used. To minimize the reflections of the glass surface oil objectives are used. Due to this label-free light optical technique, the distance between cell membrane and adhesive surface can be analysed and the contact area can be resolved. This technique allows the analysis of intransparent fluids like blood. Under static conditions it is possible to reconstruct the height profile of an object from the interference pattern of polarized light being reflected at the object's surface. In general, incoming light is refracted and partly reflected at optical interfaces of n_0 to n_1 and from n_1 to n_2, respectively, as shown in figure 6.

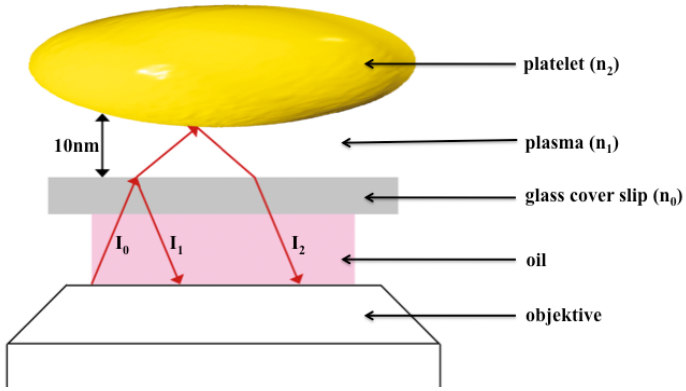

Figure 6: Principle of the RICM. The incident beam (I_0) is partially reflected from the substrate (vWF coated glass cover slip, n_0), which interferes with light reflected from the membrane of platelets (n_2) flowing in close proximity to or interacting with it. The resulting interference colours of the Newton rings give a quantitative measure of distance between the platelet membrane and the adhesive surface. I_1 and I_2 are the intensities of the refracted light. The platelet is dissolved in plasma (n_1).

The reflected parts interfere with each other in a constructive (bright rings) or destructive (dark rings) manner depending on the difference of their optical path length and form Newton rings. The resulting interferogram contains information about the vertical distance h of the object above the substrate. The height profile can be calculated from the observed intensity $I(\vartheta)$ of the interfering light beams as follows:

$$I(\vartheta) = I_1 + I_2 + 2\sqrt{I_1 I_2}\cos[2kh(x,y)\cos\vartheta + \phi] \qquad (4)$$

where ϑ is the angle of incidence, I_1 and I_2 the intensities of the refracted light, $h(x,y)$ is the distance between the substrate and the object as a function of the lateral position (x,y) and

$k = \frac{2\pi n}{\lambda}$ is the wavevector corresponding to the wavelength λ and n the refractive index of the surrounding medium. The constant phase ϕ accounts for the phase shift between two reflected light beams, which depends on the angle of incidence as well as the polarization of the light. Under flow conditions the monochromatic light reflected from the substrate coated glass surface interfered with that reflected from the membrane of platelets flowing in close proximity to or interacting with the coated surface, but a direct measurement of the height profile is not possible. Therefore, static measurements from Smith and coworkers were used to estimate the distances of the platelet and the vWF coated glass surface (Smith et al., 2008; Reininger et al., 2006; Gönnenwein 2003; Kloboucek et al., 1999).

Fluorescence images were taken using a plan neofluar objective (40x, oil immersion, N.A.=0.75, Zeiss, Germany). The measured visual field per frame was around 66,000µm^2. For epifluorescence microscopy, platelets were treated with 10µM mepacrine (quinacrine dihydrochloride, Sigma, Rödermark, Germany) for fluorescent rendering (Savage 1996).

3.2.1.4 Data aquistion

A black-and-white video camera for RICM images was used to obtain interference colours on a grey scale. Fluorescence images were taken with a colour video camera (Exwave HAD 3CCD, Sony, San Jose, USA). All experiments were recorded on DVD using a CCD camera (BC-71, AVT Horn, Aalen, Germany) and a DVD recorder (LQ-MD800 Medical Grade DVD Video Recorder, Panasonic, Germany) at the acquisition rate of 25 frames s^{-1}. Image analysis was performed off-line using Metamorph (Universal Imaging, West Chester, PA) and Matrox (Imaging, Dorval, Quebec, Canada).

3.2.2 Atomic force microscopy

3.2.2.1 Sample preparation

Immobilized multimeric vWF products (Haemate, Wilate; final concentration: 20µg/ml) in HBSS (4,760g Hepes and 7,891g NaCl dissolved in 1l H_2O) buffer were used as substrates for the high-resolution imaging. To obtain a shear coating of the vWF products, these products were aspirated over glass cover slips through the flow chamber (see chapter 3.2.1.1) with a tubing pump (Reglo; Ismatec, Glattbrugg, Switzerland) at flow rates of 6,000s^{-1} for 30min at

RT. In a final step, the vWF shear coated cover slips were fixed with 2.5% glutaraldehyde and 10% paraformaldehyde.

3.2.2.2 Imaging

All images of the vWF products (Haemate, Wilate) were obtained in HbSS buffer with an atomic force microscopy (AFM) (JPK instruments, Berlin, Germany). Liquid images were performed in tapping mode using rectangular cantilever (CSC37/noAl; Mikromash, Tallinn, Estonia). Cantilever with force constants of 0.65Nm and 0.35Nm (manufacturer information) were used.

3.2.2.3 Tip functionalization and characterization

Soft silicon nitride cantilevers (Veeco, Santa Barbara, CA) were incubated in 3-Glycidoxypropyltrimepoxysilan for 1min at RT, rinsed in toluol for 1min and briefly after in H_2O for 1min, and finally dried in a heated exicator for 30min at 80°C. Subsequently, the tips were incubated in NH_2-PEG-COOH x HCL (25mM) in a fluid chamber for 1h at RT, rinsed 4 times in ddH_2O, incubated in EDC-N-Hydroxysuccinimid C4H5NO3 (100mM) for 10min, briefly followed by 3 times rinsing in ddH_2O, and a final incubation in dimeric vWF A1 (final concentration: 0.01µg/ml) in a fluid chamber for 2h. Before each experimental series, the cantilevers were calibrated using the thermal noise amplitude analysis approach (Butt and Jaschke 1995; Florin et al., 1995). The measured spring constants were between 15-25pN/nm, in agreement with the nominal spring constant of 20pN/nm.

3.2.2.4 Force spectroscopy

The in-house-built force measurement und patch clamp set-up (Prof. Dr. Gaub Group, LMU, Munich) was mounted to the microscopic stage of an inverted optical microscope. This arrangement enabled precise positioning of the cantilever on the area of interest along the platelet membrane. The force spectroscopy steps are briefly summarized: The platelet suspension was injected in the HbSS buffer medium (4,760g Hepes and 7,891g NaCl dissolved in 1l H_2O) of the patch clamp set-up at RT. A single platelet (preparation see chapter 3.2.3) was caught with the in-house-built AFM-patch clamp device and the experimental set-up was rinsed 10 times with HbSS buffer to obtain an almost platelet free

surface around the patch clamp hole. Subsequently, the dimeric vWF A1 domain coated AFM cantilever was moved towards the platelet until getting into contact with the platelet membrane. This could be monitored by the deflection signal of the laser. The cantilever-membrane contact time varied from 1s to 3s.

3.2.3 vWF gel electrophoresis

SDS-agarose gelelectrophoresis was performed in modification to Ruggeri and Laemmli (Ruggeri and Zimmerman 1981; Laemmli 1970). The running buffer (0.375M Tris, 0.1% SDS) was adjusted to pH 8.8 and a concentration of 1% and 2% standard agarose gels was used. Agarose-acrylamide gels contained 0.8% agarose and between 1.75% and 3.5% acrylamide, with 5% crosslinking. The acrylamide soltution was preheated to 60°C and mixed with agarose at 60°C. As polymerizing agents were 3-dimethylamino-propionitrile (0.25%) and ammonium persulfate (0.025%). Agarose was solidified and flushed with a constant flow of nitrogen for 1h and left in the nitrogen atmosphere overnight at RT. The vWF Haemate proteins of different multimer size distribution (Haemate subfractions) were dissolved in 1:20 SDS loading buffer (10mM Tris, 1mM EDTA, 2% SDS, 8M urea, 0.005% bromopherol blue) at pH 8. After incubation for 15min at 60°C, 20µl samples were applied to each pocket and electrophoresis started at a constant current of 10mA/gel in a LKB-Multiphor 2117 (LKB, Bromma, Sweden) and cooled down to 15°C. The electrophoresis buffer was composed of 0.005M Tris, 0.384M glycine, 0.1% SDS at pH 8.35. The gels were connected to the buffer reservoirs by Whatman 3MM paper wicks. After the samples had run out of the pockets, these were filled with stacking gel and the current was increased to 12.5mA/gel. Electrophoresis was stopped, when the tracking dye reached the anodal end of the gel, usually within 5-6h. After the electrophoresis the gels were fixed washed and incubated with 125I-labelled affinity purified anti vWF antibody raised in emus. As a reference, plasma vWF (0.5-1µg) was run in parallel with Haemate subfractions and identified by staining with Coomassie Brilliant Blue R (Ruggeri and Zimmerman 1980).

3.2.4 Platelet aggregometry

Tumor cell mediated platelet aggregation was induced by adding either 200µl SCLC cell-suspension or 200µl MV3 cell-suspension to 200µl PRP and measured as light transmission in an aggregometer at 37°C (APACT, Labor, Germany). The steel rod at the bottom of the

measuring cuvette (1000rpm) mixed the cell suspensions. The enhanced light scattering due to the added SCLC cells or MV3 cells led to an initial drop in light transmission that was compensated by shifting the start point (t = 0min) to the nadir of this curve drop. In control experiments aggregation was also induced by adding 6.3µM ADP solution (Serva, Germany) to 200µl PRP.

3.2.5 Platelet ATP Secretion

Tumor cell mediated platelet ATP segregation was induced by adding 190µl SCLC cell suspension to 190µl PRP, which was primary incubated with 20µl Adenosine 5′-triphosphate (ATP) assay mix (stock solution 1vl/5ml; Sigma, Germany) 2min at 37°C and measured as light transmission in a chronolog aggregometer (Osburg, Germany). Experimental workflow was comparable to the platelet aggregometry experiments.

3.2.6 Flow cytometry

Either PRP or tumor cells were subjected to shear rates of 10,000s^{-1} for 3min in a cone-and-plate viscosimeter with 0.5° cone angle and 26µm cone-plate distance (Haake Rheovisco 1, Thermo Electron Corporation, Waltham, MA) in the absence of erythrocytes to avoid hemolysis at 37°C. The generated MPs in sheared PRP or tumor cells were centrifugated at 510g for 10min at RT. The supernatant of the MP suspension was used and mixed 1:1 with either PRP or tumor cells and mixtures 1:1 of PRP and tumor cells were evaluated using flow cytometry (Coulter Epics XL; Beckman Coulter, Krefeld, Germany). Platelets, tumor cells and the mixed suspensions were labelled with monoclonal antibodies against CD41 or annexin V. Detection was triggered with the fluorescence signal (FL1, FITC) or the forward scatter (FS). For data analysis a positive event was defined as an event having greater fluorescence intensity than the isotype control (FITC IgG1). Individual samples (90µl), were fixed with 10% paraformaldehyde and labelled with 10Vol% antibodies (10µl) and diluted to a final volume of 1ml with 10% paraformaldehyde diluted in HbSS. Data were acquired over 60s at a flow rate of 15mL/s for each prepared sample.

4. Influence of variations in the cytoskeleton

4.1 Introduction

The mechanical behaviour of tethers can be studied by physically extracting highly curved membrane cylinders from vesicles and living cells by applying an external point force (Brochard-Wyart et al., 2006; Glassinger and Raphael 2006; Hochmuth et al., 1996). The tether diameters can vary in the range from 10nm to 100nm (Hochmuth et al., 1996). When tethers are extracted out of vesicles, the force on the tethers linearly increases with the velocity of extraction (Hochmuth et al., 1996; Evans and Yeung 1994). Consequently, the viscous resistance in this process behaves linear or Newtonian (Hochmuth et al., 1996; Evans and Yeung 1994). The tether radius must decrease as the velocity of the tether is increased (Hochmuth and Evans 1982). In contrast, if the tension does not change during the tether formation process, the tether radius shall remain constant (Glassinger and Raphael 2006). Pulling on the tethers also leads to a surface flow of lipids from the cell body to the tethers through cytoskeleton binders (Brochard-Wyart et al., 2006).

For several reasons the analysis of the adhesion and tether forming process of platelets with variations in the cytoskeleton play an important role. First, it allows the understanding of the F-actin and the microtubuli influence in the adhesion and tether forming process. Second, it contributes to a complete picture of the cytoskeleton influence on the membrane tension and the membrane undulations. To investigate the impact on the cytoskeleton of the platelet behaviour, platelets were either treated with cytochalasin D, which disrupts the F-actin, or nocodazole, which breaks the microtubules. Platelets treated with the fungal metabolite cytochalasin D either before or after stimulation showed fewer pseudopods compared to untreated platelets. The surface of the treated platelets appeared much less convoluted and no vesicle shedding occurred (Kodali et al., 2007; Alberts et al., 2003; Koolman and Röhm 2002; Gaffet et al., 1995; Cooper 1987; Godette and Frieden 1986; Schliwa 1982; Casella et al., 1981; Flanagan and Lin 1980; Brenner and Korn 1979; Brown and Spudich 1979). Cytochalasin D inhibits the rapid polymerization of F-actin and induces depolymerization of F-actin in stimulated platelets, both resulting in variations of the platelet morphology and a prevention of the reorganisation of the cytoskeleton (Nielsen et al., 2000; Gaffet et al., 1995; Olorundare et al., 1992; Cramer et al., 1991; Fox et al., 1984; Casella et al., 1981). However, it is assumed that the amount of tubulin is not affected by cytochalasin D treatment (Casella et al., 1981). Cytochalasin D treatment impaired the migration of GPIbα and no internalization

could be observed. Thus, the GPIbα distribution on the platelet surface remained unchanged (Cramer et al., 1991). Actin polymerization is considered to be the driving force for cell spreading, since depolymerization by cytochalasin decreases the spreading kinetics to one tenth of its normal value. It is assumed that the rate of spreading depends on the rate of actin polymerization and comes to a halt, when membrane tension counteracts polymerization at the cell border (Heinrich et al., 2008). Nocodazole, a synthetic microtubule inhibitor, was developed as an antitumural drug and has been shown to have highly specific anti-microtubular activity. This drug is chemically unrelated to the microtubule disintegrating alkaloids (Malek and Izumo 1996; Eilers et al., 1989; Zieve et al., 1980; Jung et al., 1981; Tablin and Castro 1992). This microtubule inhibitor depolymerises microtubules from their minus (slow growing) end and competes with colchicine for its microtubule binding site (Tablin and Castro 1992). Nocodazole blocks aggregation and especially the release activity of platelets induced by collagen, thrombin, adrenaline, polylysine, and lectins. This inhibition effect of the polymerization of tubulin is reversible. A variation in the sensitivity of platelets from different donors was observed (Jung et al., 1981). A schematic model sketch of the blood platelet before and after cytochalasin D and nocodazole is summarized in figure 7.

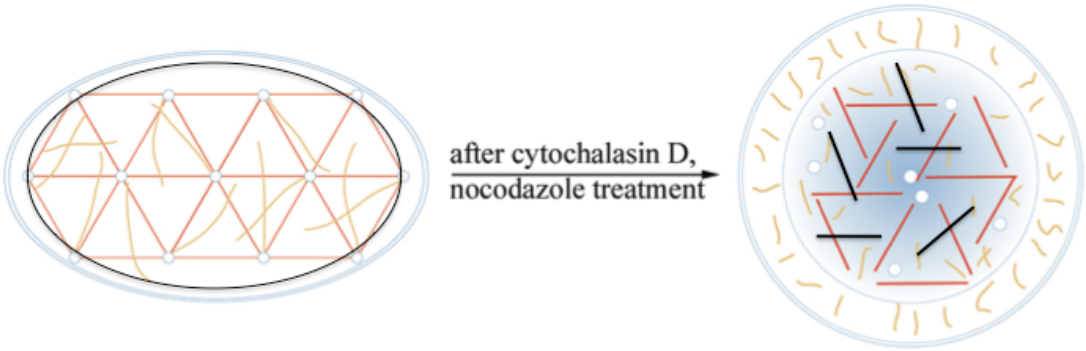

Figure 7: Schematic illustration of the actin filaments (yellow), ringlike microtuble (black) and spectrin networks (red) inside an unactivated platelet before and after cytochalasin D (F-actin disruption) and nocodazole (microtubuli disruption) treatment is shown (adapted from Barkalow et al., 2003).

Despite a large number of studies evolving the role of receptor-ligand interaction, very few studies have addressed the biophysical perspective on the platelet adhesion, tether formation and rupture. Both adhesion processes, the platelet attachment and spreading, were analysed, as the actin polymerisation is a crucial influence factor for cell spreading. The platelet-vWF interplay was investigated by using either real time reflection interference contrast microscopy (RICM) to focus directly on the behaviour of the platelets moving over a coated surface or by a combined atomic force microscopy (AFM)-patch clamp set-up. By RICM the platelet adhesion and tether formation to the surface were analysed. First, the difference

between weak and tight adhesion was quantified as well as the number of platelets adhering to the vWF surface. Second, the difference in the tether length of tethers at the platelet body and ruptured ones was elucidated as well as the comparison of the number of tethers at the platelet body, ruptured tethers and the summation of both types of tethers. Finally, the percentage spreading area coverage was measured. By an AFM tip a tether was pulled out of a platelet membrane, which had never done before, and the rupture force and tether length were measured. Next, the tether formation and adhesion rate were quantified. These two different techniques will be the basis for the understanding of the biophysical mechanism on the platelet adhesion and tether formation process.

4.2 Results and Discussion

4.2.1 Flow chamber experiments

4.2.1.1 Platelet adhesion and tether formation

Whole blocked blood (preparation see chapter 3.1.1) was perfused in a flow chamber with a vWF (Haemate) coated glass surface and subjected to shear flow using an optical accessible flow chamber equipped with a RICM (set-up see chapter 3.2.1). For shear rates of 10,000s^{-1}, increased platelet arrest from flowing blood onto the immobilized vWF at the chamber walls, leading to tethers being pulled out of the platelet membrane, was observed. This designed flow chamber set-up allowed reproducible results as depicted in figure 8.

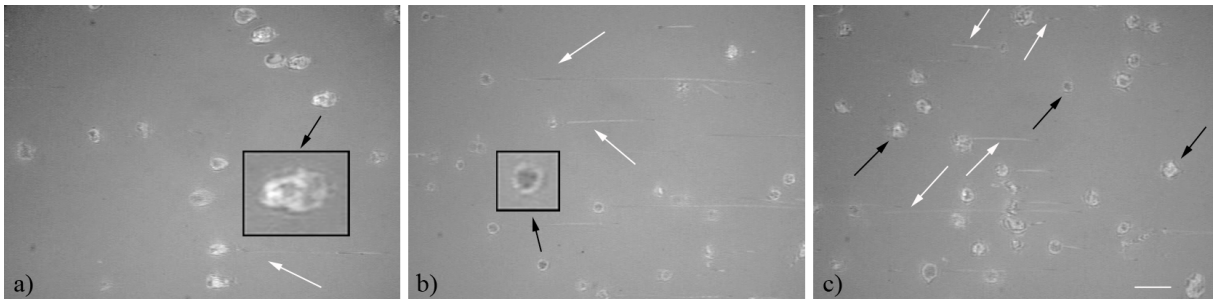

Figure 8: RICM images of blood samples (blocked) over Haemate (10U) at shear rates of 10,000s^{-1}. Image a) the cytochalasin treated, b) the nocodazole treated and c) untreated blood samples are depicted after shear was applied for 45sec. Arrested platelets, platelets with tether and ruptured tethers are shown. The black arrows indicate the platelet adhesion area, which is composed of weak and tight contact zones. Tethers and ruptured tethers are marked with white arrows. Insets exemplary demonstrate a zoomed (300%) contact area of cytochalasin (a)) and nocodazole (b)) treated platelets. Cytochalasin treated platelets show an increased weak contact area (bright regions), but a decreased tight adhesion area (dark regions) compared to platelets treated with nocodazole, which illustrate a decreased weak contact area (bright regions), but an increased tight adhesion area (dark regions). Note the large number of ruptured tethers for microtubular breakage in (b)). (In all images scale bar: 5µm.)

RICM enables to differentiate between strong and weakly adhering regions of platelets and tethers attached to the vWF surface during the flow experiment (enlarged insets in fig. 8).

Furthermore, it was also observed that the main platelet body could detach from the tether and the surface, yielding in a single tube-shaped platelet fragment (white arrows in fig. 8). These fragments translocate independently or detach completely from the surface and form ruptured tethers as previously observed by various groups (Reininger et al., 2006; Casella et al., 1981). Tethers should not be mixed up with filopodia, which are formed due to a shape change of the activated platelets. In the investigated experiments no filopodia occur as the activation of the platelets is inhibited. The adhesion of platelets from blood flow is a dynamic process as described in the introducing chapter 1.5.1. The adhesion domains are in close contact (~ 7nm) (dark regions in fig. 8) strongly adhering with the non-fluctuating regions of the substrate (Smith et al., 2008; Albersdörfer et al., 1997). The bright regions shown in figure 8 represent regions of weak adhesion, with a typical distance between membrane and substrate of ~ 100nm (Smith et al., 2008; Evans and Calderwood 2007; Gönnenwein 2003; Simson and Sackmann 1998; Albersdörfer et al., 1997). To analyze the adhesion behaviour of platelets, the contact area at the bottom of the flow chamber was measured, following the exposure of the platelets to a shear flow of $10{,}000s^{-1}$ for 45s (fig.8). The contact area is composed of two subareas, one where tight adhesion and one where weak adhesion area prevailed (insets in fig. 8). While, the weak adhesion area, which includes the tight adhesion zones, of nocodazole treated platelets showed a fairly sharp distribution with a most likely contact area around $3\mu m^2$, cytochalasin D treated and untreated platelets were more homogeneously distributed in the range between 2-$17\mu m^2$ and between 1-$13\mu m^2$ (fig. 9). This distribution indicates a drastic change in the mechanical properties of the platelet. To directly compare the two treatments, the average contact area has been calculated from integrating each histogram of the different donors and taking the average. A disruption of the F-actin led to an increase in the weak contact area, but to a decrease in the tight adhesion area, whereas for microtubule breakage the opposite was observed. The contact area was decreased and the tight adhesion area was increased compared to untreated platelets. For F-actin depolymerisation the average of the platelet adhesion area increased ($A_c \approx 8.6\mu m^2$+/-$0.7\mu m^2$) and for microtubule breakage decreased ($A_n \approx 3.8\mu m^2$+/-$0.1\mu m^2$) compared to untreated platelets ($A_u \approx 5.5\mu m^2$+/-$0.4\mu m^2$) (inset in fig. 9). The standard deviations of the weak adhesion area averages were calculated by the variations of the different donors. Due to a better general view the standard deviations are not illustrated in the inset in figure 9. Most of the tight adhesion areas of the platelets (dark regions in fig. 8) were close to the optical resolution limit (< 400nm). Keeping in mind that the adhesion process requires at least some discrete points of tight adhesion, I conclude

that the tight adhesion areas might range from 0.1µm^2 (size of a DAP measured by electron microscopy (Reininger et al., 2006)) up to the measured contact area (4µm² - 9µm²).

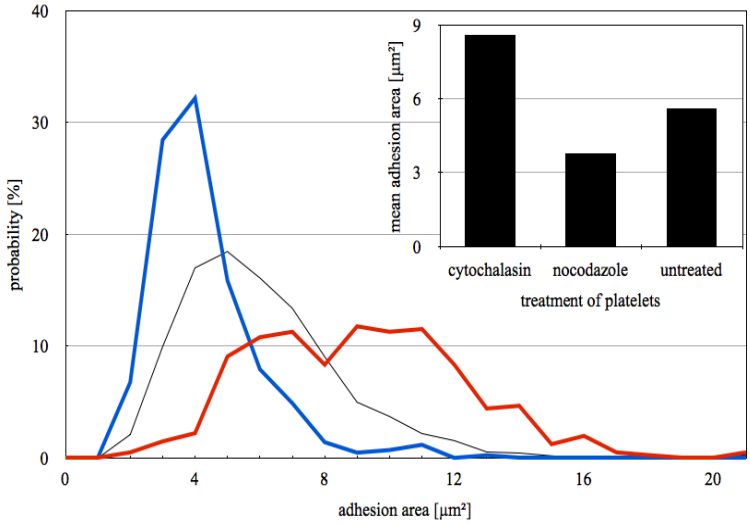

Figure 9: Weak adhesion area distribution for treated and untreated platelets at 10,000s^{-1}: the weak contact area is plotted against the probability P (∑P=100%) The red curve represents the adhesion area of cytochalasin treated platelets, the blue curve of nocodazole treated platelets and the black of untreated platelets. The inset shows the mean of the weak adhesion area of treated and untreated platelets at a flow rate of 10,000s^{-1}.

To get a more complete picture on the adhesion process, the adhered platelets on the vWF surface of the flow chamber (fig. 8) were counted by using different RICM still images of blood samples after the exposure of platelets to a shear flow of 10,000s^{-1} for 45s. Due to this static capture, it was not possible to resolve the dynamic behaviour of the platelets, e.g. the difference in rolling velocity of the platelets as well as in the adhesion time. A shear flow of 10,000s^{-1} lowered the amount of cytochalasin treated platelets adhering to the surface compared to nocodazole treated and untreated platelets of around 35%-40%. The variations of different donors were significant (~ 50%), but the tendency remained almost constant. These results indicate a strong dependence of the F-actin on the adhered platelet number, but not of the microtubuli. From the analysis of bound platelets it seemed reasonable to extract the difference in the energy of absorption ΔG of untreated and treated platelets by applying the Boltzmann equation

$$\frac{n_{untreated}}{n_{treated}} = e^{-\Delta G / k_B T} \qquad (5)$$

where k_B is the Boltzmann constant, ΔG is the change in absorption energy between untreated and cytochalasin D or nocodazole treated platelets, T the temperature and $n_{untreated}$ and $n_{treated}$ is the average fraction of the amount of untreated and cytochalasin D or nocodazole treated platelets on the surface (Fleck et al., 2002; Alberts et al., 2003). Using the average amount of untreated and cytochalasin D or nocodazole treated platelets adhering to the surface resulted

in an energy difference ΔG in the order of 0.1-0.5 k_BT. These differences in the absorption energy extracted by untreated and treated platelets are too low compared to adhesion energy differences of cells typically found in the literature. By using the Young's law, Simson and coworkers reported the lowest difference in adhesion energy of $0.8*10^{-18}$ J/μm^2 of wild type and mutant cells deficient in cortexillin II-null (Simson et al., 1998). These variations in the absorption energy and the adhesion energy are not fully understood. I propose that the adhesion energy calculated of static experiments significantly exceeds the absorption energy of a platelet or cell to withstand the shear flow. In a static process the system is able to equilibrate, as there is enough time provided for the adhesion process. However, in a dynamic one the forces acting on a platelet change over time. The absorption energy differences were also quantified in chapter 5,7 and 9, but the calculated values were also too low to be compared with the adhesion energies found in the literature. As these results show a clear dependence of the cytoskeleton on the platelet adhesion process, the cytoskeleton variations will also affect the tether formation process. To study the tether formation, they are often extracted out of membranes by aspiration micropipette techniques. This formation process stabilizes the vesicle and controls the elastic tension of the membrane (Glassinger and Raphael 2006). The aspiration method increases the observable surface area, which suggests small increases in tension (Glassinger and Raphael 2006). To overcome this enhanced tension and to simulate the tether forming process in a more physiological manner, the whole blood was exposed to shear flow. The tether formation is described in more detail in chapter 1.5.2. To understand the tether formation process the tether length at the platelet body as well as ruptured tethers on the bottom of the flow chamber (white arrows in fig. 8) were analysed after the exposure of the platelets to a shear flow of 10,000s^{-1} for 45s. While, tethers at the cytochalasin D treated platelets showed a fairly sharp distribution with a most likely tether length of around 2μm, nocodazole treated and untreated platelets were spread more homogeneously over the range between 1-34μm (fig. 10). This indicates a drastic change in the mechanical properties of the tether during the formation process after F-actin disruption. Ruptured tethers showed a fairly sharp distribution with a most likely tether length of around 6μm for F-actin disruption and around 4μm for microtubuli breakage and untreated platelets (inset in fig. 10).

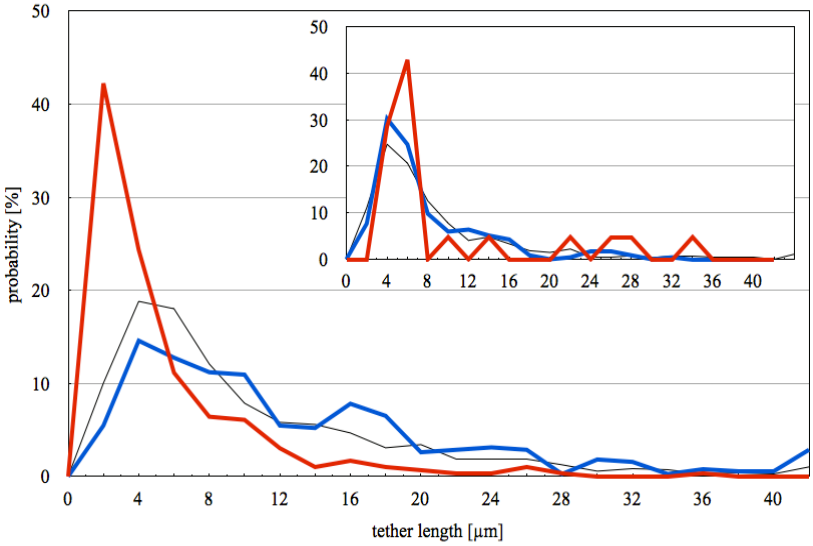

Figure 10: Tether length distribution curves at the platelet for treated platelets at a shear rate of 10,000s^{-1}: the tether length is plotted against the probability P (∑P=100%). The red curve represents the tether length of cytochalasin treated, the blue curve of nocodazole treated and the black curve of untreated platelets. The inset shows the ruptured tether length distribution of treated and untreated platelets at a flow rate of 10,000s^{-1}.

For cytochalasin D treated platelets this result is less significant, as only 7% ruptured tethers existed. Nocodazole treated platelets however exhibited 38% ruptured tethers and untreated ones 24%. Ruptured tethers finished the formation process and therefore, acted different compared to tethers at the platelet body. Consequently, cytochalasin D and nocodazole treatment of the platelets did not influence the ruptured tethers length distribution compared to control platelet ruptured tethers, as F-actin is only detected in tether ends, (Reininger et al., 2006), whereas no microtubules are located in the tethers (White and Rao 1998; Tablin and Castro 1992; Casella et al., 1981; Jung et al., 1981). The average tether length was calculated by adding tethers at the platelet body and ruptured tethers up and from integrating the histograms of each donor and finally, taking the mean. At 10,000s^{-1} for F-actin depolymerisation the average of the tether length decreased to $l_c \approx 4.9\mu m+/-1.6\mu m$ compared to reference platelets. Microtubule breakage by nocodazole elongated the average of the tether length to $l_n \approx 9.9\mu m+/-1.3\mu m$ compared to untreated platelets ($l_u \approx 8.8\mu m+/-0.8\mu m$) (the error bars were calculated by the donors variations). To directly compare the two treatments, the average amount of the total tethers and the ruptured tethers was investigated by counting the tethers adhered on the vWF surface at a shear rate of 10,000s^{-1}. Compared to cytochalasin treated platelets, the total tether count almost triplet for nocodazole treated platelets and the average amount of ruptured tethers was 13 fold higher (white arrows in fig. 8). The tendencies of each investigated donor remained almost constant (sd ~ 25%-60%). These results indicate a strong dependence of the cytoskeleton on the platelet adhesion and the tether formation. The membrane tension of cytochalasin treated platelet might be decreased compared to untreated

ones and enhanced for nocodazole treated platelets compared to controls. Consequently, a disruption of the F-actin might lead to an increase in the membrane undulations, which are induced by a decrease in membrane tension. These undulations decrease the adhesion of the platelets to the surface, especially decrease the tight adhesion domains and increase the weak contact area. In contrast, microtubular breakage showed the inverse effects. However, Hochmuth and coworkers treated neuronal growth cones with cytochalasin D and nocodazole (Hochmuth et al., 1996) and reported that after cytochalasin D treatment the apparent surface tension was decreased by around 67%, but for nocodazole treatment only by around 45% (Hochmuth et al., 1996). These changes in membrane tension can not be completely predicted for blood platelets. My results for F-actin disruption are comparable with Hochmuth's results, but for microtubular breakage the contrary for blood platelets compared to neuronal growth cones was observed. Therefore, the microtubuli in blood platelets have a different impact on the membrane tension compared to neuronal growth cones. The membrane tension is increased for nocodazole treated platelets. A reduced membrane tension as well as enhanced undulations might inhibit the clustering of the GPIbα receptor. The microtubule breakage acts contradictionary. The undulations are decreased and the membrane tension is increased. These results coincide with Cramer and coworkers, who reported that after cytochalasin D treatment of platelets the distribution of GPIbα remained unchanged and therefore, no receptor clustering occurred (Cramer et al., 1991).

4.2.1.2 Platelet spreading process

Spreading is a tight adhesion process, in which the receptor segregation and tight adhesion domain formation is more pronounced compared to the adhesion without platelet activation. After the introductory adhesion phase, the actin filaments couple to the adhesion domains and stabilise them. As the platelets completely spread and are pancake shaped, the adhesion process might be approximated by a first order wetting transition. In general, a wetting transition is described as a spontaneous formation of a thin fluid film on a solid state through completely spreading of the drop until a pancake like structure is formed. Due to a strong surface adhesion and a long-range repulsion of the solid state and the surface of the fluid film, which stabilises the finite fluid thickness, the fluid is able to spread. However, the cell adhesion is a more complex process. Long-range attraction forces of the cell through gravitation and the repulsion of undulation forces control the distance of the loose floating membrane and the surface. To decrease this distance the steric repulsion of the sugar polymers of the glycocalyx gets more pronounced compared to the long-range attraction

forces of the cell. If these polymers are compressed, they will act as macromolecules, which are jammed in between two parallel plates. These will carry out an entropic pressure, if the distance is smaller than their head groups (Sackmann and Merkel 2010). Considering the fact, that spreading requires actin polymerisation and a distinct minimal receptor-receptor distance (Geiger et al., 2009), the impact of the cytochalasin D and nocodazole treatment on the firm adhesion process was investigated by perfusion of whole blood (preparation see chapter 3.1.3) in a flow chamber with a vWF (Haemate) coated glass surface. The platelet spreading behaviour was quantified under shear flow conditions using an optical accessible flow chamber equipped with a RICM (set-up see chapter 3.2.1). For shear rates of $800s^{-1}$, platelets arrested from flowing blood onto the immobilized vWF at the chamber walls and spread over the surface. To analyze the spreading area dimensions, the area of the spread platelets on the vWF surface of the flow chamber (fig. 11) was measured by using different still RICM images of blood samples after the exposure of platelets to a shear flow $800s^{-1}$ for 1min to 9min.

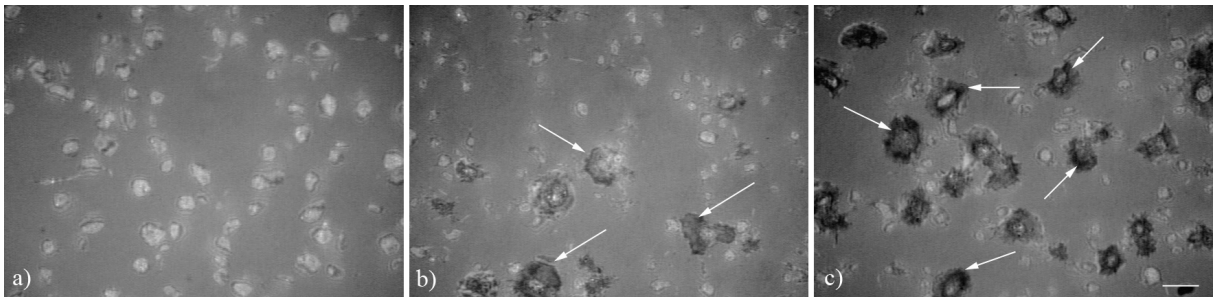

Figure 11: RICM images of blood samples (unblocked) over Haemate (10U) at shear rates of $800s^{-1}$. Image a) shows cytochalasin D, b) nocodazole treated and c) untreated blood samples after shear was applied for 9min. Spread and arrested platelets are depicted. White arrows indicate the platelet spreading area. Platelets treated with cytochalasin D show no spreading, only adhesion. Untreated platelets illustrate an increased spreading area (dark regions) compared to nocodazole treated ones. (In all images scale bar: 5µm)

For cytochalasin D treated platelets no spreading in the investigated flow time range could be observed. Nocodazole treated platelets showed lowered spreading area coverage for all flow times compared to untreated ones, indicating a drastic change in the mechanical properties of the platelet. The variations between nocodazole treated and untreated platelets were most significant at the beginning and at the end of the flow exposure. Increasing flow time exposure enhanced the spread area percentage coverage (fig. 12). However, the spread area distribution was almost similar for treated and untreated platelets. Both treatments showed a fairly sharp distribution with a most likely spread area of around $20\mu m^2$ up to 5min flow time exposure. Increasing flow time increased the most likely spread area to around $30\mu m^2$. The differences between the donors were crucial (< 100%), but the trends of the depicted results in figure 12, remained almost unchanged. For a better overview of the variation of treated and

untreated platelets, the error bars are not shown.

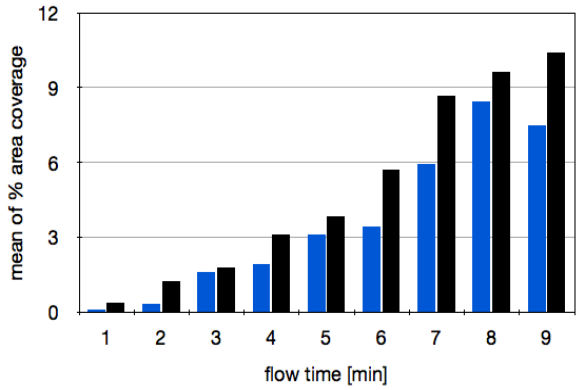

Figure 12: Percentage area coverage of spread platelets on vWF after different flow times at 800s^{-1} is shown. Cytochalasin and nocodazole were added to the blood suspension at final concentrations. For cytochalasin treated platelets no spreading could be observed. The blue histogram shows the nocodazole treated platelets and the black histogram the untreated ones.

These results show that maximum spreading is dependent on an optimal receptor-receptor distance. After F-actin disruption no spreading could be observed and after microtubuli breakage the percentage spreading coverage was decreased compared to untreated platelets. As there is no actin polymerisation and receptor clustering observed after cytochalasin D treatment, I propose that both the inhibition of the actin polymerisation and the receptor-receptor distance, which is too large to allow the platelets to spread, are crucial influence factors for platelet spreading. These results are in line with Geiger and coworkers, who reported that above a maximum distance of binding sites (in a range of 50-70nm) of individual integrin molecules almost no cell spreading occurred (Geiger et al., 2009). Furthermore, the membrane tension might also influence the binding site distance to a small extent. Thus, for F-actin disruption the binding site distance might be larger than 50-70nm. However, compared to untreated platelets the receptor-receptor distance might be slightly increased after nocodazole treatment due to an increased tension. Additionally, the receptor density is responsible for the spreading process. At a receptor density ($\rho_R \sim 10^3 \mu m^{-2}$) a homogeneous adhesion zone is formed, and the vesicles explode. Due to the adhesion and blast, an induced critical membrane tension reaches the rupture threshold of $\sigma > 3mN/m$ (Sackmann and Merkel 2010). Cytochalasin D treated platelets were not able to form a tight adhesion zone due to the non-clustering of the receptors and thus, a blast of the platelet and the formation of a spread platelet was not possible.

4.2.2 AFM-patch clamp set-up experiments

Exerting a point force on the surface of a platelet extracts a tether out of the membrane. The membrane separates from the underlying cytoskeleton and creates a long, thin cylindrically shaped tether (fig. 13 a)). As the lipid membrane is only capable of minimal area expansion in the order of 4% or less, the material for the tether forming process must be provided by the cell body (Hochmuth and Marcus 2002) (detailed information chapter 1.5.2). To get more insights in tether formation and especially measure the tether rupture force, a tether was extracted out of a platelet by a combined AFM-patch clamp set-up (see chapter 3.2.2.4 for details on set up and see chapter 3.2.2.3 for details on cantilever functionalization) for the first time (fig. 13 a)). The tip-membrane contact time varied from 1s to 3s to focus on either cluster formation by longer contact times or to clarify the role of the cantilever tip as an impurity. A plotted exemplary force curve of the retracted cantilever shows multiple rupture events as depicted in figure 13 b). The retraction profiles recorded with untreated and treated platelets exhibit a typical initial high force region (fig. 13 b), 1)). To trigger the tether forming process a substantial effort was needed. This was also confirmed by Sun and coworkers (Sun et al., 2005). This might be due to the rebinding forces. In general, the receptor-ligand binding resists external forces by increasing the adhesion strength (Sackmann and Merkel 2010). The amount of plateaus is comparable to the amount of tethers bound to the cantilever tip (fig. 13 b) 2) and 3)). The plateau length equates to the tether length (fig. 13b) 2) and 3)) (Sun et al., 2005).

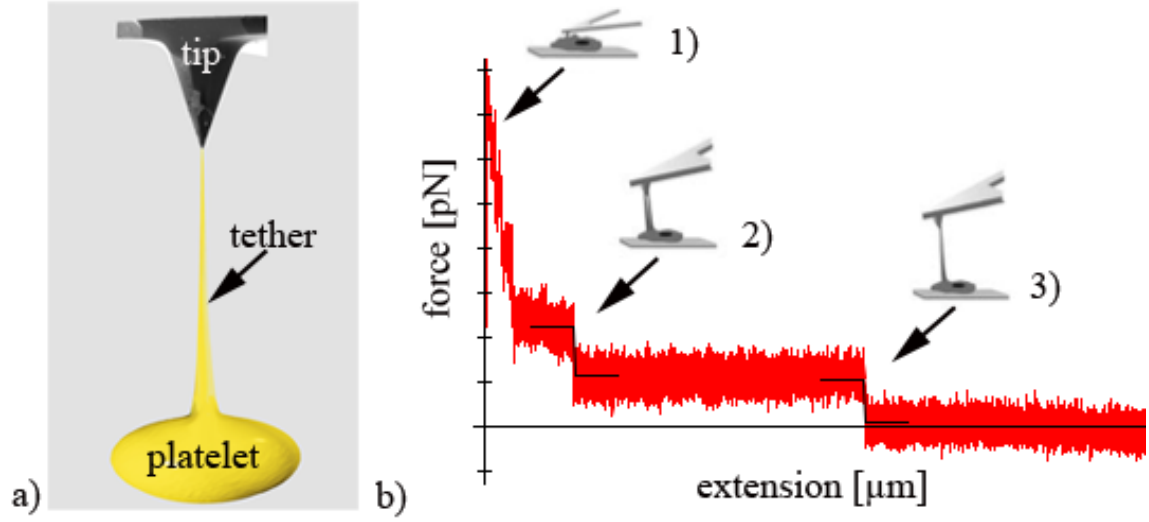

Figure 13: Sketch of an AFM tip tether extraction out of a platelet is shown in image a). In b) a typical schematic single AFM force spectroscopy retract cycle is depicted. The highlighted steps indicate the tether ruptures of multiple tethers 2) and of a single tether 3) and 1) the initial tip/surface position (adapted to Sun et al., 2005). The AFM tip remained 3s on the untreated control platelet surface. A retraction velocity of 3.4 µm/s was used.

The force necessary to exert a tether of a blood platelet was quantified. Tether pulled out of cytochalasin treated platelets showed a fairly sharp distribution with a most likely rupture force of around 40pN for a 1s duration. However, for a tip contact time of 3s these tethers were more homogeneously distributed in the range of 15-60pN. Pulled tethers from nocodazole treated platelets were homogenously distributed in the range of 10-80pN for both duration times. Control platelets showed the broadest rupture force distribution compared to treated ones. For a 1s duration time of force application, the force distribution was homogenously distributed in a range of 10-100pN and for 3s of 20-90pN (fig. 14). The comparison between treated and untreated platelets showed that the most frequent rupture force was increased for untreated platelets to 70pN compared to treated ones to 40pN after a 1s duration time. These values changed after 3s duration to 40pN for cytochalasin D treated platelets, to 50pN for nocodazole treated ones and to 60pN for control platelets (fig. 14). To compare directly the two treatments, the average rupture force was calculated from integrating the histograms of each donor and taking the average value across all donors. A disruption of the F-actin led to an increase of 20% for 1s and to a 22% decrease for 3s duration time in the rupture force compared to the control platelets, whereas for microtubule breakage a decrease of 17% for 1s and of 31% for 3s of the rupture force was observed (inset in fig. 14). The decrease in the rupture force might be due to a reduced membrane tension of treated platelets compared to untreated ones. However, a change in the receptor distribution might not be a crucial influence factor, as there were no differences observed for cytochalasin D treated platelets between 1s and 3s duration time. In addition, after a 1s duration time the variation between both treatments was negligible. The error bars were significantly large between various donors (sd ~ 40%-60%). However, the tendencies remained almost unchanged except for cytochalasin D treatment and 1s duration time. The second maximum peak of the red curve in figure 14 a) of around 110pN is donor specific. Consequently, the average of this force distribution was increased. Due to an improved general view, the error bars are not shown in figure 14.

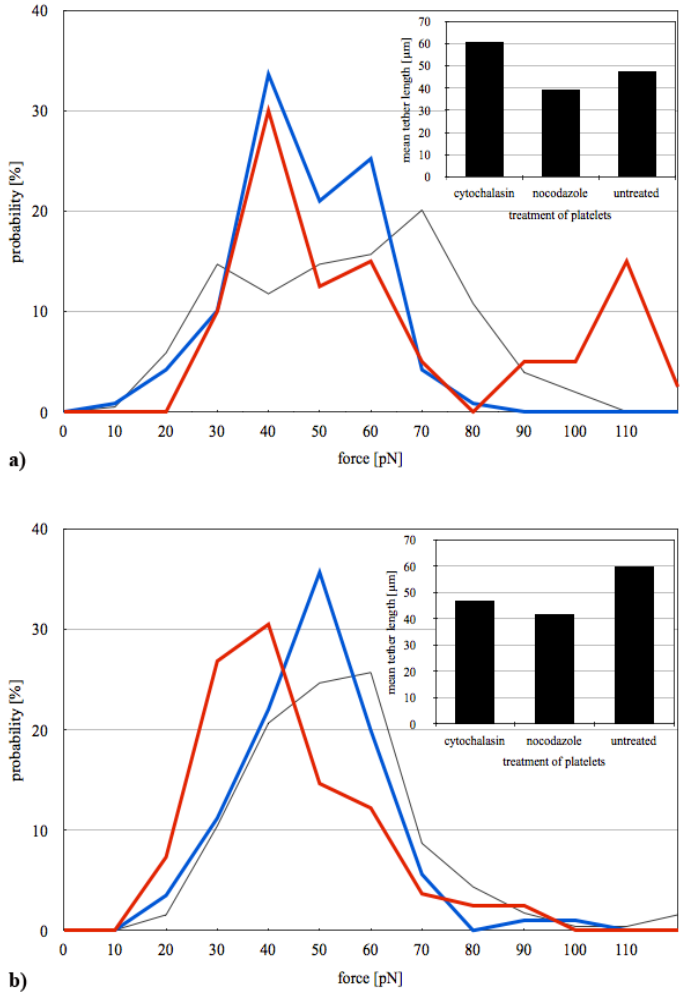

Figure 14: Single rupture force distribution curves for treated and untreated platelets: the rupture force is plotted against the probability P (∑P=100%). The red curve represents the tether length of cytochalasin treated, the blue curve of nocodazole treated and the black curve of untreated platelets. The inset shows the mean of the rupture force of treated and untreated platelets. In image a) the rupture force distribution of 1s is plotted and in b) of 3s. A retraction velocity of 3.4 µm/s was used.

These results suggest a dependence of the cytoskeleton on the tether rupture force and are coincide with previous studies, who also demonstrated for different cell types, except blood platelets, that the tether formation strongly depends on the integrity of the cytoskeleton on both the F-actin network and the microtubules (Sun et al., 2005; Sheetz 2001; Raucher et al., 2000; Raucher and Sheetz 1999; Hochmuth et al., 1996). After inhibition of actin polymerisation the tether force was reduced by 50% (Sun et al., 2005). A disruption of F-actin of bovine aortic endothelial cells with latrunculin-A resulted in a significant reduction in the threshold pulling force and the membrane viscosity (Sun et al, 2007). The effective viscosity is defined as the membrane viscosity that contains contributions associated with the intrinsic material properties of the lipid bilayer, the interbilayer slip and the association of the membrane with the underlying cytoskeleton. Whereas, the force is a direct tool to measure the membrane cytoskeleton adhesion energy and membrane stiffness (Sun et al., 2007; Hochmuth

et al., 1996). Therefore, both variables contain information on the membrane cytoskeleton interplay (Sun et al., 2007). In summary, the results of Sun and coworkers imply that the organisation of the actin cytoskeleton strongly influences the biophysical properties of the membrane (Sun et al., 2007). My results indicate that not only the cytoskeleton integrity, but also the receptor clustering are crucial influence factors for the rupture force. Following the statistical analysis of the rupture forces of the extracted platelet tethers, it seemed reasonable to use a unique relation between tether radius R_t and the apparent surface tension $T+\gamma$. This equation was derived by Hochmuth and coworkers, who formed a tether from neuronal growth cones by a laser tweezer trap (Hochmuth et al., 1996). As the tether radius depends only on the bending modulus B and the apparent surface tension and remains constant during the tether forming process. It follows

$$f_0 = \frac{2\pi B}{R_t} = 4\pi R_t (T + \gamma). \tag{6}$$

Assuming a tether radius of 120nm and using the most frequent rupture force for f_0, the surface tension and the bending modulus of treated and untreated platelets with duration times of 1s and 3s were calculated. The most frequent rupture force might reliably be used to analyse the difference in surface tension and bending modulus. The calculated values are summarized in table 1.

Table 1: Summary of the bending modulus B and the apparent surface tension T+γ

	B [pNμm]	$T+\gamma$ [pN/μm]
cytochalasin 1s	0.59	20.6
cytochalasin 3s	0.63	21.9
nocodazole 1s	0.78	27.2
nocodazole 3s	0.82	28.5
control 1s	0.97	33.8
control 3s	0.88	30.5

After cytochalasin D treatment the apparent surface tension was decreased of around 39% and of around 20% for nocodazole treatment compared to control platelets. The membrane tension of cytochalasin treated platelet was decreased compared to nocodazole treated ones. Hence, the disruption of the F-actin led to an increase in the membrane undulations, which were induced by a decrease in membrane tension. However, for microtubular breakage the membrane tension was increased compared to cytochalasin treated platelets. This led to a decrease in the membrane undulations compared to cytochalasin treated platelets. Neuronal growth cones were treated with cytochalasin D and nocodazole and the changes in apparent surface tension $T+\gamma$ were measured by Hochmuth and coworkers (Hochmuth et al., 1996).

After cytochalasin D treatment the apparent surface tension was decreased by around 67%, but for nocodazole treatment only by around 45%. The smaller effect on the membrane tension of the cytochalasin D and the nocodazole treatment of the platelets compared to neuronal growth cones, might be due to a small suction of the patch clamp set-up, to the different membrane properties of neuronal growth cones and to the other used tether formation application. As these results show a dependence of the cytoskeleton on the platelet rupture force, variations in the cytoskeleton will affect the tether length as well. To get more information on the tether formation process the tether lengths of the last ruptured exerted tether of a blood platelet were analysed. While, cytochalasin treated platelets showed a fairly sharp distribution with a most likely tether length of around 1µm for 1s and of around 2µm for 3s duration times. Nocodazole treated platelets and control platelets showed a fairly sharp distribution with a most likely tether length of around 2µm for 3s duration time. However, for 1s duration nocodazole treated and untreated platelets were more homogeneously distributed in the range between 0-8µm and 0-13µm (fig. 15). To directly compare the two treatments and the untreated platelets the average tether length was calculated from integrating the histograms of each donor and taking the average. A disruption of the F-actin led to a 51% decrease in the tether length compared to the control platelets, whereas for microtubule breakage a decrease of 22% of the tether length was observed for 1s duration time. For 3s duration the tether length of treated and untreated platelets were almost comparable (inset in fig. 15). The standard deviations of various donors were in the range between 6%-60%, but the trends remained unaffected. Due to a better general view, the error bars are not included in figure 15.

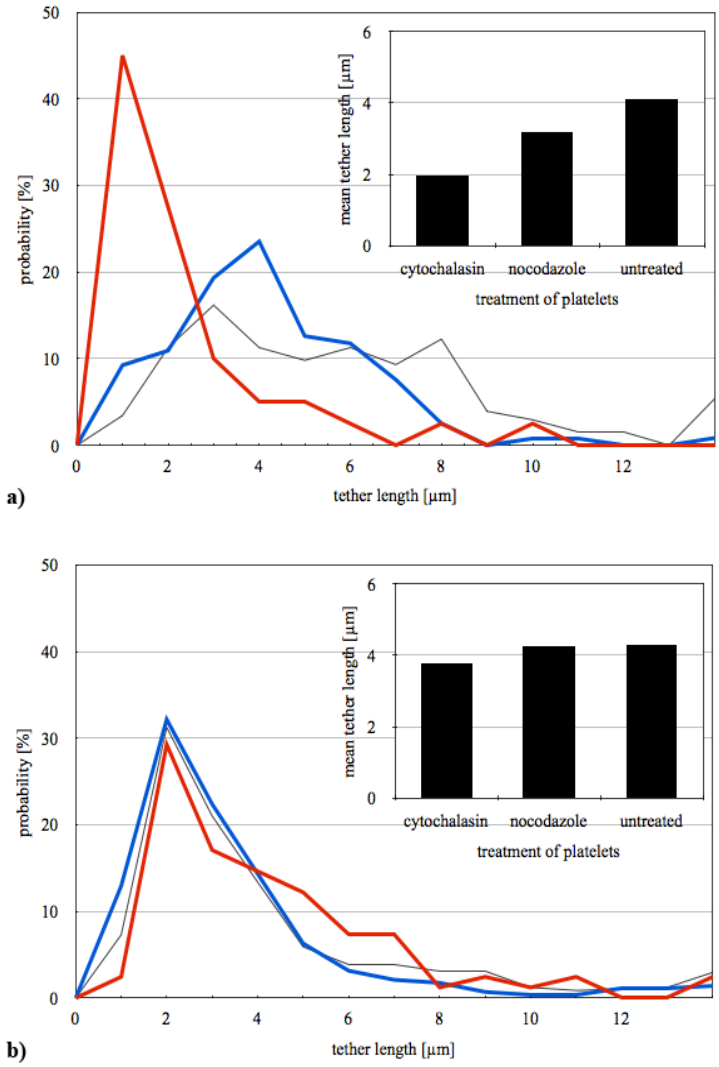

Figure 15: Single tether length distribution curves for treated and untreated platelets: the rupture force is plotted against the probability P (∑P=100%). The red curve represents the tether length of cytochalasin treated, the blue curve of nocodazole treated and the black curve of untreated platelets. The inset shows the mean of the tether length of treated and untreated platelets. In image a) the rupture force distribution of 1s is plotted and in b) of 3s. A retraction velocity of 3.4µm/s was used.

These results suggest, that the duration time of the applied force by using the cantilever tip significantly influenced the tether length. For 1s duration the membrane tension and the receptor clustering is crucial for the difference in the tether length. A decrease in membrane tension is combined with an increase in the membrane undulation, which affects the rupture of the tethers. Increased membrane undulations thus lead to a reduced tether length. As the receptor distribution remains unchanged for the cytochalasin D treated platelet (Cramer et al., 1991), the receptor-ligand pair formation is reduced. Consequently, the tethers are also shortened. However, for 3s duration times the impact of the membrane tension and therefore, the undulation vanishes and the receptor distribution becomes more significant. After F-actin disruption no receptor clustering occurred, thus 3s duration might be enough time for the receptor-ligand pairs to form as much of bonds as nocodazole treated and untreated platelets.

Another aspect might be that the tip functions as an impurity in the platelet membrane. Consequently, the symmetry of the membrane is broken and a reorientation may happen in the platelet membrane. This rearrangement might be compared with a phase separation of the lipids and the cantilever tip. Thus, the most frequent tether length of treated and untreated platelets is comparable after 3s duration time. As both the tether rupture force and the tether length were crucially influenced by the membrane cytoskeleton, the cytoskeleton could have an impact on the tether formation and the vWF A1 domain and GPIbα interaction rate. To zoom in the various impacts of the cytoskeleton on the tether formation and the adhesion rate, both rates of treated and untreated platelets were calculated. The tether formation rate was decreased for cytochalasin D treated platelets by around 58% and for nocodazole treated platelets by around 27% compared to untreated platelets. The differences in the tether formation rate between both duration times were negligible. In addition, the adhesion rate was significantly increased compared to the tether formation rate. For F-actin disruption the adhesion rate was increased around 6 times, for microtubular breakage around 4 times and for the control platelets around 3 times. The adhesion rate of cytochalasin D treated platelets was around 16% reduced compared to nocodazole and untreated platelets. Nocodazole and untreated platelets showed a comparable adhesion rate. The standard deviation for the different donors was large (< 100%), but trends remained unchanged. This indicates a strong dependence on the cytoskeleton, especially of the F-actin, on the tether formation and adhesion rate. The deciding variation in the tether formation and adhesion rate might be caused by the non-clustering of the GPIbα of cytochalasin D treated platelets, as the difference between nocodazole and untreated platelets is minimal. The binding affinity and strength of cytochalasin D treated platelets is lowered and consequently, the probability of the tether forming is reduced. For poor adhesion without tether formation only a few vWF A1 domain and GPIbα bonds are sufficient, but for the tether formation the GPIbα cluster formation is essential. The tether formation and adhesion were also significantly influenced by cytoskeleton changes. The membrane tension and therefore, the induced membrane undulations and the receptor distribution are the crucial influencing factors. After F-actin disruption the membrane tension is decreased and the membrane undulations are increased, whereas after microtubular breakage the inverse effect is observed compared to cytochalsin D treated platelets. The rupture force and the tether length were decreased for both treated platelets due to a reduced membrane tension compared to untreated ones. However, the rupture force might be neither influenced by the receptor distribution of the GPIbα nor by the phase separation. In contrast, for 3s duration times the receptor distribution and the phase

separation may influence the tether length, but not the tether formation probability. More receptor-ligand pairs might be formed between cytochalasin D treated platelets GPIbα and the vWF A1 domain after a larger duration time. Consequently, the tether length was lengthened compared to 1s duration time. On the contrary, the tether length for nocodazole treated and untreated platelets was shortened compared to 1s. Thus, the phase separation, which is caused by the cantilever tip, critically influences the tether length and results in a comparable tether length for treated and untreated platelets. The membrane tension and the receptor clustering significantly influenced the tether formation rate. Both treatments showed a reduced tether formation rate. For F-actin disruption the tether formation rate was additionally decreased due to the non-clustering of the receptors. However, the adhesion rate was only effected by cytochalasin D treatment, thus the receptor distribution might be the crucial influence factor for the adhesion rate.

The tether formation process by flow or by an AFM tip is a complete different process, which occurs in different time regimes. In a flow chamber set-up, the tether formation velocity is around 40 times faster (in the range between 108µm/s and 159µm/s) compared to the AFM retraction velocity (3.4µm/s). Furthermore, the tether formation in the flow chamber is an active process, in contrast the tether extraction by an AFM tip is passive. The variations in membrane tension of the flow chamber results and the AFM patch clamp results could be also due to a change of the membrane tension by the patch clamp set-up. The patch clamp set-up may additionally change the membrane tension. Cytochalasin D treated platelets showed a decreased membrane tension and therefore, these treated platelets might be sucked deeper into the patch clamp set-up. Consequently, the membrane tension is enhanced compared to flow experiments. However, for nocodazole treated platelets, the membrane tension is increased and therefore, the platelets might be not sucked as deep as the cytochalasin D treated or control platelets into the patch clamp hole. Thus, the change in membrane tension of nocodazole treated platelets is minimal. As control platelets did not show any change in the membrane tension compared to the treated platelets, these were sucked not as deep as the cytochalasin D treated platelets, but also not as minimal as the nocodazole treated platelets into the patch clamp hole. Therefore, the control platelets showed an enhanced membrane tension compared to treated ones. Furthermore, the variation between nocodazole treated platelets and control platelets was not as significant as the variations of cytochalasin D and untreated platelets in both set-ups.

In summary, undulations are the key characteristics of the platelet behaviour and are strongly influenced by parts of the cytoskeleton. Variations in the cytoskeleton lead to changes in the membrane tension, which change the degree of undulations. The interpretation of the results is summarized in figure 16. It depicts the correlation between the observed data and the induced membrane change with the variation in the undulations.

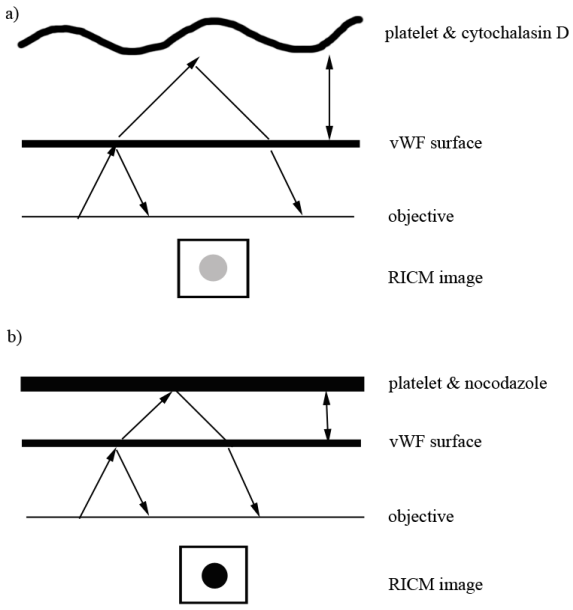

Figure 16: The sketch illustrates the combination of theory and experiment. The influence of cytochalasin D and nocodazole on the membrane tension and the induced membrane undulation is demonstrated combined with a model RICM image of the experiment. In a) the platelet is treated with cytochalasin D, which leads to a decrease in the membrane tension and to an increase in the membrane undulations. As indicated the distance between platelet to vWF surface is increased compared to nocodazole treatment. Furthermore, the model image (grey colours) shows the appearance of this configuration on the screen that the platelet only adheres weakly. In b) the opposite effect is sketched. After treatment with nocodazole the membrane tension is increased and therefore, the induced fluctuations are decreased. This induces a reduced distance between the platelet and the vWF surface and appears as black spots on the screen, which illustrates the tight adhesion of the platelet to the surface. The black arrows demonstrate the incident and refracted light, as described in figure 7.

A model system to study the integrity of the cytoskeleton and consequently, the modifications of the adhesion and tether forming process was established. Furthermore, variations in the cytoskeleton induce changes in the membrane tension, which generate alterations in the membrane undulations. These results extend the simplified picture on mechanics and thermodynamics of pure lipid bilayers with the more realistic and complex picture of a membrane shell containing the F-actin and microtubuli skeleton. These new findings can help to further understand the role that membrane tension and therefore, the induced undulations play in biological processes, especially in platelet adhesion and tether formation.

5. Impact of cholesterol loading and depletion in platelets

5.1 Introduction

Platelet free cholesterol concentration appears to influence the platelet functions (Shattil et al., 1977). Individuals with elevated levels of free cholesterol in platelets suffer from hypercholesterolemia (Shastri et al., 1980; Shattil et al., 1977). In these individuals an increased sensitivity to the aggregating agents collagen, epinephrine, and ADP is observed (Carvalho et al., 1974). These higher plasma cholesterol concentrations are a systemic trigger for the formation of atherosclerotic lesions and consequently, increase the risk of death from coronary heart disease (Davey Smith and Pekkanen 1992; Hulley et al., 1992; Oliver 1991; La Rosa et al., 1990; Dawber and Kannel 1966). When cholesterol levels are lowered in these patients, the sensitivity to the aggregating agonists ADP and collagen is lowered (Grgurevich et al., 2002; Notarbartolo et al., 1995). Lowering cholesterol levels in these patients reduces also the incidence of myocardial infarction (Haskell et al., 1994; Frick et al., 1987). However, the mechanism how cholesterol affects the platelet behaviour is still unknown. To investigate the impact of the cholesterol concentration on the platelet behaviour, platelets were either loaded or depleted with cholesterol. The cholesterol content in platelets is depleted in vitro with methyl-β-cyclodextrin (MβCD) (Grgurevich et al., 2002; Christian et al., 1997). MβCD is a cyclic heptasaccharide, which contains a hydrophobic core capable of solubilising non-polar substances and extracts membrane cholesterol from a variety of cells, in particular platelets (Grgurevich et al., 2002; Waheed et al., 2001; Kilsdonk et al., 1995; Pitha et al., 1988). The impact of the cholesterol concentration is a further step to complete the picture of the biophysical aspect of the platelet-vWF interaction introduced by the cytoskeleton disruption influence of the platelet function in chapter 4. The role of the cholesterol content on the platelet adhesion, the number of adhered platelets and the weak adhesion area, as well as the tether formation on a vWF coated surface was analysed to round up the effect of individual phenomena on the platelet-vWF interplay by changing the platelet functions. This might help to understand the increased risk of myocardial infarction by elevated cholesterol levels.

5.2 Results and Discussion

In a flow chamber equipped with a RICM (set-up see chapter 3.2.1) whole blocked blood (preparation see chapter 3.1.1) was perfused with a vWF (WT) coated glass surfaces and subjected to shear rates ranging from 5,000s^{-1} to 20,000s^{-1}, platelets arrested from flowing blood onto the immobilized vWF at the chamber walls (black arrows in fig. 17) and pulled tethers out of the platelet membrane (white arrows in fig. 17) (Reininger et al., 2006; Casella et al., 1981).

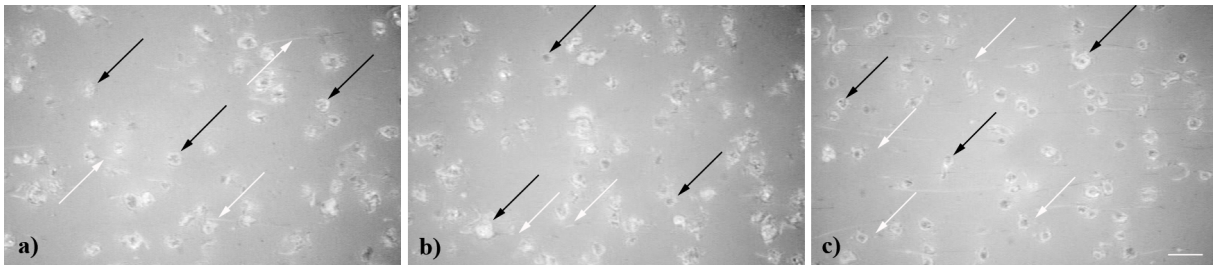

Figure 17: RICM images of blood samples (blocked) over WT (10µg/ml) at shear rates of 10,000s^{-1}. Image a) shows the cholesterol-loaded, b) cholesterol-depleted and c) control platelets adhered to the vWF surface after shear was applied for 25s. Arrested platelets, platelets with tether and ruptured tethers are shown. The black arrows indicate the platelet adhesion area. The white arrows exemplary show tethers and ruptured tethers. (In all images scale bar: 5µm)

To focus on the adhesion behaviour of platelets, the weak contact area on the bottom of the flow chamber was investigated after exposing platelets to shear flows ranging from 5,000s^{-1} to 20,000s^{-1} for 25s (fig. 18). Loaded and depleted cholesterol and control platelets were homogeneously distributed in the range between 2-14µm^2 at all investigated shear rates (fig. 18). To directly compare the impact of the cholesterol content, the average contact area was calculated from integrating the histograms of each donor and taking the average. Cholesterol-loaded platelets showed a minimal reduced average of the platelet adhesion area. Cholesterol-depleted indicated an increased platelet adhesion area and the control platelets depicted a maximum at 10,000s^{-1} at increasing shear rates from 5,000s^{-1} to 20,000s^{-1}. The differences in the shear rates and the various cholesterol contents were insignificant. The standard deviation of the various donors was calculated. For all investigated shear rates both cholesterol contents showed an increased platelet adhesion area compared to untreated platelets (table 2).

Table 2: Summary of the average contact area and the standard deviations of cholesterol-loaded, -depleted and control platelets on the vWF coated surface

mean +/- sd	5,000s^{-1} [µm^2]	10,000s^{-1} [µm^2]	20,000s^{-1} [µm^2]
cholesterol+	6.4 +/- 1.1	6.0 +/-0.8	5.9 +/-1.1
cholesterol-	5.6 +/- 1.8	6.0 +/- 0.6	6.4 +/- 0.6
control	4.4 +/- 0.3	4.9 +/- 1.0	4.3 +/- 0.6

The corresponding weak contact area distribution and average weak contact area for 10,000s^{-1} are exemplarily depicted in figure 18. The standard deviations are not depicted in the inset in figure 18 to better show the differences of treated and untreated platelets. These results denote a minimal dependence on the cholesterol concentration on the platelet adhesion area.

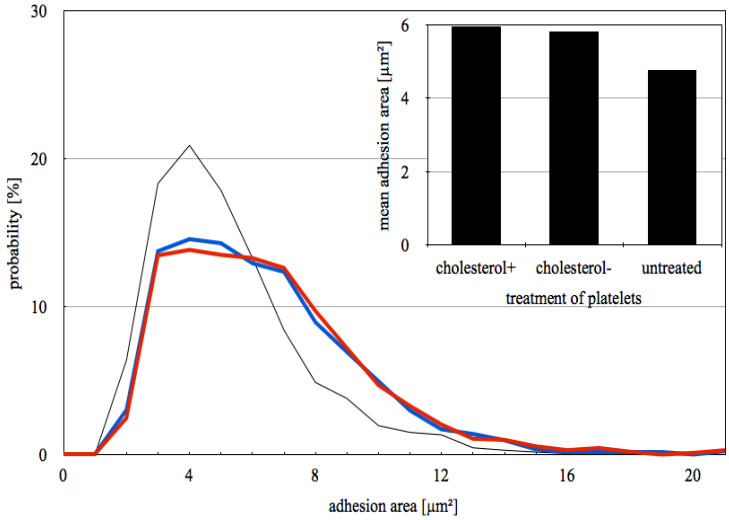

Figure 18: Weak adhesion area distribution for treated and untreated platelets at 10,000s^{-1}: the weak contact area is plotted against the probability P (∑P=100%). The red curve represents the adhesion area of cholesterol-loaded platelets, the blue curve of cholesterol-depleted platelets and the black of control platelets. The inset shows the mean of the weak adhesion area of treated and untreated platelets at a flow rate of 10,000s^{-1}.

To get a more cohesive picture on the adhesion process, the adhered platelets on the vWF coated flow chamber surface (fig. 17) were counted by using different static RICM images of blood samples following the exposure of platelets to a shear flow ranging from 5,000s^{-1} to 20,000s^{-1} for 25s. The platelet adhesion to the surface decreased for all investigated treatments with higher shear rates (fig. 19). At 5,000s^{-1} the platelet adhesion to the vWF surface was decreased by 11% for cholesterol-loaded and by 21% for –depleted platelets compared to controls. A higher shear rate of 10,000s^{-1} reduced both cholesterol contents by around 18%-19% compared to untreated platelets. In contrast, at 20,000s^{-1} the adhesion was lowered by 23% for cholesterol-loaded platelets and increased by 4% after cholesterol depletion compared to control platelets. Increasing shear flow from 5,000s^{-1} to 10,000s^{-1} reduced the adhesion of cholesterol-loaded platelets by 11%, for cholesterol depletion by 2% and for control platelets by 2%. At 20,000s^{-1} cholesterol-loaded platelet adhesion was lowered by 53%, -depleted by 28% and untreated platelet attachment by 44% compared to 5,000s^{-1}, indicating a minimal dependence on the platelet cholesterol concentration on the platelet adhesion. The standard deviation between the different donors was not significant (12%-26%), thus the error bars are not depicted in figure 19.

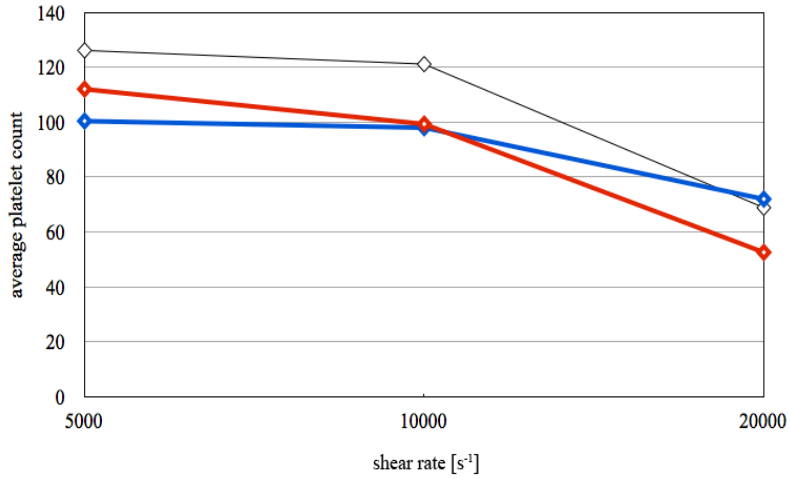

Figure 19: Average of the total platelet count per frame (5,000µm²) of treated and untreated platelets at increasing flow rates. The red curve represents the total platelet count of cholesterol-loaded platelets, the blue curve of cholesterol-depleted platelets and the black curve of controls.

These results indicate that above the shear rate threshold of vWF stretching the platelet adhesion decreases by increasing the force acting on the platelets. Above 10,000s^{-1} the force acting on the platelets reaches a maximum, thus this might be a critical shear rate threshold to significantly decrease the platelet adhesion. To zoom in the platelet absorption process, it seemed reasonable to extract the difference in the energy of absorption ΔG of untreated and treated bound platelets by applying the Boltzmann equation (adapted equation (5));

$$\frac{n_{control}}{n_{cholesterol}} = e^{-\Delta G / k_B T} \tag{7}$$

where k_B is the Boltzmann constant, ΔG is the change in absorption energy between control and cholesterol-loaded or -depleted platelets, T the temperature and $n_{control}$ and $n_{cholesterol}$ is the average fraction of the amount of control and cholesterol-loaded or -depleted platelets on the surface (Fleck et al., 2002; Alberts et al., 2003). Using the average amount of control and cholesterol-loaded or -depleted platelets adhering to the surface resulted in an energy difference ΔG in the order of 0.1-0.3 k_BT. These differences in the absorption energy extracted by untreated and treated platelets were minimal compared to the adhesion energy differences of cells typically found in the literature (Simson et al., 1998). Detailed data analysis on the comparison of absorption energy and adhesion energy in the literature is depicted in chapter 4.2. These results do not show a clear dependence of the cholesterol concentration on the platelet adhesion process, thus the tether formation process might be more sensitive compared to the adhesion process to investigate cholesterol content variations.

First, the tether length on the bottom of the flow chamber (white arrows in fig. 17) was analysed after the platelets were exposed to a shear flow ranging from 5,000s^{-1} to 10,000s^{-1}

for 25s. At 5,000s^{-1} and 10,000s^{-1} cholesterol-loaded and -depleted platelets showed a fairly sharp distribution with a most likely tether length at the platelet of around 4µm. However, untreated platelets were spread more homogeneously over the range between 1-30µm indicating a change in the mechanical properties of the tether. Instead, at 20,000s^{-1} cholesterol-loaded and -depleted and control tethers at the platelet were spread homogenously over the range between 1-26µm (loaded and control platelets: 1-26µm and depleted platelets: 1-20µm) (fig. 20). In contrast, the ruptured tethers depicted at all investigated shear rates a sharp distribution of around 4µm for cholesterol-loaded or -depleted platelets, whereas the control tethers were spread more homogenously in a range between 2-20µm (fig. 20). The ruptured tether number was significantly reduced compared to tethers at the platelet body. At 5,000s^{-1} cholesterol-loaded platelets showed 10% ruptured tethers, cholesterol-depleted platelets 14% and control platelets 27% compared to the total tether count. In contrast, at 10,000s^{-1} both cholesterol contents formed 9% ruptured tethers and untreated platelets 15%. Increasing shear rate to 20,000s^{-1} demonstrated for treated and untreated 18%-19% ruptured tethers. The tether length distribution of tethers at the platelet body and of ruptured ones was almost comparable. Afterwards, the average total tether length was calculated from integrating the histograms of each donor either at the platelet body and ruptured ones and taking the average. The standard deviation was calculated by the variations of the different donors. For all investigated shear rates, the average tether length of treated platelets was decreased compared to untreated ones (table 3).

Table 3: Summary of the average tether length and the standard deviations of cholesterol-loaded, -depleted and control platelets on the vWF coated surface.

mean +/- sd	5,000s^{-1} [µm]	10,000s^{-1} [µm]	20,000s^{-1} [µm]
cholesterol+	5.5 +/- 1.7	5.3 +/- 0.2	6.1 +/- 1.1
cholesterol-	5.4 +/- 2.1	3.7 +/- 0.3	4.9 +/- 0.2
control	10.7 +/- 0.0	7.9 +/- 1.3	7.3 +/- 1.0

The corresponding length distribution of tethers at the platelet body and ruptured tethers (inset in fig. 20) exemplarily for 10,000s^{-1} is shown in figure 20.

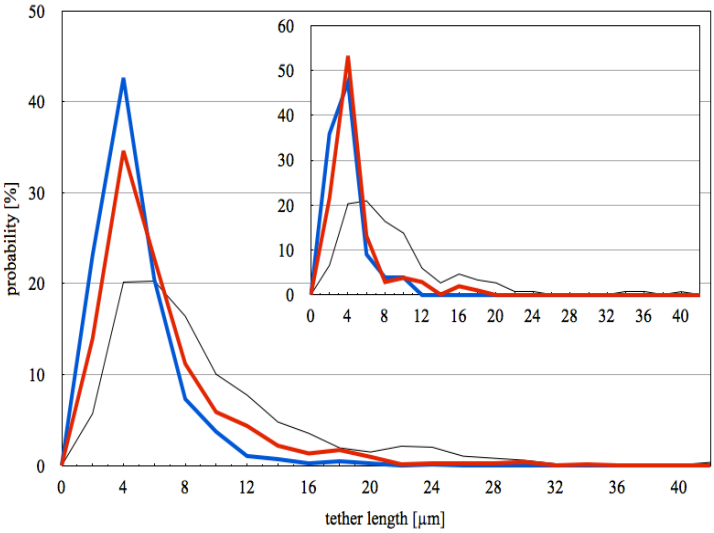

Figure 20: Tether length distribution curves at the platelet body for treated platelets at a shear rate of 10,000s^{-1}: the tether length is plotted against the probability P (∑P=100%). The red curve represents the tether length of cholesterol-loaded, the blue curve of MβCD treated and the black curve of untreated platelets. The inset shows the ruptured tether length distribution of treated and untreated platelets at a flow rate of 10,000s^{-1}.

These results show a dependence of the cholesterol content on the tether length. Thus, cholesterol might be found in tethers, failing this the ruptured tether length distribution would not be affected by cholesterol content changes. To zoom in the tether formation behaviour the influence of the shear rate on the tether formation process was investigated. For treated platelets the average of the tether length showed a minimum at 10,000s^{-1}, but the variations were minimal. In contrast, the tether length formed out of control platelets decreased with increasing shear rate. In general, it is assumed that an increase in the force or shear rate is combined with an increase in the tether length. To get an idea about the shear rate impact these results were compared with Smith and coworkers derived equation. Assuming that the tether volume is much smaller than the vesicle volume, the tether length is defined as a function of force:

$$L \cong (1 - v^{2/3}) f \tag{8}$$

with L the tether length, v the vesicle volume and f the applied force (Smith et al., 2004). As the tether length did not significantly increase for higher shear rates, this force-tether length relationship could not be applied. The variations of the most frequent tether length and the average tether length were minimal due to force changes. The impact of shear rate changes on the tether length will also be investigated in chapter 6, 7 and 9, but the variations by increasing shear rate were too minimal to be used for the force-tether length relationship (equation 8). Equation 8 will not be quantified in the following chapters. The tether length is mainly influenced by platelet function variations. The impact on the vWF on the tether forming process will be analysed in the following three chapters. To complete the tether

formation process, the average amount of the total tethers adhered on the vWF surface was calculated. The total tether count almost bisected for cholesterol-depleted platelets compared to cholesterol-loaded and untreated ones at shear rates of 5,000s^{-1}. At 10,000s^{-1} the total tether amount was 9% and 26% reduced for cholesterol-loaded and -depleted platelets compared to controls. Whereas, at 20,000s^{-1} the total tether amount was lowered by 31% and 42% for cholesterol-loaded and -depleted platelets compared to untreated ones. The standard deviation between the different donors was significant (30%-60%), but the tendencies remained almost unchanged. These results indicate that the tether formation process is more sensitive on the cholesterol concentration changes in the platelet as the platelet adhesion. The tether formation and the tether length were reduced due to cholesterol content changes. The platelet adhesion was minimal reduced and the weak contact area was minimal increased compared to untreated platelets. As the variations in the platelet adhesion are minimal, the changes in the cholesterol content might be too low. These variations in the tether length and the platelet adhesion might be due to a slightly increased membrane-cytoskeleton adhesion. Due to the increased membrane-cytoskeleton adhesion the formation of adhesion domains might be lowered, thus more lock and key interactions have to be formed to achieve the same adhesion strength compared to an untreated membrane-cytoskeleton adhesion. The enhanced lock and key interaction formation increase the weak adhesion area. Due to this lowered adhesion strength the tether formation and the tether length are reduced. These results are almost in line with Sun and coworker except for cholesterol-enriched platelets. For different cell types, except blood platelets, the membrane-cytoskeleton adhesion is decreased for cholesterol-enriched cells and increased for cholesterol-depleted ones (Sun et al., 2007). Every variation out of the platelets biological equilibrium, which is the status of a healthy platelet, might influence the tether formation and adhesion in the same direction. The concentration of cholesterol loading and depletion may also be responsible for the same impact on the platelet adhesion and tether formation processes, as low and large cholesterol concentrations influence the permeability and the thermomechanics of membranes contrary (Mouritsen and Zuckermann 2004). Cholesterol depletion diminishes collagen induced platelet aggregation by first, altering the platelet ultrastructure critical in mediating secretion and second, influencing intracellular events, such as a reduction in microtuble ring formation and tyrosine phosphorylation (Grgurevich et al., 2002). The spreading on vWF (Van Lier et al., 2005) and the platelet volume is also lowered suggesting a decreased platelet reactivity. However, morphological changes, variations in the granule structure, the $\alpha IIb\beta 3$ distribution and the platelet activation state are not observed (Gousset et al., 2004; Grgurevich et al., 2002). Human platelets

depletion with 10mM MβCD leads to a 24%-54% reduction in total cholesterol concentration of the platelets (Grgurevich et al., 2002). These effects of cholesterol depletion analysed by Grgurevich and coworkers showed that MβCD changes the platelet biochemistry. The presented results coincide with the other groups, but the influence on the platelet adhesion and tether formation was minimal compared to the changes in adhesion on collagen and spreading on vWF. Thus, a higher change in the cholesterol concentration might stronger influence these investigated processes.

Taken together, these small variations in the cholesterol concentration might not crucially affect the GPIbα-vWF A1 domain interaction. The investigated changes in the cholesterol concentration were in the physiological relevant range. In contrast, physically more effective would be an increased cholesterol concentration change. The platelet-vWF interaction might not be the main risk factor for mycardinal infarctions.

6. Importance of the multimer size for von Willebrand factor function

6.1 Introduction

Essential in the coagulation cascade is a functional vWF. Defect of the vWF results in a decrease of the vWF antigen content and in alterations in its functionality. The multifunctional character of vWF, its complex biosynthesis, intercellular transport, secretion pathways and structure are responsible for its marked heterogeneity of clinical symptoms in von Willebrand disease (vWD) (Schneppenheim 2004; Schneppenheim and Budde 2004). In general, three different main types of vWD can be observed. The vWD type 1 shows a low vWF antigen concentration, type 3 the loss of vWF and type 2 qualitative mutations independent of the vWF antigen content. Type 2 is devided into several subgroups. The vWD type 2A is characterised by a disordered platelet dependent function due to loss or relative reduction of the high molecular weight multimers, which are most active in primary hemostasis. Type 2B is distinguished by an increased GPIbα binding affinity independent of either a loss of the large multimers or a normal vWF multimer distribution. Platelet dependent defects of the vWF are described by type 2M and defects in the factor VIII-vWF interaction by type 2N (Schneppenheim and Budde 2006; Schneppenheim 2004; Schneppenheim and Budde 2004; Sadler 1994). The severity and the type of the vWD are the basis for the therapy plan. For example, vWD type 3 patients are treated with commercial available vWF products. Crucial for this therapy are the large multimers of the vWF products, as these are more active and important for the primary haemostasis step (Schneppenheim and Budde 2006). VWF products used for patient treatment exhibit a large variation in multimeric distribution, which may reflect in vivo effectiveness. Up to now, the influence of various multimer size lengths is not fully understood. This knowledge is important for the differentiation and classification between the various vWF product types. To directly point out the impact on different lengths of the vWF multimer distribution, subfractions from one vWF product, Haemate, were as well investigated. The platelet adhesion, the number and the weak adhesion area, and the tether formation on a vWF product coated surface were analysed by a flow chamber set-up equipped with a RICM. It is a suitable tool to test the efficiency of vWF products in vitro. Over collagen the percentage coverage area was quantified by epifluorescence microscopy with the vWF products and Haemate subfractions in the blood suspension.

6.2 Results and Discussion

Either washed blocked cell suspensions (preparation see chapter 3.1.2) with immobilized multimeric vWF products coated on a glass surface or blocked or not blocked blood containing EDTA, PPACK (preparation see chapter 3.1.2 and 3.1.3) and multimeric vWF over fibrillar type I collagen were perfused in a flow chamber (set-up see chapter 3.2.1). The vWF products Fanhdi, Haemate, Haemoctin, Immunate, Octanate and Wilate were investigated. The effect of shear rates and vWF products on the platelet-vWF interaction by increasing the shear rate from $400s^{-1}$ to $40{,}000s^{-1}$ was examined. To point out the differences of the multimer size length on the platelet-vWF interplay, especially in the adhesion on collagen, the subfractions of the vWF product Haemate were quantified. The vWF proteins were used in a final concentration of 100µg/ml or 10µg/ml. The physiological vWF blood concentration is 10µg/ml. The increased vWF concentration was investigated to clarify the role of an increased vWF concentration on the platelet-vWF interaction to study the possibility of an increased vWF content for patient treatment. To resolve the structure of a few Angström and the distribution of vWF after shear surface coating, two vWF products, Haemate and Wilate, were shear coated onto a glass surface under constant shear conditions of $6{,}000s^{-1}$ for 30min. These coated glass slides were preliminary analysed by AFM operating in tapping mode (set-up see 3.2.2.1) not to manipulate the sample by the AFM tip. The vWF coated glass cover slips were fixed with 2.5% glutaraldehyde and 10% paraformaldehyde to provide stable immobilization. Only for Haemate multimer fibers on the coated cover slips could be observed. Wilate showed a homogenous distribution of globular vWF molecules. The presence of elongated vWF fibers might be due to the largest multimers of Haemate compared to Wilate (fig. 21).

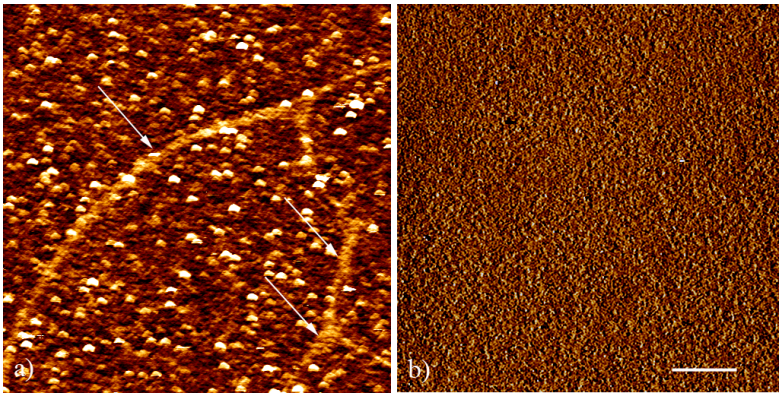

Figure 21: Atomic force microscopy images of vWF multimer fibers (see arrows) in a) the Haemate product adsorbed to glass under shear rates of 6,000 s^{-1} versus lack of those structures in b) the Wilate product. (In all images scale bar: 5µm)

This suggests that the largest multimers might be responsible for the fibre formation of the vWF protein on surfaces. The absorption of vWF on a glass surface is obtained by unspecific interactions and not by lock and key interactions.

6.2.1 vWF products coated on the chamber surface

To quantify the adhesion of platelets in detail, first the adhered platelets on the vWF surface of the flow chamber were statistically calculated by using still RICM images of blood samples after the exposure of platelets to a shear flow ranging from 1,500s^{-1} to 40,000s^{-1} for 45s. Unfortunately, due to this static capture it was not possible to resolve the dynamic behaviour of the platelets. The rolling velocities of the vWF products were determined to clarify the differences in adhesion time of the GPIbα and the vWF A1 domain. The amount of the adhered platelets on the vWF surface was dependent on the shear rate and on the coating concentration, but not on the vWF products. For a coating concentration of 100µg/ml most of the vWF products showed a maximum for the platelet adhesion at 10,000s^{-1}. In contrast, Fandhi exhibited a maximum at 4,000s^{-1} and Haemate at 20,000s^{-1}. The average value of the platelet adhesion per frame and their standard deviation, calculated by various donors, are depicted in table 4.

Table 4: Summary of the average platelet adhesion and the standard deviations to the vWF surface per frame (5,000µm^2) coated by different vWF products (10U).

vWF products (mean +/- sd)	1,500s^{-1}	4,000s^{-1}	10,000s^{-1}	20,000s^{-1}	40,000s^{-1}
Fanhdi	42.1 +/- 16.4	95.6 +/- 30.5	88.8 +/- 24.5	87.5 +/- 34.7	52.4 +/- 35.2
Haemate	28.9 +/- 12.7	95.2 +/- 15.5	110.0 +/- 24.8	109.2 +/- 27.4	57.7 +/- 53.8
Haemoctin	38.3 +/- 8.6	58.2 +/- 19.5	71.5 +/- 21.9	68.7 +/- 20.6	29.4 +/- 30.5
Immunate	44.2 +/- 8.1	95.9 +/- 21.5	117.4 +/- 18.4	101.9 +/- 21.7	64.4 +/- 40.7
Octanate	52.3 +/- 15.8	90.9 +/- 24.7	116.0 +/- 16.7	79.5 +/- 38.7	20.5 +/- 7.0
Wilate	56.2 +/- 18.8	93.2 +/- 32.2	96.9 +/- 22.9	82.5 +/- 19.9	43.4 +/- 25.4

For the lower vWF coating concentration the shear rates with the most significant differences and only one vWF product from Octapharma were chosen to investigate the adhesion and tether formation processes on vWF as well as the aggregate formation on collagen. A lower vWF coating concentration of 10µg/ml showed more than twice as much adhered platelets on the vWF surface compared to the higher vWF coating concentration. The increase from 1,500s^{-1} to 10,000s^{-1} doubled for all investigated vWF products the platelet adhesion. However, the variations of the different vWF products were minimal as for the higher vWF

concentration. The mean of the platelet adhesion and their standard deviation is summarized in table 5.

Table 5: Summary of the average platelet adhesion and the standard deviations to the vWF surface per frame (5,000µm^2) coated by different vWF products (1U).

vWF products (mean +/- sd)	1,500s^{-1}	10,000s^{-1}
Fanhdi	102.1 +/- 18.0	222.4 +/- 20.5
Haemate	103.3 +/- 19.0	217.6 +/- 11.5
Haemoctin	108.3 +/- 18.7	214.1 +/- 12.3
Immunate	93.2 +/- 21.8	219.7 +/- 23.0
Wilate	107.8 +/- 6.3	208.3 +/- 11.2

These results indicate a significant dependence on the vWF concentration and the exposed shear rate. In contrast, the variations in the platelet adhesion of the vWF products were minimal. The differences in the vWF multimer distribution might be too small to influence the platelet adhesion. The significant increase in the platelet adhesion amount from 1,500s^{-1} to 10,000s^{-1} might be due to the stretching of the vWF protein above a critical shear rate. In the range between 2,000s^{-1} and 5,000s^{-1} the vWF protein gets activated (Schneider et al., 2007). Above a shear rate of 10,000s^{-1} the adhesion decreased due to an increased applied force, which pushed most of the platelets over the surface without the possibility of detaching. The platelet-vWF interaction might be not strong enough at 20,000s^{-1} to provide the same number of adhered platelets. Thus, at high shear rates more lock and key interactions and the formation of adhesion domains are essential. An increase in the vWF product concentration is combined with a decrease in platelet adhesion. The platelet count on the surface was almost bisected by a higher vWF concentration. Therefore, increased vWF surfaces coating contents might not provide more binding sites, as vWF products might tend to self assemble on the vWF surface. Consequently, the availability of the receptors for platelet adhesion is reduced. To elucidate the dynamic behaviour of the platelets, the rolling velocities of the platelets over the different vWF products (c = 100µg/ml) coated surfaces were investigated. All vWF products showed comparable velocities. By trend Wilate had a decreased rolling velocity compared to Haemate, these resulted in a longer binding time of the GPIbα and the A1 domain of the Wilate product. The average value of the rolling velocities and their standard deviations due to the various donors are depicted in table 6. The rolling velocities minimal increased with increasing shear rate.

Table 6: Summary of the platelet rolling velocities and the standard deviations of vWF product coated surfaces (10U).

vWF products (mean +/- sd)	1,500s^{-1} [µm/s]	4,000s^{-1} [µm/s]	10,000s^{-1} [µm/s]
Fanhdi	3.7 +/- 2.6	4.0 +/- 2.9	6.8 +/- 4.1
Haemate	3.8 +/- 2.0	5.1 +/- 4.7	6.9 +/- 4.2
Haemoctin	2.7 +/- 1.9	7.1 +/- 4.7	9.3 +/- 4.4
Immunate	3.0 +/- 2.0	3.6 +/- 2.7	5.0 +/- 3.2
Octanate	3.0 +/- 2.0	4.5 +/- 3.2	6.8 +/- 3.4
Wilate	2.9 +/- 2.1	3.8 +/- 3.0	5.2 +/- 3.9

For lower vWF coating concentrations the differences in rolling velocities were not investigated, as no differences for the comparison of products at higher coating concentrations were present. These results show that the difference in the multimer distribution of the investigated vWF products is too low to influence the platelet rolling velocities. The rolling velocity increased with the flow rate, as the force acting on the platelets was enhanced and therefore, the probability for binding events and time was reduced. Next, the contact area on the bottom of the flow chamber after the exposure of the platelets to different shear flows ranging from 1,500s^{-1} to 40,000s^{-1} for 45s was quantified. All vWF products were homogeneously distributed in the range between 1-15µm^2 at all investigated shear rates and for both vWF coating concentrations (fig. 22). To point out the variation of low and high shear rates for the lower vWF coating concentration were 1,500s^{-1} and 10,000s^{-1} investigated. To highlight the impact of the vWF products, the average contact area was calculated from integrating the histograms of each donor and taking the average. All investigated products were comparable to each other. The differences of the vWF products were in the range of the standard deviation of the various donors. The average of the contact area showed a maximum at 10,000s^{-1}. However, the changes in the investigated shear rates were minimal. A detailed list of the average contact area and the standard deviations on all investigated vWF coated surfaces and for both coating contents is summarized in table 7 and 8.

Table 7: Summary of the average platelet adhesion and the standard deviations to the vWF surface coated by different vWF products (10U).

vWF products (mean +/- sd)	1,500s^{-1} [µm^2]	4,000s^{-1} [µm^2]	10,000s^{-1} [µm^2]	20,000s^{-1} [µm^2]	40,000s^{-1} [µm^2]
Fanhdi	5.4 +/- 0.7	5.5 +/- 0.7	6.0 +/- 0.2	7.0 +/- 0.4	6.4 +/- 1.1
Haemate	5.5 +/- 0.2	5.7 +/- 0.2	6.2 +/- 0.7	7.0 +/- 0.4	6.2 +/- 1.5
Haemoctin	4.9 +/- 0.4	6.6 +/- 1.3	6.7 +/- 0.6	7.6 +/- 1.1	6.2 +/- 1.0
Immunate	6.5 +/- 0.5	6.5 +/- 0.9	6.5 +/- 1.2	7.3 +/- 1.1	7.6 +/- 1.6
Octanate	6.0 +/- 0.5	6.6 +/- 1.2	7.0 +/- 1.0	7.0 +/- 0.9	6.7 +/- 0.4
Wilate	5.5 +/- 0.8	5.9 +/- 0.3	6.9 +/- 0.5	7.1 +/- 0.6	7.2 +/- 0.5

Table 8: Summary of the average platelet adhesion and the standard deviations to the vWF surface coated by different vWF products (1U).

vWF products (mean +/- sd)	1,500s^{-1} [µm^2]	10,000s^{-1} [µm^2]
Fanhdi	4.6 +/- 0.1	5.2 +/- 0.3
Haemate	4.8 +/- 0.5	5.3 +/- 0.2
Haemoctin	4.8 +/- 0.2	5.2 +/- 0.3
Immunate	4.8 +/- 0.2	5.4 +/- 0.4
Wilate	4.9 +/- 0.2	5.2 +/- 0.2

Exemplarily for 10,000s^{-1} the weak contact area and exemplary RICM still images of platelets adhering to the Haemate surface of both coating concentration are depicted in figure 22.

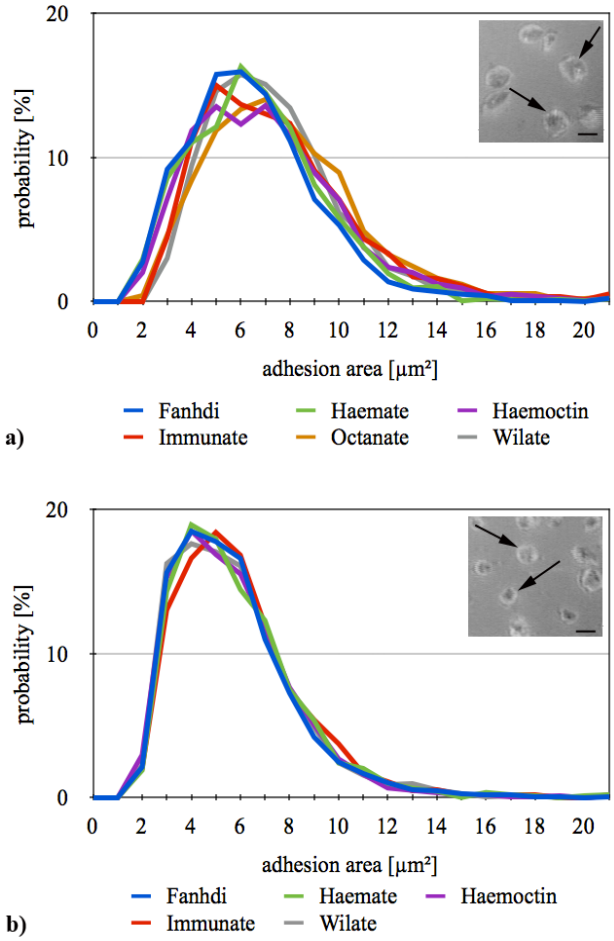

Figure 22: Adhesion area distribution of platelets over a vWF product coated surface at 10,000s^{-1}: the contact area is plotted against the probability P (∑P=100%). a) shows the adhesion area distribution of a vWF coating concentration of 100µg/ml and b) of a concentration of 10µg/ml. The insets show RICM still images of platelets adhering exemplary to a Haemate surface of both vWF concentrations at 10,000s^{-1}. The black arrows indicate the platelet weak contact area. (In all images scale bar: 2µm)

These results suggest that the platelet weak adhesion area on the vWF coated surface remained constant by minimal variations in the multimer distribution of the investigated vWF products and also by a drastic change in the vWF coating concentration. Additionally, the weak adhesion area was minimal increased by increasing shear rate. The influencing factor of the weak adhesion area might be the platelet and not the vWF protein, especially the large multimers, as variations in the platelet cytoskeleton significantly changed the weak adhesion area (details see chapter 4). However, the effect of the vWF protein will be analysed in the next two chapters, to confirm this assumption. The tether length might be more sensitve in multimer distribution variations. To zoom in the platelet-vWF interaction, the tether length on the bottom of the flow chamber was analysed, following the exposure of the platelets to shear flows ranging from 1,500s^{-1} to 40,000s^{-1} for 45s. The variations between the different products and different coating concentrations were minimal. All products showed a fairly sharp distribution between 3-10µm at all investigated shear rates (fig. 23). The tether length distribution varied between tethers at the platelet body and ruptured ones minimal. However, the amount of ruptured tethers was significantly reduced. Almost all investigated products showed approximately 10% ruptured tethers, except Wilate, which formed approximately 30% ruptured tethers. The average tether length was calculated to better compare the variations of the vWF products by integrating each histrogram and taking the average. All investigated vWF products were comparable to each other. The tether length reached a maximum at 10,000s^{-1}, but the changes by the shear rate were minimal. The detailed values of the average tether length and the standard deviations of the various donors are depicted in tabele 9 and 10.

Table 9: Summary of the average tether length and the standard deviations to the vWF surface coated by different vWF products (10U).

vWF products (mean +/- sd)	1,500s^{-1} [µm]	4,000s^{-1} [µm]	10,000s^{-1} [µm]	20,000s^{-1} [µm]	40,000s^{-1} [µm]
Fanhdi	4.8 +/- 0.7	7.6 +/- 3.0	8.1 +/- 1.0	6.1 +/- 1.0	5.9 +/- 0.5
Haemate	4.1 +/- 1.3	6.4 +/- 0.6	6.9 +/- 1.0	6.9 +/- 0.8	5.9 +/- 0.9
Haemoctin	5.0 +/- 0.6	5.8 +/- 1.1	9.5 +/- 1.4	7.2 +/- 1.0	6.3 +/- 0.9
Immunate	4.4 +/- 1.1	5.6 +/- 0.4	9.0 +/- 2.5	8.6 +/- 0.8	6.5 +/- 0.9
Octanate	4.9 +/- 0.7	5.4 +/- 1.0	7.5 +/- 0.9	6.6 +/- 0.3	5.2 +/- 0.5
Wilate	4.6 +/- 0.6	5.0 +/- 0.8	7.8 +/- 1.1	8.2 +/- 0.7	6.4 +/- 1.4

Table 10: Summary of the average tether length and the standard deviations to the vWF surface coated by different vWF products (1U).

vWF products (mean +/- sd)	1,500s^{-1} [µm]	10,000s^{-1} [µm]
Fanhdi	4.4 +/- 0.7	9.4 +/- 1.8
Haemate	4.3 +/- 1.5	9.8 +/- 3.2
Haemoctin	3.6 +/- 0.4	7.4 +/- 2.2
Immunate	3.9 +/- 1.3	8.6 +/- 2.4
Wilate	3.9 +/- 1.6	7.5 +/- 2.2

Exemplarily, for a shear flow of 10,000s^{-1} the total tether length distribution and RICM still images of tethers and platelets adhering to the Haemate coated surface of both coating concentrations are depicted in figure 23.

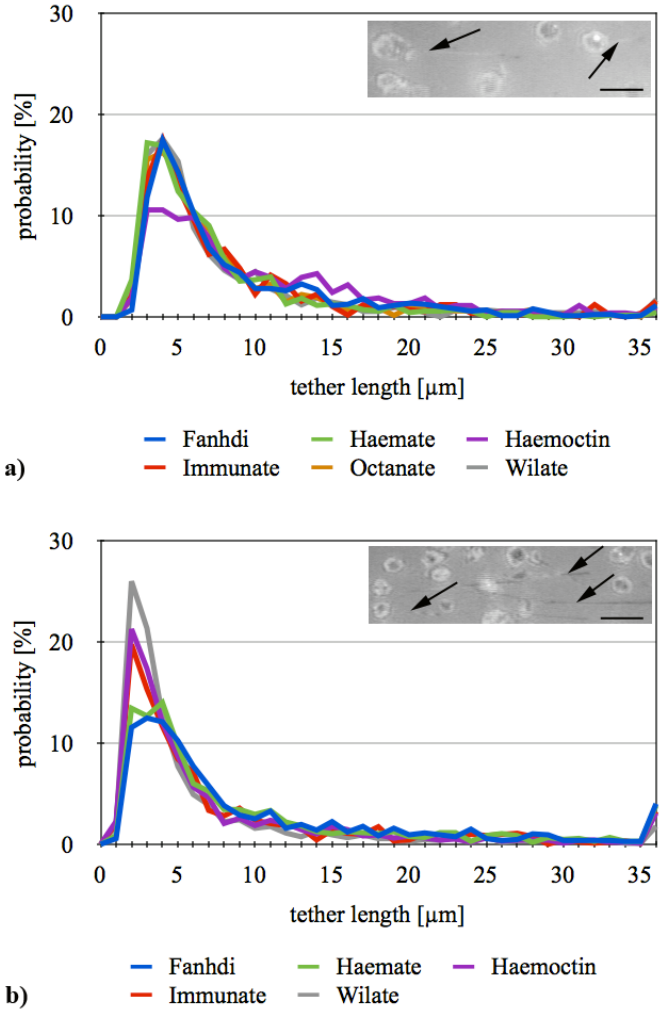

Figure 23: Total tether length distribution for platelets over a vWF product coated surface at 10,000s^{-1}: the tether length is plotted against the probability P (∑P=100%). a) shows the tether length distribution of a vWF coating concentration of 100µg/ml and b) of a concentration of 10µg/ml. The insets show RICM still images of tether and platelets adhering exemplary to a Haemate surface of both vWF concentrations at 10,000s^{-1}. The black arrows indicate tethers. (In all images scale bar: 5µm)

Finally, the total tether count was quantified. At higher vWF coating concentrations the tether adhesion was maximal at 20,000s^{-1} for all investigated vWF products, except Fanhdi, which depicted most of the tethers at 10,000s^{-1}. These results were also comparable with the lower vWF coating concentration. At all investigated shear rates and a higher vWF surface coating Haemoctin showed the fewest total tether number. In contrast, at lower vWF coating concentration Fanhdi showed the fewest tethers. Wilate significantly increased the ruptured tethers number by increasing shear rate and both coating concentrations compared to the other vWF products. In general, the tether count increased with increasing shear rate. The calculated standard deviations were < 50%, however, the tendencies remained unchanged. These results show that the tether length is minimal controlled by the shear rate. The average value of the tether length slightly increased until 10,000s^{-1} and decreased above that shear rate threshold. However, the tether count depends on the shear rate, due to an increased platelet adhesion probability. The tether formation rate increases until 10,000s^{-1} like the platelet adhesion. Consequently, the increased platelet adhesion to the surface might be the key impact factor on the tether formation. The various vWF products and both coating contents did not regulate the tether formation process, except for Wilate. Wilate showed most of the tethers adhering to the surface, especially ruptured ones. Thus, Wilate might offer an increased binding affinity for GPIbα compared to the other products.

Over all, all investigated products were comparable to each other for all investigated platelet functions and no impact of the large multimers on the platelet-vWF interplay was observed.

6.2.2 Collagen coated surface

To analyse the aggregate formation of platelets, the formed platelet aggregates on the collagen surface of the flow chamber were statistically quantified. The adhesion on collagen might simulate in more detail the in vivo blood flow compared to the vWF coated surface, as collagen is exposed to the blood flow after vascular injury. By using epifluorescence microscopic images of unblocked blood samples (preparation see chapter 3.1.3) containing vWF products or Haemate subfractions the aggregate formation was examined after the exposure of platelets to a shear flow of 400s^{-1} to 10,000s^{-1} for 30s to 5min (fig. 24). Both coating contents were quantified to point out the impact on the vWF concentration in the blood suspension on the platelet-vWF interplay.

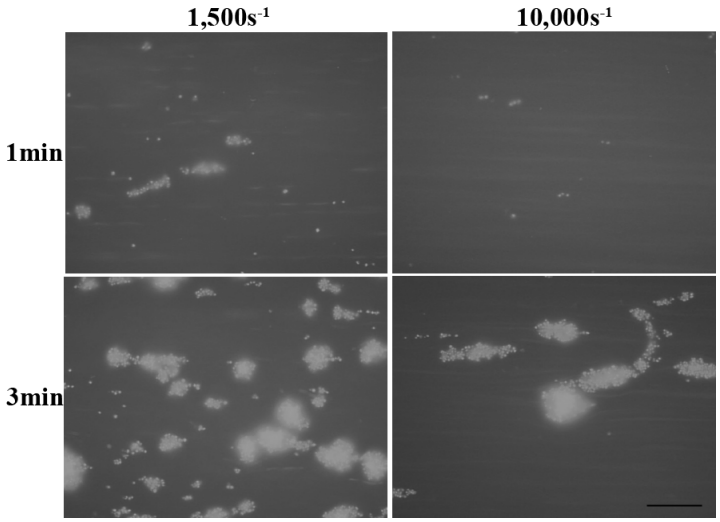

Figure 24: Epifluorescence microscopic picture of platelet aggregates over collagen exemplary added Haemate (10µg/ml) to the blood suspension arrested single platelets and platelet aggregates are shown. Black arrows indicate the platelet aggregates on collagen. (In all images scale bar: 40µm)

For high vWF concentrations, a shear rate of 1,500s^{-1} and a flow time duration of 1min showed that Haemate provided most of the vWF-platelet aggregates on collagen. However, at increasing flow time duration all products were comparable except Wilate, which had the greatest amount of small aggregates (≤ 200µm²). This amount was almost doubled compared to the other products. At 10,000s^{-1} Wilate showed most of the aggregates on collagen compared to the other products. From summing up the amount of aggregates a percentage area coverage was calculated, which exactly demonstrated the results of the single aggregate observation. The differences between the products for 1,500s^{-1} were not significant (fig. 25 a)), but for 10,000s^{-1} the percentage area coverage was increased for Wilate (fig. 25 b)). In contrast, for the low vWF concentration the aggregate distribution varied. At 1,500s^{-1} and for 30s and 1min flow exposure the difference between the products was significant (fig. 25 c)). Haemate and Immunate showed most of the aggregates, but at increasing duration times this effect vanished. However, at a duration time ≥ 4min Wilate showed most of the aggregates, which was comparable to ten times of the vWF concentration (fig. 25 c)). On the contrary, at 10,000s^{-1} and a flow exposure of 30s Haemate formed most of the aggregates on collagen (fig. 25 d)). Instead, at increasing flow time duration the products were comparable except for Fanhdi and Haemoctin (fig. 25 d)). This result was completely contrary to the higher vWF concentration. For the higher vWF concentration Wilate formed most of the aggregates. The percentage area coverage showed the same results (fig. 25). The standard deviations between the donors were significantly large (< 100%), however, the trends remained almost constant. Due to a better overview, the error bars are not depicted in figure 25.

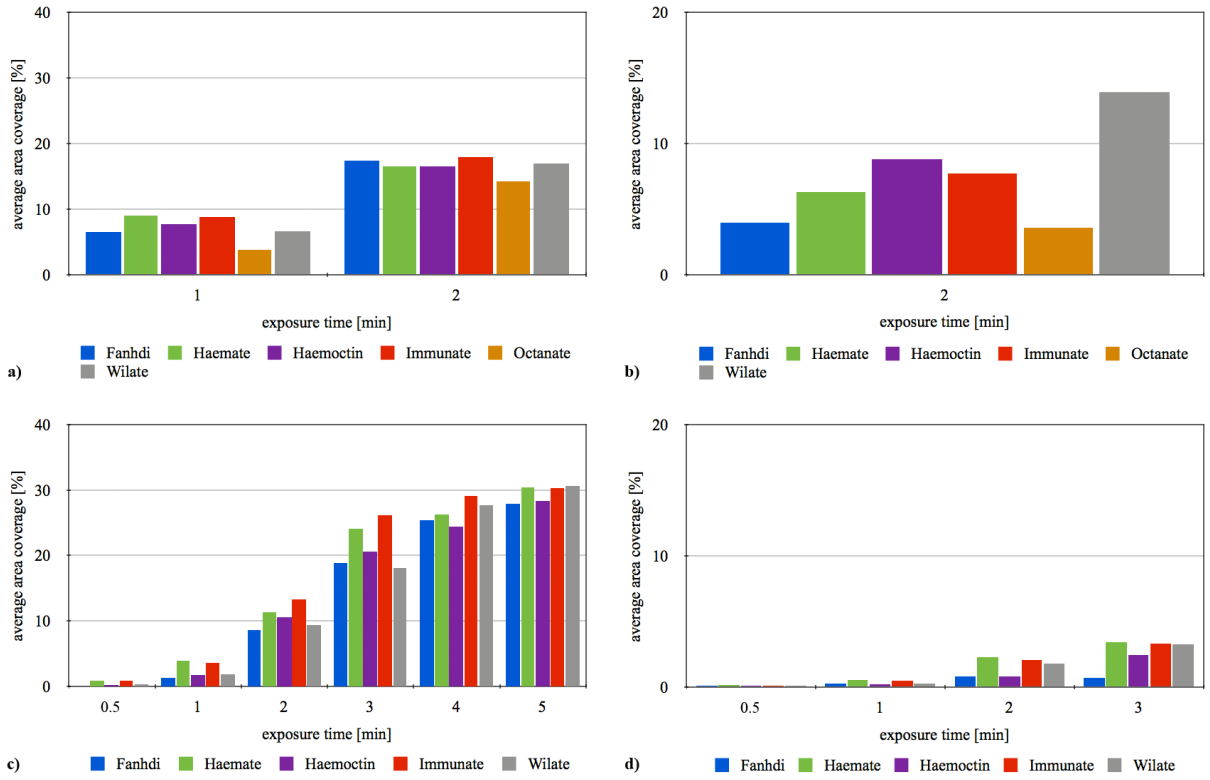

Figure 25: Percentage area coverage of platelet aggregates on collagen. VWF products were added to the blood suspension at final concentrations of a), b) of 100µg/ml and c), d) of 10µg/ml. Image a) shows platelet aggregate formation at shear rates of a), c) of 1,500s^{-1} and b), d) of 10,000s^{-1}.

For shear rates of 400s^{-1} the vWF products were comparable until 4min duration time of the shear flow except Immunate, which showed for all duration times a lower amount of aggregates. However, at 4min the variation of the vWF products increased and for Haemoctin and Wilate most of the aggregates were observed. At 800s^{-1} and at the beginning of the flow perfusion Haemoctin and Immunate formed most of the aggregates on collagen. In contrast, with increasing flow time the products were comparable (fig. 26). These flow measurements at shear rates of 400s^{-1} and 800s^{-1} were only performed for the lower vWF concentration, as no variation for the higher vWF concentration could be observed at 1,500s^{-1}. The standard deviations between the donors were significantly large (< 100%), however, the trends remained almost constant. Due to a better overview, the error bars are not depicted in figure 26.

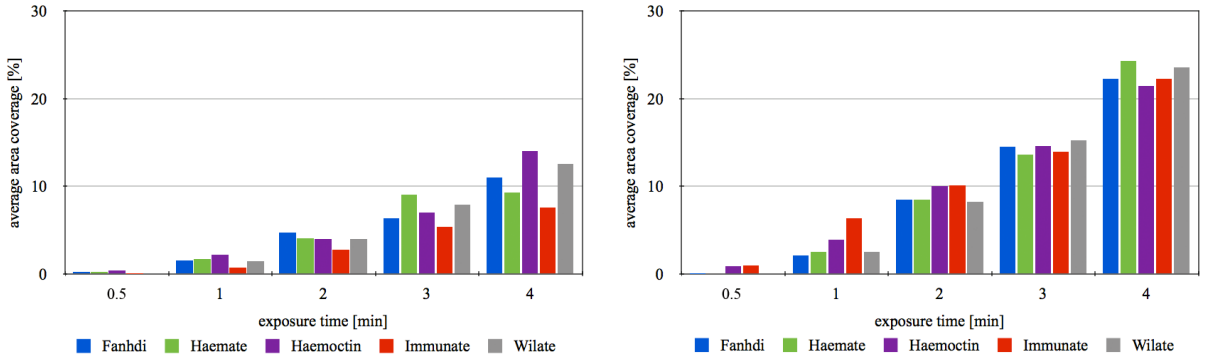

Figure 26: Percentage area coverage of platelet aggregates on collagen. VWF products were added to the blood suspension at final concentrations of 10µg/ml. Image a) shows platelet aggregate formation at shear rates of a) of 400s^{-1} and b) of 800s^{-1}.

These results indicate that the differences in the multimeric distribution of the vWF products over collagen are significant at lower vWF concentrations compared to higher ones. At the beginning of the flow exposure (30s, 1min) at 1,500s^{-1} and at 10,000s^{-1} Haemate formed most of the platelet aggregates compared to the other investigated vWF products. Therefore, the largest multimers might be a key characteristic for the aggregate formation over collagen, as Haemate was the only vWF product, which was composed of the whole multimer distribution of the normal plasma vWF. The other products did not consist of the largest multimers. In contrast, at increasing flow exposure at 1,500s^{-1} the effect of the largest multimers vanished. After two minutes flow exposure the vWF multimers might conglomerate and were able to replace the influence of largest multimers due to self assembling. Contrary, for higher vWF concentration the influence of the largest multimers vanished. At 1,500s^{-1} the variation in the aggregate formation of the different vWF products was minimal, but for 10,000s^{-1} Wilate showed most of the aggregates. Although Wilate was not composed of the largest multimers, to overcome the effect of the largest multimers Wilate might tend to self assemble more effective at 10,000s^{-1} compared to the other vWF products. The influence of the largest multimers might be neglected due to a ten times increased vWF protein concentration. To directly clarify the effect of each multimer group and to understand the possibility of self assembly, Haemate subfraction of the same production process containing only small, middle or large size multimers (multimer distribution in fig. 27) were analysed by using a collagen coated flow chamber equipped with epifluorescence microscopy. The variation in the multimer distribution of the Haemate subfractions was biochemical analysed by agarose gel electrophoresis to better understand the differences of small, middle and large multimers. The main differences in the multimer length are shown by the black circles and arrows in the upper bands in figure 27.

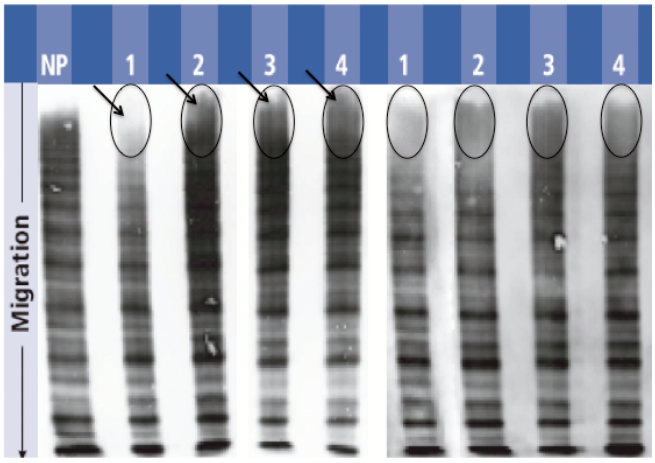

Figure 27: Analysis of vWF multimer patterns of 4 different subfractions of Haemate by sodium dodecyl sulfate–agarose gel electrophoresis. NP, normal plasma; lane 1, E100 (low molecular weight); lane2, E140 (low intermediate molecular weight); lane 3, E180 (high intermediate molecular weight; lane 4, E250 (high molecular weight). Concentration of vWF as determined by ristocetin cofactor activity assay was adjusted to 1.0U/mL. The black arrows and circles indicate the changes in the multimer distribution size.

On the basis of the gel electrophoresis the amount of aggregates and the aggregate size was investigated to quantify the influence of shear rate, flow duration time, vWF multimer size length and the vWF concentration. To get an idea of the various aggregation formation processes due to the multimer size difference, shear rate and exposure, exemplarily for the physiological vWF concentration the adhesion pattern on collagen at 1,500s^{-1} and flow times of 1min, 2min and 5min (fig. 28 a)) and at 10,000s^{-1} of 3min (fig. 28 b)) is depicted for small multimers (E100), Haemate and large multimers (E250) in figure 28. The variation in the different multimer sizes at higher vWF contents was minimal at 1,500s^{-1} except for the large multimers. The large multimers formed at any investigated flow exposure time at 1,500s^{-1} less aggregates compared to the other subfractions. At duration times between 30s and 1min the larger intermediate multimer fraction showed most of the aggregates compared to the other investigated subfraction. However, after 2min flow exposure the subfraction were comparable except the large multimers, which showed significantly decreased amounts of the aggregates on collagen (fig. 29 a)). At a higher shear rate of 10,000s^{-1} the influence of differences of the Haemate subfractions was more pronounced compared to 1,500s^{-1}. For all investigated flow exposure times at 10,000s^{-1} the larger multimers formed most of the aggregates and also the largest aggregates (fig. 29 b)).

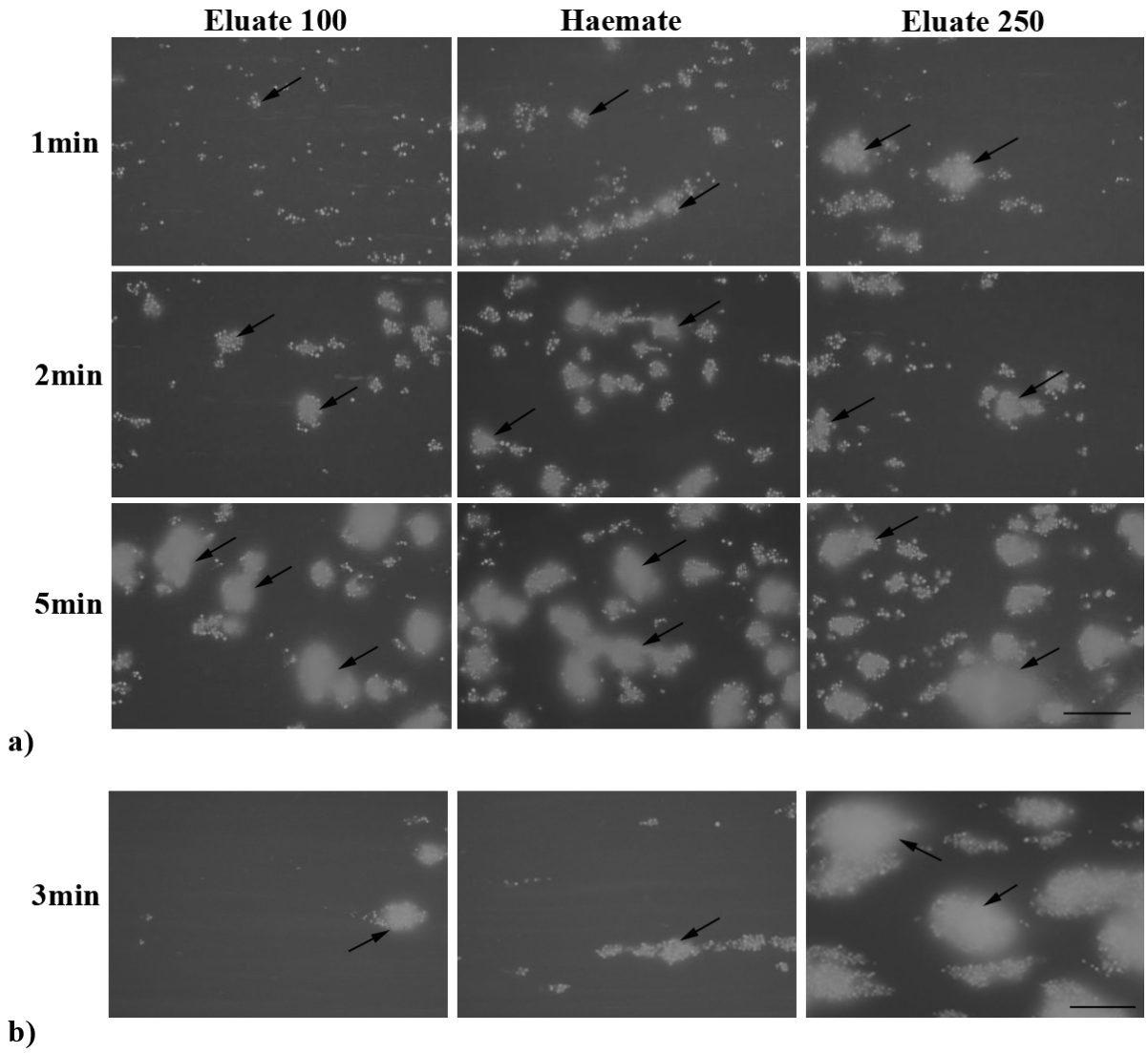

Figure 28: Epifluorescence microscopic picture of platelet aggregates over collagen by adding E100 (small multimers), Haemate (comparable with normal plasma) and E250 (large mulltimers) at a final concentration of 10µg/ml to the blood suspension. Arrested single platelets and platelet aggregates are shown. Black arrows indicate the platelet aggregates on collagen. Image a) shows aggregate formation at 1,500s^{-1} and b) at 10,000s^{-1}. (In all images scale bar: 40µm)

The percentage area coverage showed the same results and is demonstrated exemplarily for 1,500s^{-1} and 10,000s^{-1} in figure 29 a) and b). The influence of the larger multimers was more significant at lower vWF concentrations compared to higher ones. At 1,500s^{-1} and at the beginning of the flow exposure the large multimers were crucial for the aggregate forming process, at flow times increasing 2min the multimers were comparable (fig. 29 c)). The large multimers were essential for all flow duration times at 10,000s^{-1} (fig. 29 d)). To show the difference between the multimers the percentage area coverage for 1,500s^{-1} and 10,000s^{-1} is illustrated in figure 29 c) and d). The standard deviations between the various donors were pronounced (in the range 10% - 100%, depending on the multimer size, the shear rate and the

duration time), but the distributions remained almost constant. To better outline the impact on the multimer size length, no standard deviations are depicted in figure 29.

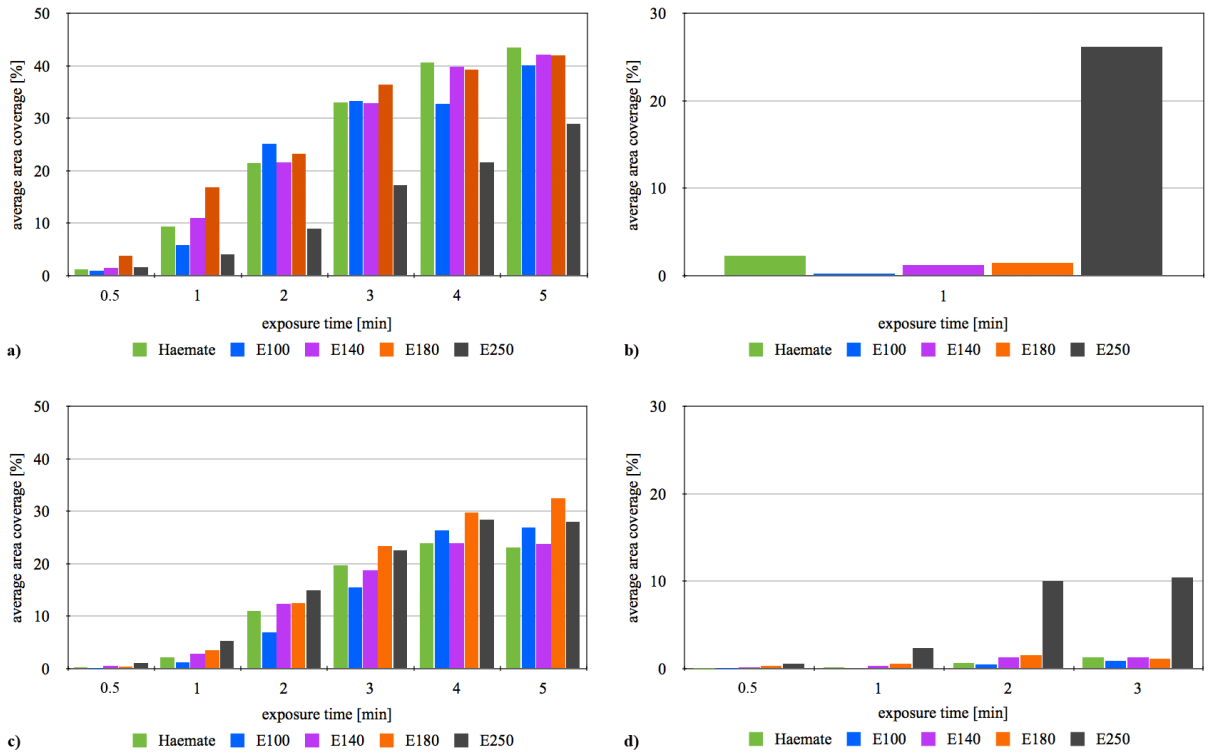

Figure 29: Percentaged area coverage of platelet aggregates on collagen. Haemate and Haemate subfractions were added to the blood suspension at final concentrations of a), b) of 100µg/ml and c), d) of 10µg/ml. Image a), c) shows platelet aggregate formation at shear rates of 1,500s^{-1} and b), d) at 10,000s^{-1}.

These results indicate that at low vWF concentrations the large multimers were essential for the aggregate formation process at the beginning of the flow exposure (30s, 1min) at 1,500s^{-1} and at 10,000s^{-1}. This was comparable with the effect of Haemate by comparing the vWF products. Increasing the vWF concentration could minimize or even invert the effect of the large multimers. For 1,500s^{-1} the large multimers showed less aggregates compared to the other subfractions. These results fit to the results observed for the vWF products. In contrast, at 10,000s^{-1} and the higher vWF concentration the large multimers showed most of the formed aggregates, which was contrary to the result of the vWF products. By increasing the vWF concentration the effect of the large multimers could be disregarded according to the self assembly of the smaller multimers. Next, the influence of the vWF products on the vWF-collagen and on the platelet-vWF interaction was carried out with washed blocked blood cell suspensions. At high vWF concentrations increasing shear rates decreased the platelet adhesion. For 1,500s^{-1} and 4,000s^{-1} Wilate showed almost four times more adhered platelets on the surface compared to the other vWF products. For 10,000s^{-1} almost all products were equal in their adhesion and for 20,000s^{-1} Haemate and Haemoctin showed most of the adhered platelets. Instead, for lower vWF concentrations the adhesion behaviour of the platelets

changed. At 1,500s^{-1} the single platelet adhesion on collagen was comparable for all investigated vWF products, but for 10,000s^{-1} Wilate showed only one half adhered platelets compared to the other products. The error bars between the donors were large (< 90%), but the effects remained almost unchanged. This suggests that the vWF-collagen and platelet-vWF interaction is slightly influenced by the multimer distribution size except for Wilate. At physiological vWF concentration the binding affinity of Wilate and collagen might be reduced by an increasing Wilate concentration. Overall, the differences in the multimer distribution only minimal influence the platelet functions and vWF interactions with platelets or collagen. These results are comparable with Mouton and coworkers. They reported that there were no significant differences among 6 commercially available vWF concentrates (Haemate HS, Immunate STIM lus, Facteur Willebrand-LFB, Octanate, Wiloctin Alphanate) with regard to platelet adhesion to de-endothelialized, human vessel walls under arterial flow conditions, although these concentrates varied considerably in terms of content of high molecular weight vWF multimers (Mouton et al., 2004). While, some products have multimeric patterns very similar to that of normal human plasma, no concentrate contains the full amount of the largest vWF multimers, as plasma does (Metzner et al., 1998; Mannucci et al., 1994).

In conclusion, for patient treatment the physiological concentration of vWF products is crucial. As the variations of the various vWF products were minimal in the investigated platelet functions, all vWF products might be applicable for patients' treatment, but further in vivo investigations need to be done.

7. Influence of the von Willebrand Factor loss of function mutant

7.1 Introduction

Dysregulated interactions between the GPIbα and vWF A1 domain or mutations in both cause bleeding either in vWF disorders such as vWD or in thrombotic disorders such as thrombotic thrombocytopenic purpura (Yago et al., 2008; Sadler et al., 2006). Due to the multifunctional vWF properties vWD is known for its marked heterogeneity (Schneppenheim 2004; Schneppenheim and Budde 2004) (more details on vWD types see chapter 6.1). In 1989 the genomic vWF structure was solved by polymerase chain reaction (PCR) based methods. This was the first step to qualitatively describe the different vWD types and to elucidate new vWD types in patients (Schneppenheim 2004; Schneppenheim and Budde 2004; Mancuso et al., 1989). This investigated vWF loss of function mutant (lofm) is genetically recombinant produced by Schneppenheim and coworkers after PCR analysis of the patient's vWF protein. Schneppenheim and coworkers will publish the genomic structure and more clinical details of the vWF mutant. Up to now the impact of this patient vWF lofm on the platelet functions is unknown. As the diagnosis and classification of vWD in the different subtypes is difficult, the biophysical mechanism of platelet-vWF mutant interaction will be in the focus of the following chapter. The platelet functions were investigated by a flow chamber set-up, equipped with a RICM or an epifluorescence microscopy, to analyse the platelet adhesion on either vWF or collagen as well as the tether formation on and the rolling velocities over vWF.

7.2 Results and Discussion

7.2.1 vWF coated surface

Whole unactivated blood (preparation see chapter 3.1.2) was perfused in a flow chamber equipped with a RICM (set-up see chapter 3.2.1) and a surface coating of either a vWF WT or vWF lofm. For shear rates ranging from 1,500s^{-1} to 20,000s^{-1}, platelets arrested from flowing blood onto the immobilized vWF and pulled tethers (fig. 30).

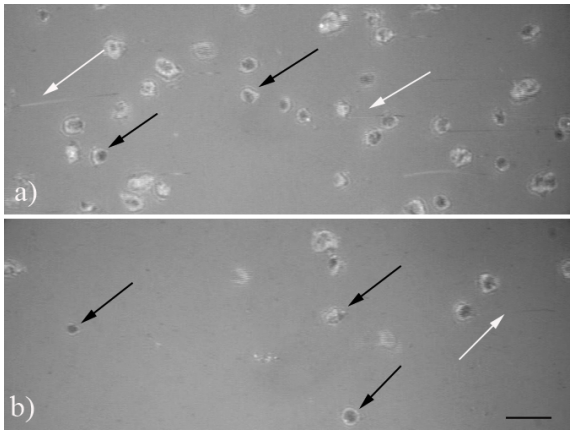

Figure 30: RICM images of blood samples (blocked) over different vWF coatings at shear rates of 10,000s^{-1}. Image a) vWF WT coating and b) vWF lofm coating after shear was applied for 25s. Arrested platelets, platelets with tether and ruptured tethers are shown. Black arrows exemplary indicate the platelet contact area and the white arrows exemplary show tethers and ruptured tethers. Note the large number of platelets and tethers for vWF WT coating. (In all images scale bar: 5 µm)

To analyze the platelet adhesion in detail, the adhered platelets on the vWF surface of the flow chamber (fig. 30) were counted by using different still RICM images of blood samples after the exposure of platelets to a shear flow of 1,500s^{-1} and 20,000s^{-1} for 25s. Due to this static capture the dynamic behaviour of the platelets remained unresolved, e.g. the differences in the rolling velocity as well as in the adhesion time. To clarify the dynamic platelet function the platelets rolling velocities over the vWF surface were calculated. The adhered platelet amount on the vWF surface and the rolling velocities of the platelets were strongly influenced by the vWF coated surface and the shear rate. With increasing shear rate the platelets adhered to the surface increased for vWF WT until 10,000s^{-1} and for the vWF lofm until 4,000s^{-1}. For higher shear rates the difference between the vWF WT and vWF lofm was more significant compared to lower shear rates. At 1,500s^{-1} and 4,000s^{-1} the average amount of platelets adhered to the vWF WT surface is about 50% increased compared to the vWF lofm surface and at 10,000s^{-1} even by 75% (fig. 31 a)). However, the rolling velocities enhanced with higher shear rates and there was no reduction observed until 10,000s^{-1}. For vWF WT the slope was almost linear (~ 1) between 1,500s^{-1} and 10,000s^{-1}, but for the vWF lofm the slope between 1,500s^{-1} and 4,000s^{-1} was almost 4 and for 4,000s^{-1} and 10,000s^{-1} was almost 0.5. The rolling velocities at 1,500s^{-1} were reduced by 42% for vWF WT coating compared to the vWF lofm, at 4,000s^{-1} by 61% and at 10,000s^{-1} by 51% (fig 31 b)). The standard deviations in the platelet adhesion of the various donors were in the range between 20%-30%. However, the tendencies remained almost unchanged, thus the error bars are not depicted in figure 31.

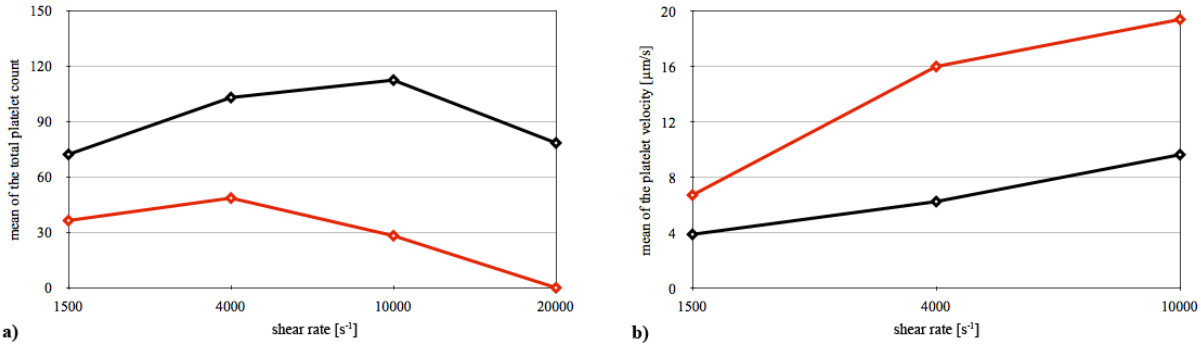

Figure 31: a) Average of the total platelet count per frame (5,000µm²) and b) average rolling velocities of different vWF coatings at increasing flow rates. The black curve represents the total platelet count on vWF WT, the red black curve on vWF lofm.

Following the presented results it can be concluded, that the stretching properties of the vWF protein might be essential for the platelet adhesion behaviour. Above the critical shear rate the vWF protein is activated and increases the A1 domain exposure and thus, the platelet adhesion to the surface. Above 10,000s^{-1} the force acting on the platelets is too large to show the same amount of platelet adhesion. Due to a vWF lofm the platelet-vWF interaction is reduced and therefore, the platelet adhesion to the vWF surface. The shear rate influence on the platelet adhesion is also discussed in chapter 5 and 6. From this statistical analysis of bound platelets it seemed reasonable to extract the difference in adhesion energy ΔG of platelets adhered on a vWF WT or a vWF lofm surface by applying the Boltzmann equation (adapted to equation (5));

$$\frac{n_{WT}}{n_{lofm}} = e^{-\Delta G / k_B T} \tag{8}$$

where k_B is the Boltzmann constant, ΔG is the change in adhesion energy between vWF WT and vWF lofm, T the temperature and n_{WT} and n_{lofm} is the average fraction of the amount of platelets on the vWF WT and vWF lofm surface (Fleck et al., 2002; Alberts et al., 2003). Using the average amount of platelets adhering to the vWF WT and to the vWF lofm surface resulted in an energy difference ΔG in the order of 0.7 k_BT for 1,500s^{-1}, 0.7 k_BT for 4,000s^{-1} and 1.4 k_BT for 10,000s^{-1}. These variations in the absorption energy extracted by platelets adhering to vWF WT or lofm surface are too low compared to adhesion energy differences of cells typically found in the literature (Simson et al., 1998). The detailed discussion is depicted in chapter 4.2. To complete the adhesion behaviour of platelets on vWF, the weak contact area on the bottom of the flow chamber was analysed after platelets were exposed to a shear flow ranging from 1,500s^{-1} to 20,000s^{-1} for 25s. For vWF WT surface coating and at all investigated shear rates the platelets were homogeneously distributed in the range between 1-15µm^2, whereas for vWF lofm surface coating the distributions ranged from 1-13µm^2 (fig.

32). The average contact area was calculated by integrating the histograms of each donor and taking the average, to better compare both investigated vWF proteins (inset in fig. 32). The average of the platelet adhesion area at all investigated shear rates was comparable for both vWF coatings and is listed in table 11.

Table 11: Summary of the average weak contact area and the standard deviations to the vWF surface

(mean +/- sd)	1,500s^{-1} [µm²]	4,000s^{-1} [µm²]	10,000s^{-1} [µm²]	20,000s^{-1} [µm²]
WT	4.8 +/- 0.5	5.1 +/- 0.7	5.4 +/- 0.9	5.6 +/- 0
lofm	4.8 +/- 0.6	5.4 +/- 0.2	5.3 +/- 0.6	0

Exemplarily at 10,000s^{-1} the weak adhesion area and the average weak adhesion area are depicted in figure 32. The standard deviations were calculated by the changes of various donors. Due to a better overview the error bars are not shown in figure 32.

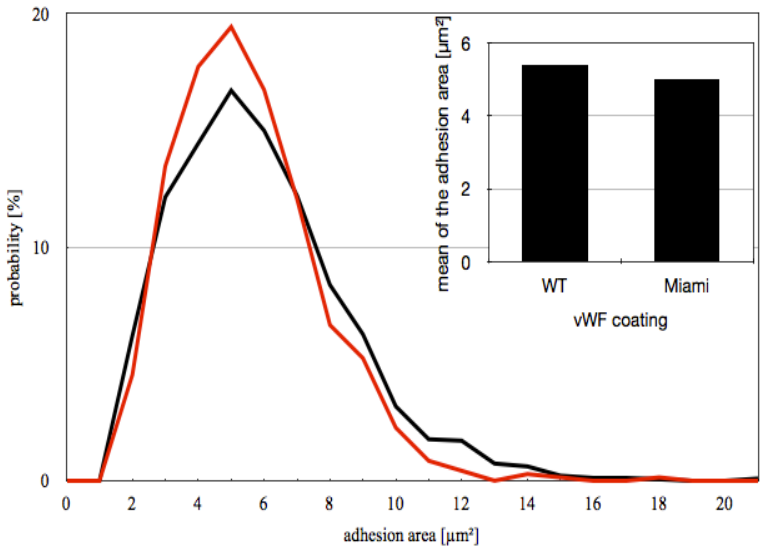

Figure 32: Platelet weak adhesion area distribution on vWF WT and vWF lofm at 10,000s^{-1}: the weak contact area is plotted against the probability P (∑P=100%). The black curve represents the adhesion area of platelets on vWF WT, the red one on vWF lofm. The inset shows the mean of the weak adhesion area of platelets of variable vWF coatings at a flow rate of 10,000 s^{-1}.

These results indicate a massive influence of the different vWF coatings on the platelet adhesion amount on the surface, but the adhesion area itself remained unaffected. Thus, vWF mutations will as well affect the tether formation process like the adhesion processes. To qualitatively understand the tether formation process, the tether length on the bottom of the flow chamber (white arrows in fig. 30) was quantified after exposing platelets to a shear flow of 1,500s^{-1} to 20,000s^{-1} for 25s. While, for 1,500s^{-1} and 4,000s^{-1} the tethers at the platelet body showed for both vWF coatings a fairly sharp distribution with a most likely tether length of around 2µm. However, at 10,000s^{-1} the tethers at the platelets were more homogeneously

spread over the range between 1-28µm for vWF WT and in the range between 1-16µm for vWF lofm. As at 20,000s^{-1} no platelets adhered to the vWF lofm surface, the tether formation was hindered, but for vWF WT the tethers at the platelet were homogenously spread over the range between 1-24µm. The ruptured tethers on vWF WT at 1,500s^{-1} were more homogenously spread in a range between 2-7µm, whereas the ruptured ones on vWF lofm showed a fairly sharp distribution with a most likely tether length of around 2µm. The number of ruptured tethers on vWF lofm was bisected compared to vWF WT. At 4,000s^{-1} on vWF WT, the ruptured tethers showed a fairly sharp distribution with a most likely tether length around 3µm. On vWF lofm formed 14% of vWF WT ruptured tethers. This small amount was randomly distributed in a range between 3-7µm. However, at 10,000s^{-1} on vWF WT the ruptured tethers were more homogenously distributed in a range between 2-17µm. On vWF lofm the ruptured tethers formation was hindered. At 20,000s^{-1} on vWF WT the ruptured tethers showed a fairly sharp length distribution of around 2µm. The corresponding length distribution of tethers at the platelet and ruptured ones is exemplarily shown for 10,000s^{-1} in figure 33.

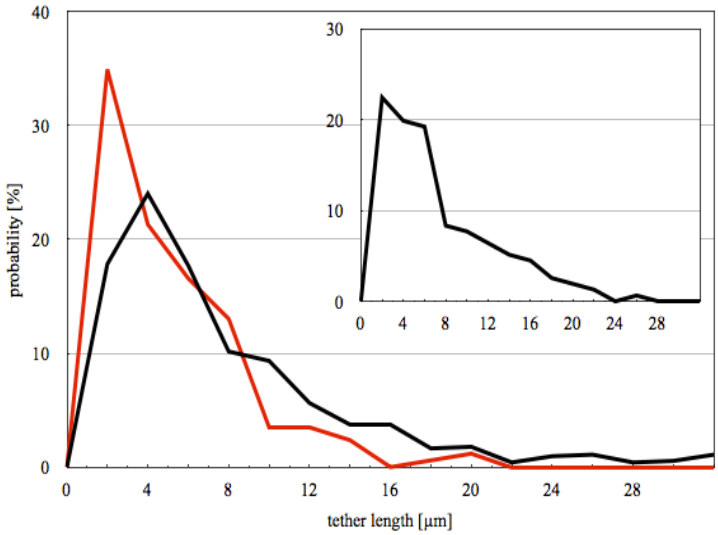

Figure 33: Tether length distribution curves for platelets on vWF WT and vWF lofm coatings at a shear rate of 10,000s^{-1}: the tether length is plotted against the probability P (∑P=100%). The black curve represents the tether length of vWF WT surface and the red curve of vWF lofm surface. The inset shows the ruptured tether length distribution of platelets at a flow rate of 10,000s^{-1}. The vWF lofm did not form any ruptured tethers at the depicted shear rate.

Next, the total average tether length was calculated by integrating the histograms of each donor and taking the mean. The standard deviations of the various donors were as well evaluated to better estimate the variations of both vWF coatings. At all investigated shear rates the average of the tether length was different for the vWF WT and the vWF lofm coating. The vWF WT coating showed a maximal average tether length at 10,000s^{-1} and vWF

lofm at 4,000s^{-1}. The shear dependent increase and decrease were minimal. To better compare both coatings the total average tether length and their standard deviations are listed in table 12.

Table 12: Summary of the average tether length and the standard deviations to the vWF surface coated by different vWF products (10U).

(mean +/- sd)	1,500s^{-1} [µm]	4,000s^{-1} [µm]	10,000s^{-1} [µm]	20,000s^{-1} [µm]
WT	4.5 +/- 0.8	6.5 +/- 0.8	6.8 +/- 0.5	5.6 +/- 1.2
lofm	2.8 +/- 0.5	3.8 +/- 1.3	3.7 +/- 1.1	0

To complete the influence of the vWF coatings on the tether formation process the average amount of the total tethers was analysed by counting the tethers adhered on the vWF surface. The changes between vWF WT and the vWF lofm were significant. The total tether count almost bisected for a shear rate of 1,500s^{-1} for vWF lofm, at 4,000s^{-1} the amount of tethers was 64% decreased and at 10,000s^{-1} even 80% lowered compared to tether numbers on vWF WT (data not shown) (fig. 30, white arrows). On vWF WT surface at 1,500s^{-1} 7% ruptured tethers were formed, on vWF lofm 12% compared to each total tether count. In addition, at 4,000s^{-1} vWF WT showed 13% ruptured tethers and vWF lofm 4%. In contrast, at 10,000s^{-1} vWF WT demonstrated 18% ruptured tethers and vWF lofm 1%. At 20,000s^{-1} vWF WT formed 32% ruptured tethers. The changes of the different donors were significant (in the range between 20%-60%, depending on the vWF coating and the shear rate), but the effects remained almost constant. These results indicate a crucial dependence of the vWF coating on the tether formation process and the platelet adhesion to the vWF surface, but not on the weak adhesion area on the vWF surface. By studying the specific interactions between platelets and vWF under controlled flow conditions, the effect of alterations of a vWF lofm on the platelet behaviour was identified. A reduction in the apparent platelet adhesion to the vWF lofm surface was observed. This was combined with an increased platelet rolling velocity. This behaviour is assumed to be a consequence of the reduced GPIbα and A1 domain binding affinity of the vWF lofm. The platelets adhesion area on the vWF surface is not influenced by alterations in the vWF A1 binding site. Consequently, after the initial platelet-vWF interaction the adhesion area formation takes place independent of a reduced A1 binding affinity. The A1 domain is crucial for the number of first platelet adhesion contacts as well as for the platelet adhesion time on the vWF surface, but the platelet weak adhesion area is unchanged by variations in the number of adhesion contacts and the adhesion time. In contrast, the tether formation is governed by alterations in the A1 domain, as the first contact and the adhesion

time are critical for the tether formation process. A reduction in the binding affinity of the vWF A1 domain and the GPIbα causes a decrease in the tether length. For optimal and maximal tether formation a strong binding of the GPIbα to the surface is coactive. The force acting on the platelets, which is altered by the shear rates, is also a stringent requirement for the investigated platelet properties. At a specific force or shear rate for most vWF coatings at 10,000s^{-1}, which is dependent on the platelet-vWF interaction, the platelet adhesion and the tether number are maximal, however the adhesion area and the tether length are minimal affected. After this threshold force point the adhesion and the tether formation process is reduced. As the probability of platelet adhesion is reduced due to the increased applied force, the possibility of tether formation is also decreased. To mimick the in vivo situation of platelet aggregate formation, the surface was coated with collagen and both vWF types were added to the blood suspension.

7.2.2 Collagen coated surface

To quantify the platelets aggregate formation, the aggregate formation was examined by using static epifluorescence microscopic images of blood samples after the exposure of platelets to a shear flow of 1,500s^{-1} to 10,000s^{-1} for 30s to 2min. The aggregate dimensions were dependent on the shear rate, the time of exposure of the shear rate, and the vWF added to the blood suspension. For vWF WT blood suspension the aggregate formation increased with the duration time and the shear rate. In contrast, for the vWF lofm containing blood suspension the aggregate formation was enhanced with duration time, but reduced for increasing shear rates. At all investigated shear rates and duration times the difference in the percentage area coverage was maximal at 120s duration time between vWF WT and vWF lofm. At 1,500s^{-1} and a 120s flow time duration vWF WT showed twice the average of the area coverage compared to vWF lofm, at 4,000s^{-1} the increase was 7 times higher and at 10,000s^{-1} even 25 times higher compared to vWF lofm (fig. 34). The standard deviations of the various donors were calculated. The error bars for vWF WT were in the range of 21% and 30% and for vWF lofm of 42%-100%, but the trends remained unaffected. Due to a better overview the error bars are not depicted in figure 34.

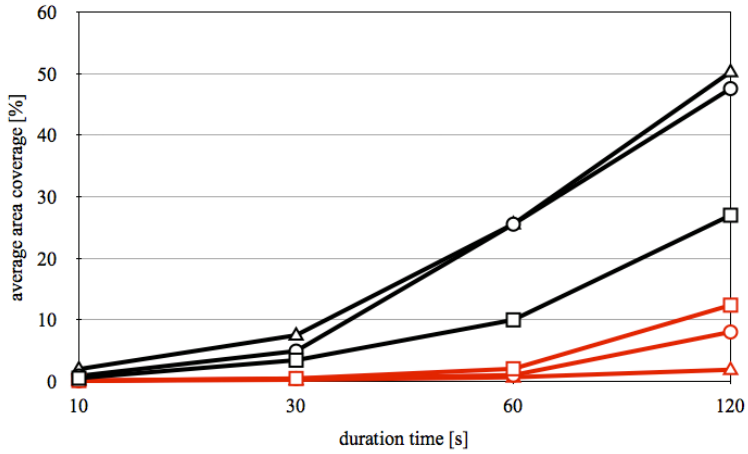

Figure 34: Percentage area coverage of platelet aggregates on collagen. VWF WT or vWF lofm were added to the blood suspension at final concentrations of 10µg/ml. The black curve represents the vWF WT blood suspension and the red curve the vWF lofm one. The curves with a quadrat symbol show platelet aggregate formation on collagen at shear rates of 1,500s^{-1}, the curves with the circle of 4,000s^{-1} and the ones with a triangle of 10,000s^{-1}.

Furthermore, the most frequent aggregate size was analysed. This size was comparable for both vWF WT and vWF lofm at all investigated shear rates and duration times. However, the average aggregate size increased for both vWF types with increasing duration time. For vWF WT the aggregate size increased with shear rate, but for vWF lofm the aggregate size reached a maximum at 4,000s^{-1}. Differences in the aggregate size between vWF WT and vWF lofm were pronounced at all investigated shear rates and duration times of 120s. At 1,500s^{-1} and 4,000s^{-1} the aggregate size of vWF WT was 3 times higher and at 10,000s^{-1} 15 times enhanced compared to vWF lofm. The standard deviations were calculated by the changes of the various donors. As aggregate size is homogenously distributed, the error bars were significantly high (< 100%). These results show a significant impact of the soluble vWF in the blood suspension on the amount of platelet adhesion to the collagen surface. The soluble vWF lofm showed a clear reduction in the apparent platelet adhesion to the collagen surface compared to vWF WT. This behaviour might be a consequence of the reduced binding affinity of the vWF lofm to platelets and maybe to collagen. The most frequent aggregate size was not influenced by alterations in the vWF-binding site. In addition, the force acting on the platelets, which is altered by the shear rates, and the duration time are a stringent requirement for the platelet adhesion to collagen and therefore, for the aggregate formation. Increasing shear rate and flow duration time enhanced the platelet adhesion and aggregate formation for vWF WT due to the increased platelet probability near the vessel and an enhanced vWF-platelet and vWF-collagen binding affinity compared to vWF lofm. The closure of the vascular injury is strongly decreased for vWF lofm compared to vWF WT, as the adhesion and aggregate formation on collagen is strongly lowered for the vWF lofm.

Over all, the presented results showed that the vWF lofm strongly influenced the platelet adhesion, aggregate formation and tether forming processes. This can help to further understand the role of this specific short-range lock and key interaction, especially the effect of vWF mutants in the vWD. Furthermore, these investigations might be the first step for a new testing tool for the difficult and complex classification of the various vWD types. This knowledge might help to improve clinical therapy plans.

8. Characterization of platelet-vWF aggregates

8.1 Introduction

Thrombotic arterial occlusion requires fast accrual and prolonged arrest times of initially unstimulated platelets. This process is controlled by shear rate activation of vWF. Exclusively at high shear rates, this leads to the reversible platelet aggregate-vWF network formation. This exclusively occurs at the interface of immobilized and soluble vWF. The vWF mediated platelet aggregation is independent of the activation of the αIIbβ3 and their functionality. The interplatelet connections are formed by adhesive vWF proteins functionally altered by tensile stress (Ruggeri et al., 2006). Multimeric vWF normally does not agglutinate circulation platelets, except from being immoblized at sites of vascular injury or being exposed to massively high shear rates, exceeding 20,000s^{-1} (Ruggeri et al., 2006; Dong et al., 2001). However, in patients with type 2B vWD plasma vWF may spontaneously interact with platelet GPIbα (Szanto et al., 2007; Sadler 2005; Matsuhita and Sadler 1995). These mutations in the vWF protein directly affect the mechanical properties of the isolated A1 domain bonds with GPIbα. Due to the agglutination the large vWF multimers are depleted, which might cause thrombocytopenia (Yago et al., 2008). The characterization of the platelet-vWF aggregate formation remains unresolved until now. To clarify the role of the vWF multimer distribution size and the sugar content in the platelet agglutination, the formation of platelet-vWF aggregates in a flow chamber device with adjustable shear rates with dimeric vWF A1 domain coating was investigated. Over collagen the impact of vWF mutations compared to recombinant full-length vWF was examined. The shear rates were varied from 0s^{-1} to 50,000s^{-1} to report the thrombus growth rates.

8.2 Results and Discussion

8.2.1 Dimeric vWF A1 surface coating

Whole blocked blood as well as washed blocked blood cell suspensions (preparation see chapter 3.1.2) reconstituted with various labelled or unlabelled multimeric vWF proteins were perfused in a flow chamber (set-up see chapter 3.2.1) with an immobilized recombinant isolated dimeric vWF A1 domain or a collagen surface coating. Recombinant full-length

vWF, healthy donor plasma vWF, commercially vWF preparation from pooled human plasma (Haemate), subfractions from the same production process containing only small (E100) or large (E250) size multimers and sugar free and sugar containing vWF added to the blood cell suspension were investigated. The main differences in the investigated vWF proteins are the vWF multimer distribution and the sugar content. Recombinant full-length vWF shows the largest multimers and additionally, the whole multimer distribution of normal plasma vWF. In the vWF product Haemate the multimer distribution is comparable to normal plasma vWF, whereas E100 contains only the small multimers and E250 only the large multimers (fig. 27). Additional detailed information on commercially vWF preparations from pooled human plasma is depicted in chapter 6. Both sugar free and sugar containing vWF show comparable multimer size distributions. The effect of serial increasing shear rates from $0s^{-1}$ to $50{,}000s^{-1}$, as the thrombus growth rate was reported to be a linear function of very high shear rates beyond $40{,}000s^{-1}$ (Ku and Flannery 2007) on the the platelet-vWF aggregate formation was investigated. Above a critical threshold of $10{,}000s^{-1}$ to $30{,}000s^{-1}$ dependent on the vWF protein in the blood suspension inactivated platelet-vWF aggregates started to roll over the immobilized dimeric vWF A1 domain surface without adhering. The progressive disappearance of rolling aggregates below the shear rate threshold point could be visualized in real time and therefore, the absence of platelet-vWF conglomerates in areas exposed to lower shear rates. These conglomerates continually rolled in the flow direction above the threshold shear rate, grew in size with increasing shear rate, and were completely reversible below the critical shear rate threshold, although platelet activation was completely inhibited. Additionally, these formed aggregates differed in size in dependence to the added multimeric vWF proteins. The formation of vWF strands in and around those platelet-platelet aggregates, which grew up to several microns thickness and up to several tens of microns length, was observed. These resulting large vWF networks could be visualized and analysed for the first time. These results showed that platelets were enmeshed in the vWF networks. The threshold aggregate forming shear rate and the size of the platelet-vWF conglomerates were analysed. For recombinant full-length vWF the shear rate threshold was at around $15{,}000s^{-1}$ (fig. 35 b) and d); supplemental material). The reversibility of activation-independent aggregate formation is shown in figure 35.

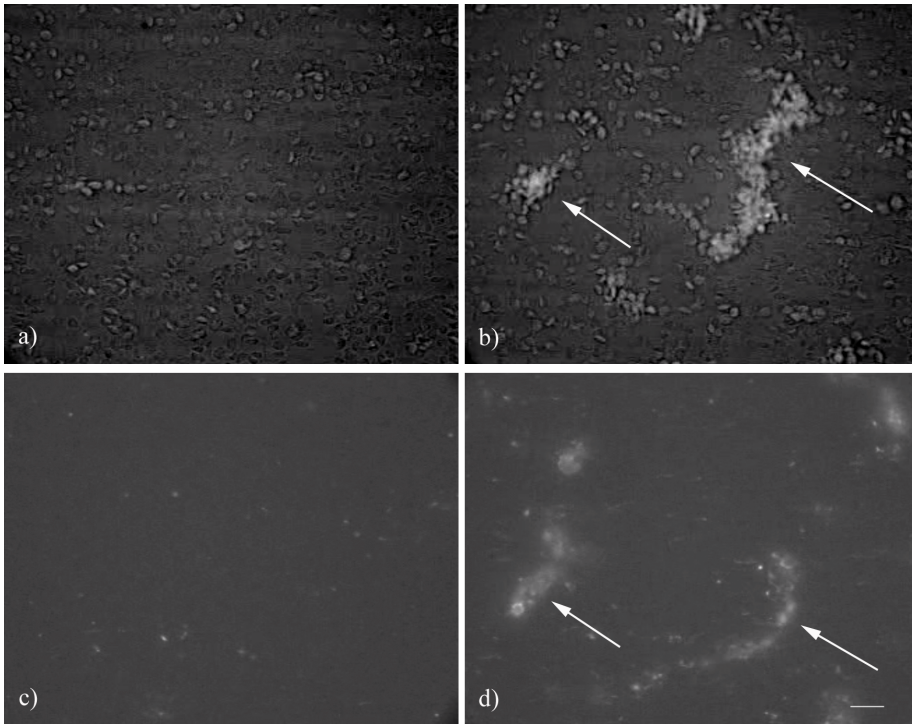

Figure 35: Microscopic still images taken from real-time video-recording of blood flow over immobilized dimeric vWF A1 domain at shear rates a) and c) of 10,000s^{-1} and b) and d) of 30,000s^{-1}. The blood cells were washed plasma-free and resuspended in buffer containing recombinant full-length vWF. Image a) shows the single platelet adhesion occurring below the critical shear rate threshold of 15,000s^{-1} and images b) and d) depict reversible platelet-vWF aggregates formed above the critical shear rate and rolling over the surface without attaching to it. In images a) and b) double illumination with fluorescence and bright field was used, and thus the aggregate appears brighter due to the enmeshed fluorescently labelled recombinant full-length vWF. Comparison between c) and d) demonstrate appearance of reversible, fluorescent vWF networks rolling over the surface only above the critical shear rate threshold in d) (white arrows). Image c) and d) depict the identical region. (In all images scale bar: 10µm)

Due to the various preparation processes healthy donor plasma vWF and commercial vWF preparation from pooled human plasma (Haemate) and subfractions from the same production process containing only small (E100) or large (E250) size multimers in solution could not be labelled. On the one hand the extraction of the poor vWF out of the whole blood is difficult and on the other hand the fluorescence labelling of the vWF requires at least 4 days, thus the same whole blood from the healthy donor could not be used for the flow experiments, as the whole blood would be too long not under physiological conditions. The vWF commercially prepared from pooled plasma contains a large amount of factor VIII, due to the labelling the vWF protein agglomerated. To solve this problem the enmeshed platelets were fluorescently labelled to observe the reversible rolling aggregate formation in real time. Plasma vWF (fig. 36 a); supplemental material) and Haemate (fig. 36 c); supplemental material) in the plasma-free and resuspended in buffer platelet suspension exhibited the same critical shear rate as the recombinant vWF (15,000s^{-1}), but for E100 no rolling aggregates could be observed (data not shown) and for E250 the critical shear rate decreased to 10,000s^{-1} (fig. 36 b); supplemental

material). The reversible aggregate formation was not influenced by the different vWF protein preparations.

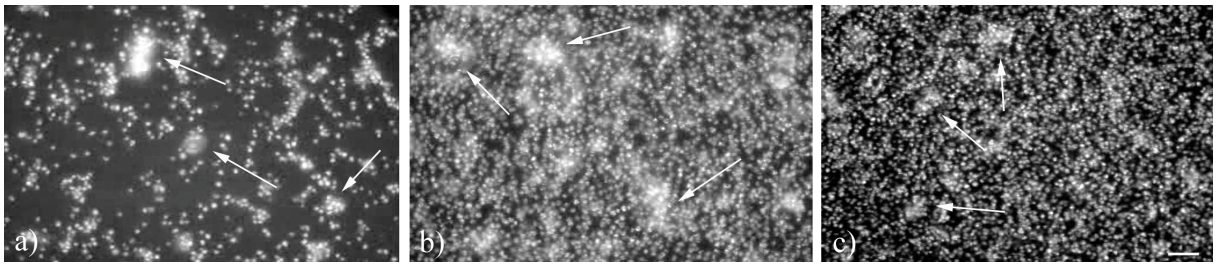

Figure 36: Fluorescent microscopic still images taken from real-time video-recording of blood flow over immobilized dimeric vWF A1 domain at shear rates of 20,000s^{-1}. The blood cells were washed plasma-free and resuspended in buffer containing the fluorescent dye mepacrine (10µM) and a) plasma vWF, b) E250 and c) Haemate over dimeric vWF A1 domain (20µg/ml). Although, activation was completely inhibited, platelet-vWF aggregates formed in varying size dependent on the added vWF. White errors indicate exemplarily the reversible platelet-vWF aggregates rolling over the surface without attaching to it. (In all images scale bar: 20µm)

Sugar free vWF showed no rolling aggregates formation (data not shown), but sugar containing vWF exhibited rolling aggregates above a critical shear rate of 30,000s^{-1} (fig. 37 b); supplemental material). The reversible platelet-vWF conglomerate formation process was crucial dependent on the content of sugar of the vWF protein. Due to the fluorescence labelling the sugar containing vWF networks could be visualized and compared with the recombinant vWF formed networks and aggregates (fig. 37 a)).

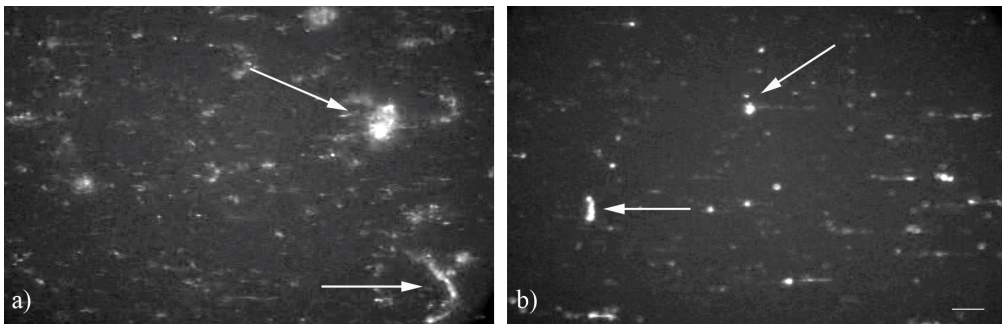

Figure 37: Fluorescent microscopic still images taken from real-time video-recording of blood flow over immobilized dimeric vWF A1 domain (20µg/ml). The blood cells were washed plasma-free and resuspended in buffer containing fluorescently labelled a) recombinant full-length vWF at a shear rate of 20,000s^{-1}, b) sugar containing vWF at a shear rate of 40,000s^{-1}. White errors indicate exemplarily the platelet-vWF aggregates. Although, activation was completely inhibited, platelet-vWF aggregates formed in varying size dependent on the added vWF. (In all images scale bar: 10µm)

These results are in line with Ruggeri and coworkers, who described platelet-vWF aggregates, so called “rolling aggregates” over fibrillar collagen type I and vWF (c = 20µg/ml) coated surfaces. By electron microscopy the presence of membrane protrusions connecting platelets to one another and to the surface was demonstrated (Ruggeri et al., 2006). The effects of perfusion fixation on the vWF networks could be analysed by vWF labelling and thus, observed microscopically. After fixation the morphology of rolling aggregates was preserved, but the vWF networks vanished. Consequently, the vWF networks resolve was hindered due

to perfusion fixation. In the experiments of Ruggeri only the platelets were labelled and only the platelet-platelet aggregates without the interconnecting part could be visualized by fluorescence microscopy. Due to the vWF labelling, it was possible to resolve the interconnecting parts of the platelet-platelet aggregates. To zoom qualitatively in the aggregate formation process the size distribution of the formed platelet-vWF conglomerates was quantified. The recombinant vWF networks showed an increasing maximal aggregate length with increasing shear rate. The maximal length for 20,000s^{-1} was around 43µm, for 30,000s^{-1} around 87µm and for 40,000s^{-1} around 146µm, but the aggregate count decreased with increasing shear rate (fig. 38). As the aggregates increased in size by increasing the shear rate, the larger conglomerates picked up the smaller ones and assembled. The amount and the maximal size of the sugar containing vWF aggregates were reduced by more than 90% of the recombinant vWF. The maximal size for 40,000s^{-1} was around 8µm.

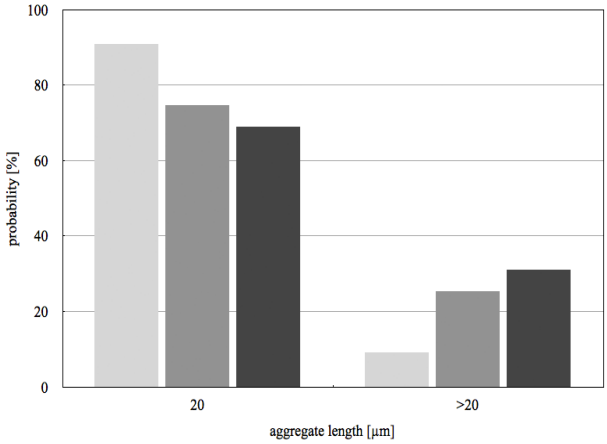

Figure 38: VWF conglomerate length distribution of recombinant vWF with different shear rates: the aggregate length is plotted against the probability P (∑P=100%). The bright grey histogram represents a shear rate of 20,000s^{-1}, the middle grey histogram a shear rate of 30,000s^{-1} and the dark grey histogram a shear rate of 40,000s^{-1}.

For the other vWF proteins the vWF labelling was not possible and therefore, only the length of the formed labelled platelet aggregates was measured. These aggregates were different in size compared to the labelled vWF networks. The labelled platelet conglomerates formed visually larger aggregates then the vWF networks alone. For 20,000s^{-1} washed blocked cell suspension formed aggregates with a maximal length of around 57µm, Haemate of around 32µm and E250 of around 43µm. However, Haemate formed most of the aggregates, followed by E250 and whole blocked blood had less aggregates (fig. 39).

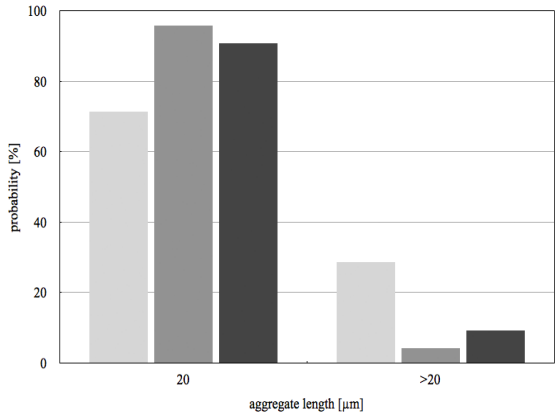

Figure 39: Platelet-v WF conglomerates length distribution at 20,000s^{-1} shear rate: the aggregate length is plotted against the probability P (∑P=100%). The bright grey histogram represents washed blocked blood containing plasma vWF, the middle grey histogram containing Haemate and the dark grey histogram containing E250.

These results show a massive influence of the vWF multimer distribution, the vWF sugar content and the shear rate on the platelet-vWF conglomerate formation. The differences in the aggregate length distribution are mainly due to the variation in the size distribution of the multimers, which expose various numbers of A1 domains and thus, a different number of binding sites for GPIbα. In the elongated vWF structure the concentration of the A1 domains, which are exposed to the blood flow, is higher for the recombinant full-length vWF compared to plasma vWF. The size of the aggregates of normal plasma vWF was larger than for E250, although E250 was assembled of the largest multimers of the vWF Haemate protein. Therefore, the exposure of the A1 domain should be increased for E250 compared to normal plasma vWF. Not only the A1 domain exposure might be a crucial factor for the formation of rolling aggregates, but also the binding strength and the stretching properties of the vWF molecule. Instead, the shear rate threshold was decreased for E250 compared to plasma vWF. A possible reason could be the enhanced binding strength or stretching properties of E250 compared to plasma vWF. This assumption might be in line with Ayra and coworkers, who reported that the recombinant vWF bond is around one third more powerful as the plasma vWF bond (Ayra et al., 2002 a)). Consequently, the bond strength might not be the influencing factor for the shear rate threshold point, as the recombinant vWF and the plasma vWF showed the same critical shear rate for aggregate formation. Thus, the stretching properties might be enhanced for E250 compared to the recombinant and the plasma vWF. The large vWF multimers might play the major role in the formation of the platelet-vWF conglomerates as no rolling aggregates were formed in the absence of larger multimers. The small multimers of the vWF might not expose enough binding sites for the GPIbα and might not be as functional and active as the larger ones. The reduced elongation probability might be

as well a crucial factor. Furthermore, rolling aggregates of sugar free vWF were not observed. Sugar free plasma vWF might not provide the possibility to increase the exposure of the A1 domain, as the stretching properties are limited compared to the sugar containing plasma vWF. A model opinion that sugar free vWF might not be able to recoil at the same shear rate as the sugar containing vWF is introduced. At a critical shear rate in the range of $2{,}000s^{-1}$ to $5{,}000s^{-1}$ vWF is elongated (Schneider et al., 2007). The sugar free vWF might stretch at higher shear rates and thus, expose only at higher shear rates a higher concentration of A1 domains, as the globular vWF might be more compact and adhesive due to the loss of sugar molecules. Each vWF monomer contains N- and O-linked olgiosaccaride chains, which together account for almost 20% of the final monomeric mass (Titani et al., 1986). The presented results coincide with previous studies, which have shown that glycan structures cause protein-protein interactions through either conformational and/ or charge-induced mechanisms (Mitra et al., 2006; Toyoda et al., 2002; Nishiyama et al., 2000; Wormald and Dwek 1999; Kimura et al., 1998; Wyss et al., 1995; Narhi et al., 1991). The sugar content is crucial not only for the stretching properties, but also recently reported for the vWF clearance and the cleavage by ADAMTS 13. The absence of sugar on vWF reduces the probability of cleavage, but increases the likelihood of clearance (McGrath et al., 2010). The investigated shear rate range might be not high enough to observe platelet-vWF conglomerates of sugar free vWF. Increasing the shear rate was the basis for the formation of huge conglomerates for the other investigated vWF proteins, due to a “fishing” mechanism by collecting platelets and even small platelet-vWF aggregates from the blood flow. Not only the fishing mechanism, but also the exposure of active A1 domain within the vWF protein is crucial for the larger aggregate length by higher shear rates, as the probability of vWF stretching is enhanced by increasing the shear rate. These results are mainly in compliance with Yago and coworkers, who reported that the mean lifetime of the GPIbα and the vWF A1 domain increased with increasing force. As the lifetimes of A1 bonds with GPIbα are too short at arterial shear rates ($500–5{,}000s^{-1}$), the GPIbα-A1 domain is not able to agglutinate. Only at shear rates of $20{,}000s^{-1}$ shear induced platelet-vWF aggregation is possible (Yago et al., 2008; Ruggeri et al., 2006; Dong et al., 2001). However, the presented results showed a decreased threshold shear rate for platelet-vWF aggregate formation over dimeric vWF A1. The physical basis for the enhanced formation of vWF-platelet aggregates close to the surface was discussed by Alexander-Katz, Netz and coworkers. The unfolding of the vWF occurs mostly close to the surface of the blood flow, as the flow gradient and thus, the shear rate is maximal (Alexander-Katz and Netz 2008). Additionally, the blood cell wall dramatically enhances the unfolding

and decreases the critical shear rate due to an increase in hydrodynamic stress (Alexander-Katz and Netz 2008; Alexander-Katz and Netz 2007; Sing and Alexander-Katz 2010). Therefore, the unwanted binding of the vWF to platelets in the vessel interior is reduced and the vWF is directed to the surface of the capillaries (Alexander-Katz and Netz 2007). Due to the results reported by Yago and coworkers, eliminating deformability of the platelets did not alter the descending phase of the velocity curve for rolling on WT A1 (Yago et al., 2008), changing the deformability of the platelets might not alter the effect of the formation of the rolling aggregates.

8.2.2 Collagen coated surface

Perfusion of washed blood cell suspensions containing recombinant vWF or a vWF gain of function mutant type 2B (J1309V) over a collagen coated surfaces caused shear dependent assembly of vWF networks anchored to the collagen fibrils and captured discoid activation-blocked platelets within them (fig. 40, supplemental material).

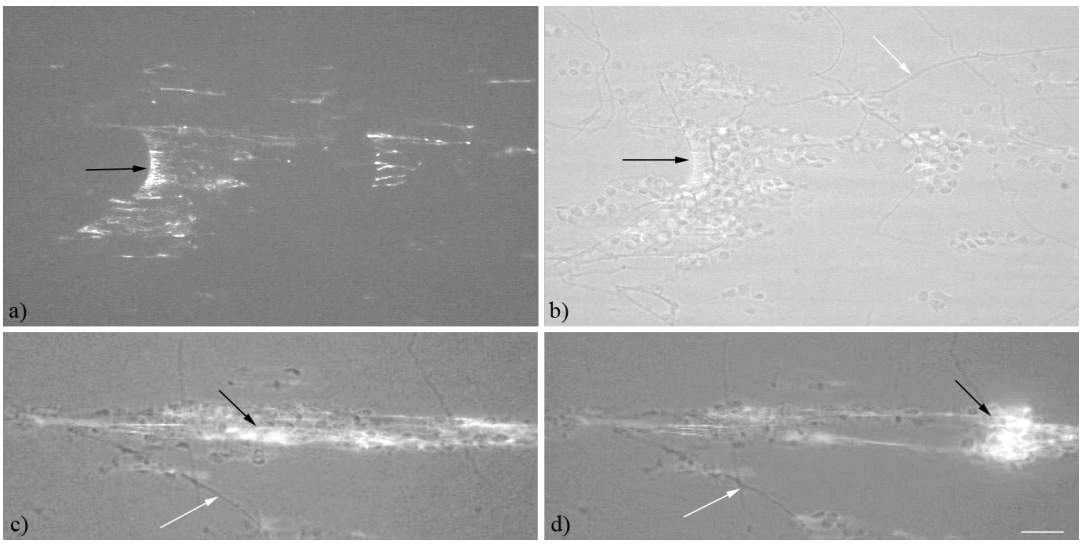

Figure 40: Microscopic still images taken from real-time video-recording of blood flow over immobilized collagen type I at shear rates of a), b) 2,000s^{-1} and of c), d) 40,000s^{-1}. The blood cells were washed plasma-free and resuspended in buffer containing recombinant full-length vWF. In the fluorescence illumination image a) the black arrow shows fluorescently labelled vWF, which has attached permanently to collagen fibres during the flow, thereby forming vWF strands and nets. In b) the identical region of a) is depicted in bright field. The black arrow demonstrates the attachment of platelets to the vWF nets. The completely activation-inhibited platelets adhere nevertheless permanently to the vWF strands. In images c) and d) double illumination with fluorescence and bright field is used to observe vWF networks (black arrows) closely interwined with platelets. Image d) shows the identical region of c). In d) a detaching vWF-platelet conglomerate can be seen. The white arrows indicate a collagen fibre. (In all images scale bar: 10µm)

These detaching of the aggregates was due to the hydrodynamic drag. These platelet-vWF conglomerates arrested more than a minute and reached a total length of 100-200µm. Recently, formed platelet conglomerates could be visualized eventually detaching and rolling

over the surfaces. Flow measurement with shear rates ranging from 1,500s^{-1} to 50,000s^{-1} were performed. The threshold shear rate for recombinant vWF formation of platelet-vWF conglomerates was around 2,000s^{-1} (fig. 40). However, for the mutant vWF type 2B individually slowly rolling aggregates formed at 1,500s^{-1} (fig. 41; supplemental material). The vWF mutant type 2B is recombinant genetically produced and grown in a protein media, therefore the fluorescence labelling of the vWF mutant was not possible. Although, the platelets were completely activation inhibited, these platelet-vWF conglomerates formed, detached from and rolled over the surface. These aggregates had a decreased rolling velocity and size compared to the ones formed with recombinant full-length vWF at the same shear rate.

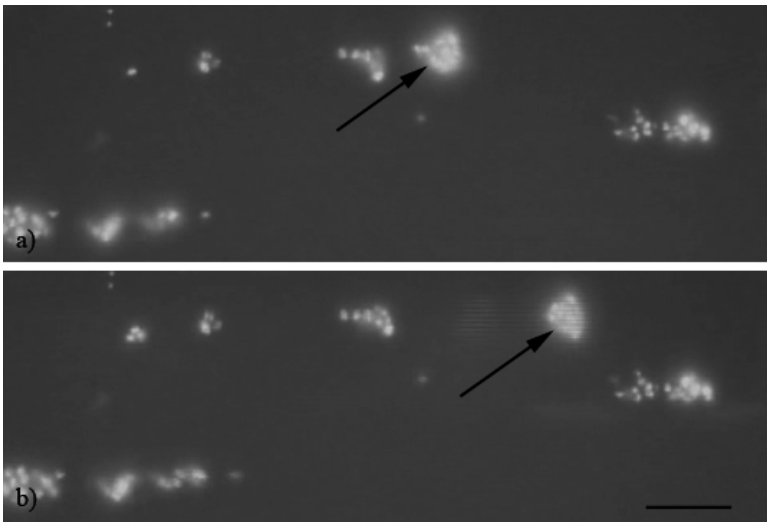

Figure 41: Fluorescence microscopic still images taken from real-time video-recordings of blood flow over immobilized collagen type I at a shear rate of 1,500s^{-1}. The blood cells were washed plasma-free and resuspended in buffer containing mutant vWF type 2B and fluorescently labelled platelets. Black arrows in image a) and b) delineate a detaching platelet-vWF conglomerate subsequently rolling over the surface. Although platelet activation was completely inhibited, platelet aggregate formation and rolling was observed. (In all images scale bar: 10µm)

These results indicate that variations in the bond strength and the bond lifetime of the GPIbα and the vWF A1 domain influence the shear rate threshold and the size of the rolling aggregates over collagen, but not in the vWF multimer distribution. The gain of function mutant showed over collagen a decreased shear rate threshold of 1,500s^{-1} and an increased rolling aggregate size. This is comparable to previous studies, which reported on patients with type 2B vWD plasma vWF may spontaneously interact with platelet GPIbα and spontaneously agglutinate, as the lifetimes of vWF with GPIbα is increased at low shear rates (200s^{-1}) (Yago et al., 2008; Ruggeri et al., 1980). Therefore, the GPIbα-A1 domain bond strength effects the formation of the rolling aggregates over collagen.

In summary, the exposure of the A1 domain of the vWF protein, the bond strength, bond lifetime of the GPIbα and the vWFA1 domain, the vWF sugar content and the shear rate are the key characteristics for the formation of the platelet-vWF aggregates rolling over the surface. Only due to the interplay of the various influence factors the formation of rolling aggregates is possible. The knowledge of the key features of the platelet-vWF aggregate formation process is essential for the therapy of patients with stenotic arteries, which leads to acute thrombotic occlusions. The experiments are the first step to understand the biophysical mechanism involved in the rolling aggregate formation process.

9. Influence of the hematocrit

9.1 Introduction

The impact of the hematocrit (HCT) on the platelet adhesion and the tether formation is not fully understood. In particular, the consequences of a change in the HCT, like the occupancy platelet probability near the vessel wall or a variation in the platelet-erythrocyte collision, will analyse fundamental insights in the biophysical mechanisms of the platelet-vWF interaction. Detailed information of the physical properties of the blood flow is described in the introducing chapter 1.4. The following chapter will be the starting point for the investigation of collective phenomena on the platelet GPIbα and vWF A1 domain crosstalk. The influence of the solid components of the blood on the platelet adhesion, especially the first platelet contact with the vWF coated surface, the number of adhered platelets and the weak adhesion area, as well as the tether formation will be quantified by a flow chamber set-up equipped with a RICM.

9.2 Results and Discussion

Over a vWF (Haemate) coated surfaces whole blocked blood (preparation see chapter 3.1.1) was perfused in a flow chamber equipped with a RICM (set-up see chapter 3.2.1). The shear rates ranged from $400s^{-1}$ to $20{,}000s^{-1}$. By the RICM technique platelets (black arrows in fig. 42) and tethers (white arrows in fig. 42) adhered to the vWF coated surface can be observed.

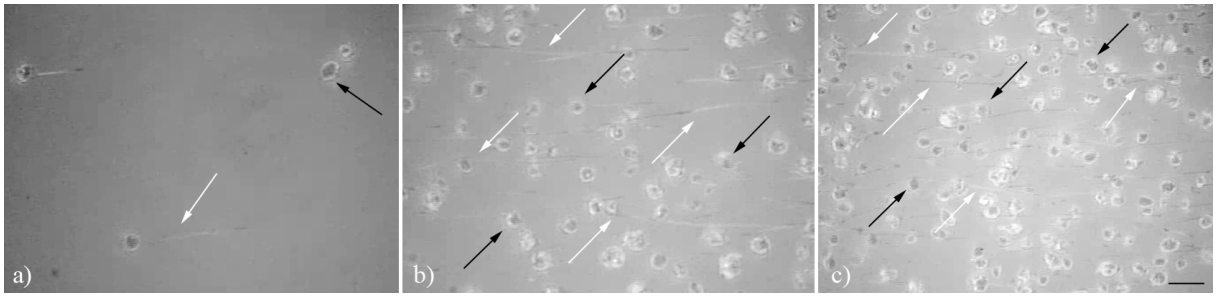

Figure 42: RICM images of blood samples (blocked) over Haemate (10U) at shear rates of $10{,}000s^{-1}$. Image a) HCT of 20%, b) of 40% and c) of 60% after shear was applied for a) 46s, b) 32s and c) 34s. Arrested platelets, platelets with tether and ruptured tethers are shown. Black arrows exemplarily indicate the platelet contact area and the white arrows exemplarily show tethers and ruptured tethers. Note the large number of platelets and tethers for HCT 40% (b)) and 60% (c)). (Scale bar in all images: 5µm)

To understand the impact of the HCT on the platelet adhesion processes, the first dynamic attachment of the platelet was analysed. At $400s^{-1}$ for HCT of 20% no platelet adhered to the

vWF surface and for 40% and 60% the first platelet interacted after 19s with the vWF coated surface. For a 20% HCT a shear flow of 1,500s^{-1} was applied for 82s, before the first platelets adhered to the vWF surface. For a 40% HCT this value was lowered of around 87% and for 60% HCT of around 91%. Shear rates of 10,000s^{-1} showed almost the same percentual variations in the first platelet-surface contact time, but adhered significantly faster. For HCT of 20% the first platelets adhered after 16s of flow exposure, of 40% after 2s and of 60% after 4s. However, for 20% HCT the shear rate of 4,000s^{-1} had to be applied for 17s and for 40% and 60% for 8s and 7s, respectively. Additionally, at 20,000s^{-1} and a HCT of 20% not a single platelet adhered in between the first few minutes. For the other hematocrit values rolling platelet-vWF aggregates (details see chapter 8) formed in between the first seconds and collected all adhered platelets on the surface. Due to this accumulation process also parts of the vWF coating were ruptured. Therefore, the platelet adhesion was hindered after around 60s. To get an idea on the platelet adhesion count changes, the adhered platelets on the vWF surface of the flow chamber (fig. 42) were counted. The average amount of platelet adhesion was significantly enhanced for an increase in shear rate from 400s^{-1} to 1,500s^{-1} for all HCTs. The curve progression for all three HCTs was crucial altered. HCT of 20% and 40% showed an almost linear increase from 400s^{-1} to 4,000s^{-1}. For 60% HCT the slope between 400s^{-1} and 1,500s^{-1} was around 4 and between 1,500s^{-1} and 4,000s^{-1} around 3. From 4,000s^{-1} to 10,000s^{-1} the curve of HCT of 20% decreased linearly and the curve slopes of the HCTs 40% and 60% were comparable (fig. 43). The standard deviations between the different donors were in the range of 20%-50% at 400s^{-1} and 1,500s^{-1} and in the range between 8%-25% at 4,000s^{-1} and 10,000s^{-1}. In contrast, the trends remained almost constant, thus, the error bars are not depicted in figure 43.

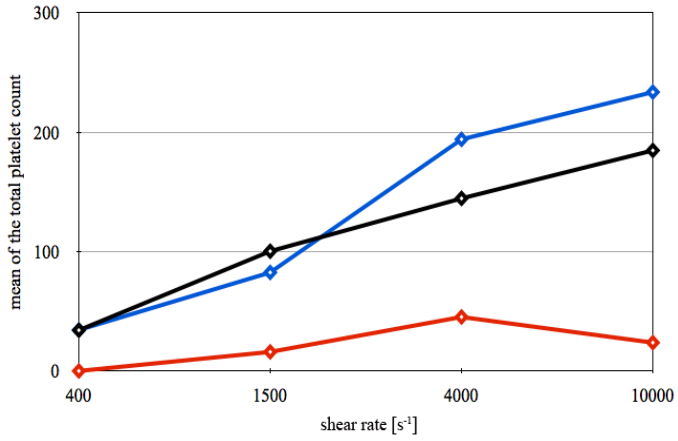

Figure 43: Average of the total platelet count per frame (5,000µm²) of different HCTs at increasing flow rates. The red curve represents the total platelet count of 20% HCT, the black curve of 40% and the blue curve of 60%.

This indicates that the activation of the vWF protein is crucial for the platelet adhesion increase. This behaviour was also observed in chapter 5,6 and 7. The significant decrease in platelets adhere to the vWF surface at a HCT of 20% compared to a HCT of 40% or 60% might be due to a reduced near wall platelet concentration. The difference of 40% HCT and 60% HCT remained still unexplained, but above 1,500s^{-1} the variation might be due to an increased near wall platelet concentration. From this statistical analysis of bound platelets it seemed reasonable to extract the difference in adhesion energy ΔG of platelets influenced by variable HCTs using the Boltzmann equation (adapted to equation (5));

$$\frac{n_{20}}{n_{HCT}} = e^{-\Delta G / k_B T} \qquad (9)$$

where k_B is the Boltzmann constant, ΔG is the change in adhesion energy between 20% HCT and 40% or 60% HCT, T the temperature and n_{20} and n_{HCT} is the average fraction of the amount of platelets on the surface at 20% HCT and at 40% or 60% HCT (Alberts et al., 2003; Fleck et al., 2002). Using the average platelets amount adhering to the surface of HCT of 20% and of 40% or 60% resulted in an energy difference ΔG in the order of 1.6-1.8 k_BT at 1,500s^{-1}, 1.2-1.5 k_BT at 4,000s^{-1}, 2.0-2.3 k_BT at 10,000s^{-1} and at 20,000s^{-1}. These differences in the absorption energy extracted by untreated and treated platelets are too low compared to adhesion energy differences of cells typically found in the literature (Simson et al., 1998). The detailed information is depicted in chapter 4.2. To complete the adhesion behaviour of platelets, the weak contact area on the bottom of the flow chamber was analysed after exposing the platelets to a shear flow of 1,500s^{-1} and 10,000s^{-1}. As the highest differences compared to the other investigated shear rates were expected, these two shear rates were chosen. At 1,500s^{-1} as well as at 10,000s^{-1} the platelets were homogeneously distributed in the range between 1-11μm^2 for all investigated HCTs (fig. 44). The average contact area was calculated from integrating the histograms of each donor and taking the average. The standard deviations were calculated from the variations in the donors. The average of the platelet adhesion area at 1,500s^{-1} was comparable for all hematocrits. The variations at 10,000s^{-1} between the different fractions of solid parts to fluid parts were minimal (inset in fig. 44). The average platelet weak adhesion values are summarized in table 13.

Table 13: Summary of the average weak adhesion area and the standard deviations on the vWF coated surface

mean +/- sd	1,500s^{-1} [μm^2]	10,000s^{-1} [μm^2]
20%	5.8 +/- 0.3	6.2 +/- 1.0
40%	4.7 +/- 0.4	4.9 +/- 0.8
60%	4.6 +/- 0.6	3.9 +/- 0.1

The weak adhesion area distribution and the average weak adhesion area are exemplarily shown at 10,000s^{-1} in figure 44. Due to a better overview of the influence of the HCTs, the error bars are not depicted in figure 44.

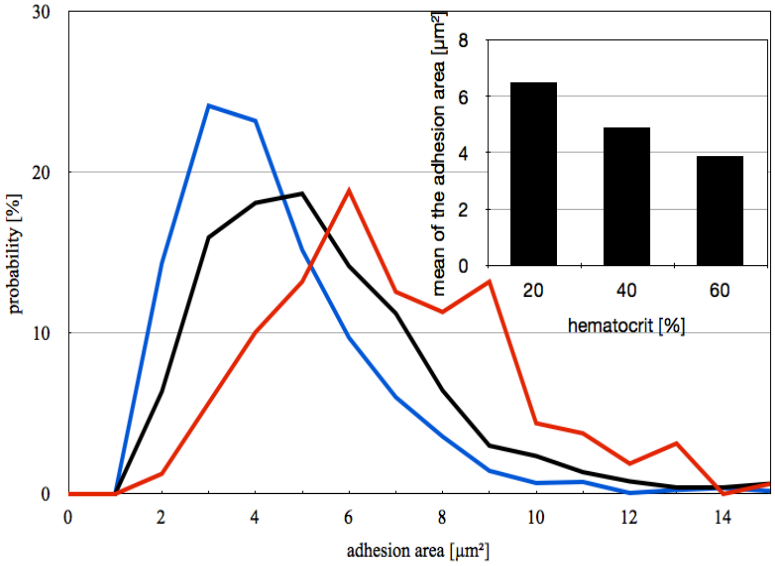

Figure 44: Weak adhesion area distribution for different HCTs at 10,000s^{-1}: the weak contact area is plotted against the probability P (∑P=100%). The red curve represents the adhesion area of platelets of 20% HCT, the black curve of 40% and the blue of 60%. The inset shows the mean of the weak adhesion area of platelets of variable HCTs at a flow rate of 10,000s^{-1}.

These results demonstrate that the HCT strongly influences the platelet adhesion amount and the first contact of the platelets with the vWF surface. On the contrary, the adhesion area itself remained constant. Variation in the solid parts content of the blood will affect the tether formation process. To unravel this, the tether length on the bottom of the flow chamber (white arrows in fig. 42) was measured after the exposure of the platelets to a shear flow of 1,500s^{-1} and 10,000s^{-1}. These two shear rates were again selected, as the most difference for these compared to the other investigated shear rates was expected. While, for 1,500s^{-1} the tethers at the platelets showed for all different HCTs a fairly sharp distribution with a most likely tether length of around 2µm, at 10,000s^{-1} the tethers at the platelet body were spread more homogeneously over the range between 1-28µm (fig. 45). In contrast, the formation of ruptured tethers was almost hindered for HCT of 20% and 40% at 1,500s^{-1}. For HCT of 60%

only 9% ruptured tethers compared to the total tethers amount were formed and were homogenously distributed in the range between 2-20µm. At 10,000s^{-1} the ruptured tethers for 20% HCT were spread more homogenously in a range between 2-31µm, for 40% and 60% HCT the ruptured tethers showed a fairly sharp distribution of around 3µm (inset in fig. 45). All investigated HCTs formed 9%-10% ruptured tethers compared to each investigated total tether amount at 10,000s^{-1}. Exemplarily, at 10,000s^{-1} the tether length distribution of tethers at the platelet and the ruptured ones is depicted in figure 45.

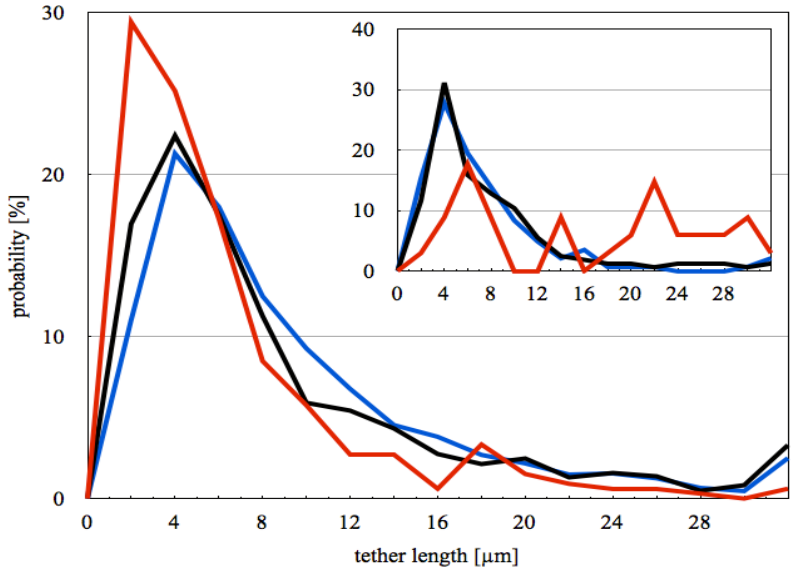

Figure 45: Tether length distribution curves for tethers at the platelets of different HCTs at a shear rate of 10,000s^{-1}: the tether length is plotted against the probability P (∑P=100%). The red curve represents the tether length of HCT 20%, the black curve of 40% and the blue curve of 60%. The inset shows the ruptured tether length distribution at a flow rate of 10,000s^{-1}.

To highlight the influence of the solid components of the blood on the tether formation the total average tether length was calculated from integrating the histograms of each donor and taking the mean. The standard deviation was calculated due to variations of the donors. At 1,500s^{-1} the average of the tether length was almost comparable for all HCTs. Instead, at 10,000s^{-1} the average of the tether length was significantly decreased for 20% HCT compared to HCT 40% and 60% (table 14).

Table 14: Summary of the average tether length and the standard deviations on the vWF coated surface

mean +/- sd	1,500s^{-1} [µm]	10,000s^{-1} [µm]
20%	4.3 +/- 2.5	6.6 +/- 1.8
40%	3.7 +/- 1.7	8.1 +/- 2.0
60%	4.8 +/- 0.3	8.5 +/- 1.5

To elucidate the changes in the tether count the average amount of the total tethers on the vWF surface was counted. The total tether count almost triplet for a shear rate of 1,500s^{-1} for HCT of 40% and of 60% and was 5 and 7 times higher for HCT of 40% and of 60% compared to 20% HCT (fig. 42, white arrows). The standard deviations of the various donors were in the range between 30%-60% at 1,500s^{-1} and between 20%-40% at 10,000s^{-1}. The trends remained almost constant. These results suggest that the tether formation process is influenced by the HCT changes from 20% to 40% or 60%, but 40% HCT and 60% HCT were comparable. This is comparable with the number of platelet adhesion to the vWF surface and the first platelet adhesion contact time. The variation between a HCT of 20% and of 40% and 60% were significant, but the differences between 40% and 60% were minimal. However, the adhesion area on the vWF surface remained unhindered by HCT changes. Due to an increased amount of platelets near the vessel wall and of platelet-erythrocyte collisions, the probability of the platelets to adhere to the surface might be enhanced and thus, the tether formation rate. The tether length is only slightly influenced due to an enhanced platelet adhesion and tether formation rate, therefore the probability of the formation of longer tethers is increased. In contrast, the weak adhesion area and the tether formation were significantly influenced by variations in the platelet cytoskeleton (see chapter 4). Consequently, it is assumed that the red blood cells do not exert an additional high enough force or pressure on the platelets adhering on the surface. These results are coincide with the literature. The platelets experience a complex motion during blood flow that was roughly characterized as enhanced diffusion (Turitto et al., 1972). More recently, an increased platelet concentration near the vessel wall compared to the centre was observed in flowing blood under arterial or arteriolar flow conditions (Tilles and Eckstein 1987; Tangelder et al., 1985). In flowing blood, even at high HCTs, it was observed that red blood cells were shifted towards the centre of the channel due to their deformability (Goldschmith 1971). Additional experimental studies by Aarts and coworkers showed that red blood cells in whole blood migrated towards the centre of the vessel and pushed the plasma containing the platelets near the vessel wall (Aarts et al., 1988). The size of the cell free layer near the vessel wall strongly depends on the HCT (Crowl and Fogelson 2009). At 50-60% HCTs the blood flow behaves non-Newtonian and thus, flattens the velocity profile and the off-wall lateral migrations of the red blood cells. These variations of the Poisseuille flow increase the near wall shear rate as well as the near wall platelet concentration (Tokarev et al., 2011; Yeh and Eckstein 1994; Eckstein et al., 1989; Goldsmith and Turitto 1986; Goldsmith and Skalak 1975). A graphical illustration summarizing the

influence of the HCT on the blood flow and on the particle distribution is presented in figure 46.

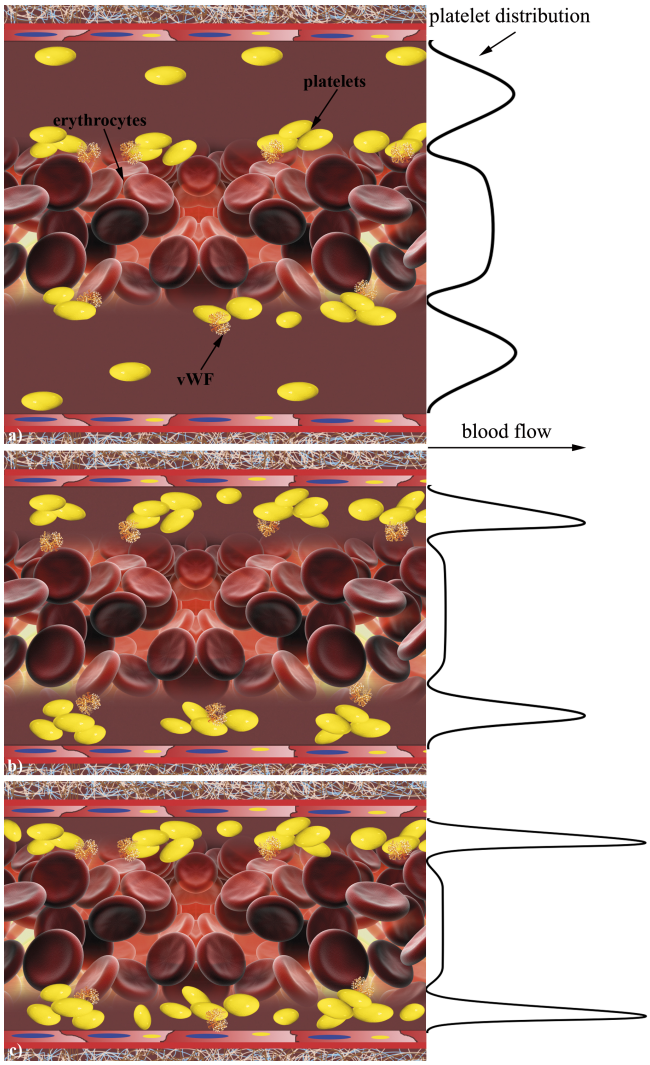

Figure 46: The sketch schematically illustrates the influences of the HCT on the distribution of the solid components of the blood flow and the platelet distribution across the blood vessel. The black curves indicate the platelet distribution. A reduced HCT of 20% shows a reduced near wall platelet concentration. The platelets are spread more homogenous in the vessel (image a)). However, an increase in the HCT of 60% enhances the near wall platelet concentration (image c)). In image b) physiological HCT concentrations (40%) are illustrated.

In summary, these results can help to unravel the role that increased red blood cell concentrations play in disease for example chronic obstructive pulmonary disease (Edelman et al., 1992) and for high performance sports. Furthermore, these results might be the first step to understand the biophysical mechanism of probability changes and external force on the complex platelet-vWF interplay. The impact on the HCT on the platelet functions might be the basis to understand the influence of collective phenomena on the platelet-vWF interplay.

10. Interaction of tumor cells with platelets

10.1 Introduction

Tumor metastasis is a dynamic process, in which tumor cells interact with platelets and the vessel wall, before colonizing on secondary sites (Terraude et al., 2007; Terraude et al., 2006). Metastasis may depend on the ability of tumor cells to interact with platelets (Nash et al., 2002). The presence of the platelets could protect the tumor cells from the clearance by the immune system (Nieswandt et al., 1999). Furthermore, platelets might mediate tumor cell arrest and the adhesion to the endothelium, thus facilitating cell extravasation (Terraude et al., 2007; Terraude et al., 2006; Dardik et al., 1997; Felding-Habermann et al., 1996). On the one hand a direct interaction of vWF with tumor cells is observed (Morganti et al., 2000), but on the other hand vWF is not absolutely required for haematogenous metastasis. VWF might be responsible for tumor cell death (Terraude et al., 2007). In a mouse model platelet deficient mice as well as mice with mutations rendering non functional platelets, showed reduced metastases from lung carcinoma and melanoma cell injection (Terraude et al., 2007; Boucharaba et al., 2004; Nash et al., 2001). As coagulation and platelet function support tumor metastasis, functional absence of GPIbα resulted in a decreased metastasis (Terraube et al., 2007). The thrombin formation is enhanced in small cell lung cancer (SCLC) and malignant melanoma cells (Kirszberg et al., 2005). Tumor cells activate circulating platelets and thus, platelet-derived microparticles (PMPs) are shed in the vicinity of tumor cells in the vasculature. PMPs are small encapsulated by plasma membrane due to activation of platelets. MPs are defined as cell derived membrane fragments, which range in the size from 0.1µm to 1µm. The MPs are present at the surface of negative phospholipid moieties that are essential in the case of PMPs for initiation of blood coagulation (Gosh et al., 2008; Reininger et al., 2006). MPs bear at least one of the antigenic markers distinctive of the parent cell (Reininger et al., 2006; Abid Hussein et al., 2003). Enhanced levels of PMPs were observed in the circulation of patients with different cancers (Tilley et al., 2008; Del Conde et al., 2007; Zwicker et al., 2007; Kim et al., 2003). Dashevsky and coworkers reported a direct correlation of PMPs and prostate cancer cells, Clone-1 (CL-1). Preincubation of CL-1 with PMPs showed an increased invasion through a gelatin coated (a denaturated form of collagen) membrane of the Boyden chamber system. An incorporation of PMPs into the tumor cell membrane might be possible, thus PMPs can firmly adhere to the cancer cell membrane (Dashevsky et al., 2009). Pancreatic and lung cancer cells produce microparticles (MPs), which aggregate

platelets. Endogenous cancer cell derived MPs shed from growing tumor are able to accumulate at the site of injury in mice (Thomas et al., 2009). In mouse models the presence of an ectopic tumor increased the quantity of MPs present in the bloodstream and accelerate thrombus formation. However, cancer cells themselves may not participate in thrombus formation (Thomas et al., 2009). While, the relation between blood platelets, PMPs und tumor cells in mouse models is well described, the interaction of platelets and the influence of PMPs with tumor cells in in vitro models is entirely unclear. The stimulatory effect of SCLC and maligne melanoma cells (MV3) on platelet aggregation in an aggregometer was analysed. To investigate the stimulatory agonist the tumor cell impact on ATP secretion of the platelets in a chronology aggregometer was measured. The platelet-tumor interaction in a parallel flow chamber device was investigated. Finally, the receptor transition or MP increase due to stimulation was measured in a flow cytometry. As MPs might increase the stimulatory effect of tumor cells, the supernatant of the tumor cells was investigated due to MP fractions in the supernatant solution. Additionally, tumor cells and platelet were sheared in a cone and plate to generate an increased amount of MPs.

10.2 Results and Discussion

10.2.1 Tumor cell induced platelet aggregation in solution

Adding SCLC cells suspended in Tyrode buffer to platelet rich plasma (PRP) induced platelet aggregation in the aggregometer (solution preparation see chapter 3.1.4 and 3.1.3; set-up see chapter 3.2.4). The average maximal amplitude reached was around 20% after 45s. The curve decreased and reached a steady state around 0%-5% due to a platelet deaggregation. However, adding MV3 cells suspended in Tyrode buffer reduced the maximal aggregation amplitude by 80% compared to SCLC cells in Tyrode buffer. SCLC cells in medium bisected the maximal aggregation amplitude compared to SCLC cells in Tyrode buffer. The maximal aggregation amplitude of MV3 cells in medium was comparable with the ones in Tyrode buffer. To measure the effect of tumor cell derived MPs on the aggregation behaviour of platelets either the supernatants of the tumor cells or sheared tumor cells in Tyrode buffer at $10{,}000s^{-1}$ for 3min in a cone and plate viscosimeter were used. The supernatant SCLC cell maximal aggregation amplitude was 37% decreased compared to SCLC cells in Tyrode buffer. The supernatant MV3 cells showed no aggregation. For sheared SCLC cells maximal aggregation amplitudes was bisected and for sheared MV3 cells lowered by 71% compared to

SCLC cells in Tyrode buffer (fig. 47). The standard deviations were significant, but the trends were unaffected, thus the error bars are not shown in figure 47.

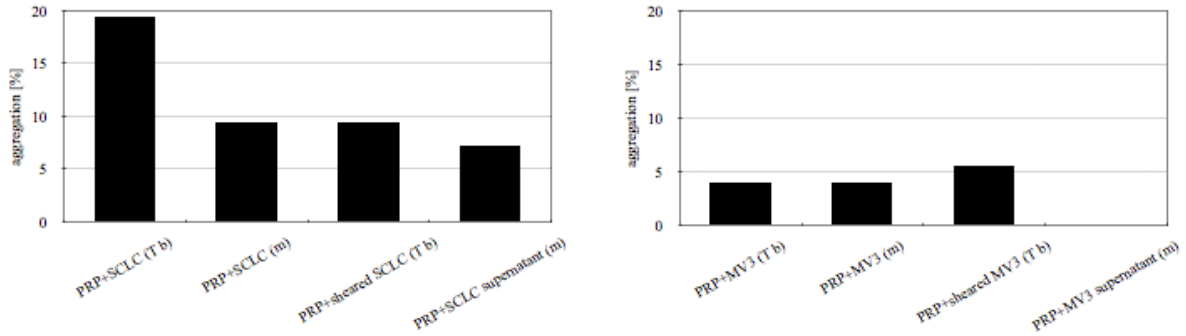

Figure 47: Average percentage aggregation of PRP and tumor cells in buffer or medium, stimulated tumor cells in buffer and the supernatant of the tumor cells are depicted. Image a) shows SCLC cells and b) MV3 cells.

These results indicate that the platelet stimulation was significant dependent on the tumor cell solution as well as on the tumor cell type. For all investigated solutions and treating procedures the SCLC cells showed an increased average maximal aggregation amplitude compared to the MV3 cells. The SCLC cells might be more active compared to the MV3 cells. As the SCLC cells grow as aggregates and the MV3 cells as individual cells, the aggregates of the SCLC cells might precipitate faster compared to MV3 cells. This assumption is supported by the reduced difference between sheared SCLC and MV3 cells compared to the other solutions investigated. The MV3 supernatant solution showed no platelet aggregation, as there are no cells or cell derived microparticles in the MV3 cell supernatant solution. SCLC cell-supernatant induced aggregation was lowered compared to SCLC cell suspension. As the aggregation curve did not drop to zero, an ongoing ATP release during aggregometry can be proposed. The enlarged amount of SCLC cells compared to MV3 cells does not influence the aggregation process. The tumor cells stimulate platelets, may be due to an ATP secretion. To verify this hypothesis the ATP secretion of the tumor cells was measured.

10.2.2 Induced ATP secretion by tumor cells

To clarify the ATP secretion of platelets the same varying tumor cell solutions as for the aggregation measurements were used (solution preparation see chapter 3.1.4 and 3.1.3; set-up see chapter 3.2.5). As a control, the ATP secretion after adding the poor Tyrode buffer or tissue medium was measured. No ATP secretion was observed. The ATP secretion of SCLC cells in Tyrode buffer was bisected compared to MV3 cells in Tyrode buffer. SCLC cells in Tyrode buffer showed a 6 time higher secretion compared to SCLC cells in medium, 4 times

higher than the supernatant of SCLC cells and 3 times bigger as SCLC cells, which were sheared for 3min (fig. 48 a)). However, Tyrode buffer incubated and sheared MV3 cells showed a comparable secretion average value and MV3 cells in medium secreted only a tenth of MV3 cells in Tyrode buffer (fig. 48 b)). The standard deviations were significantly large, in the range of 40%-100%, however the trends remained unchanged. Except for PRP and collagen the error bar was only 9%. Due to a better overview the error bars are not depicted in figure 48.

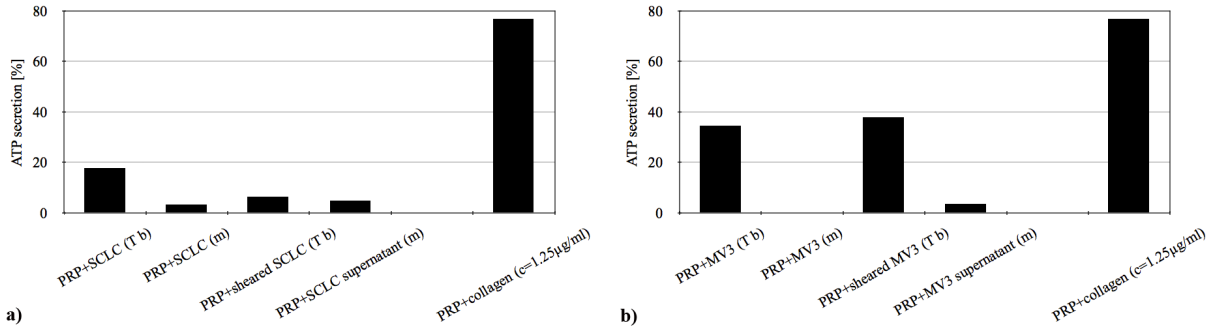

Figure 48: Average percentage ATP secretion of PRP by addition of tumor cells in buffer or medium, stimulated tumor cells in buffer and the supernatant of the tumor cells is shown. a) SCLC cells and b) MV3 cells.

The platelet aggregation is stimulated due to an ATP secretion. As the MV3 stimulated ATP secretion is increased compared to the SCLC stimulated one, the cell count might unhinder the measured results for all investigations. The ATP secretion characteristics did not correlate directly with the aggregation measurements. The observed differences of ATP secretion and aggregation remained unexplained. To observe in real time and analyse the interaction of platelets and tumor cells in vitro a flow chamber set-up was used.

10.2.3 Tumor cell adhesion to vWF under blood flow conditions

Perfusion of immobilized multimeric vWF with whole blood without further stimulation at flow rates of $100s^{-1}$ caused single platelet adhesion (see solution preparation see chapter 3.1.4 and 3.1.3; set-up see chapter 3.2.1). No tumor cell adhesion or platelet-tumor cell interaction was observed. Incubation of tumor cells with PMPs did not change the adhesion or interaction pattern. The tumor cells are pushed towards the centre of the channel due to the hydrodynamic drag. The Fahraeus-Lindquist effect might be an explanation for the observed phenomenon. In contrast, to Thomas and coworkers, who reported an increased amount of MPs from platelets and tumor cells, which were able to accelerate the thrombus formation in a mouse model (Thomas et al., 2009). The tumor cell adhesion to immbolized multimeric vWF or collagen type I in buffer solution was observed (Fallah et al., 2010). The interaction of

tumor cells with platelets or the interaction with their derived MPs is reported by various groups in vitro or in mouse models (Dashevsky et al., 2009; Thomas, et al., 2009; Gosh et al., 2008; Tilley et al., 2008; Del Conde et al., 2007; Zwicker et al., 2007; Abid Hussein et al., 2003; Kim et al., 2003), but not in a comparable flow chamber set-up with whole blood. Flow chamber studies, which focus on the platelet-tumor cell interaction are still lacking. It remains unclear, if mouse models could fully replace in vitro studies. Investigations by comparing both in vitro and mouse models could elucidate this problem. The interaction of platelets and tumor cells was measured by an aggregometry and it was shown that this interplay cause the activation of platelets. To clarify the role of an effect on the receptor distribution on the cell's surface, the MP increase or receptor adaption was tested by flow cytometry.

10.2.4 Flow cytometry measurements

The receptor transfers of platelets to tumor cells or vice versa alone and after incubation of platelets or tumor cells or PMPs was investigated by flow cytometry (solution preparation see chapter 3.1.4 and 3.1.3; set-up see chapter 3.2.6). Incubation times of 0h, 1h, 2h, 24h and 48h were tested. After 48h the investigated cells were in an apoptotic condition, thus only incubation times from 0h to 24h are depicted. The increase in MPs after different incubation times is the multiple times MP amount compared to the 0h measurements for not mixed suspension due to a better overview of the differences in the MP amount increase. However, for mixed suspensions it is the multiple times increase of one half of each suspension partner of 0h measurement. The annexin V labelled MPs of platelets and tumor cells showed a maximum after 2h incubation, except SCLC cell MPs. However, the variations between the different incubation times were not significant, as the standard deviations, especially for the 2h incubation time measurement, were crucial large. As the measured values obtained by the variation of the 0h measurement the difference due to various donors or growth sections might be minimal. The CD41 labelled MP amounts demonstrate a maximum at 2h for PMPs, MV3 derived MPs, PRP-MV3 MP solution and for both tumor cell-PMPs solutions. In contrast, SCLC derived MPs, both tumor cell-platelet solution and PRP-SCLC MP solutions increased continuously. Both tumor cell-PMPs solution depicted an enlarged MP amount compared to the other investigated solutions. The difference between these investigated solutions were minimal, as error bars were significantly large. Comparing both individual labels showed that each investigated solution showed annexin V label as well as CD41 label. The MP amount of CD41 label was significantly increased compared to the annexin V label.

These results indicate that these tumor cells might exhibit the platelet integrin receptor αIIbβ3 as well as platelets. The increase of the MPs of the tumor cell-PMPs solution might be due to the incorporation of the PMPs into the tumor cells or due to an increased amount of PMPs after shearing. The various cell counts of both tumor cell lines did not affect the results, as all results were related to the 0h measurements. Over all, a drastic increase due to stimulation or an induced receptor transfer could not be observed. An assembly of the investigated increases in MPs of various tumor cells, platelets and MPs incubation and the standard deviations are shown in figure 49. As the trends did not remain unaffected, the error bars are depicted in figure 49.

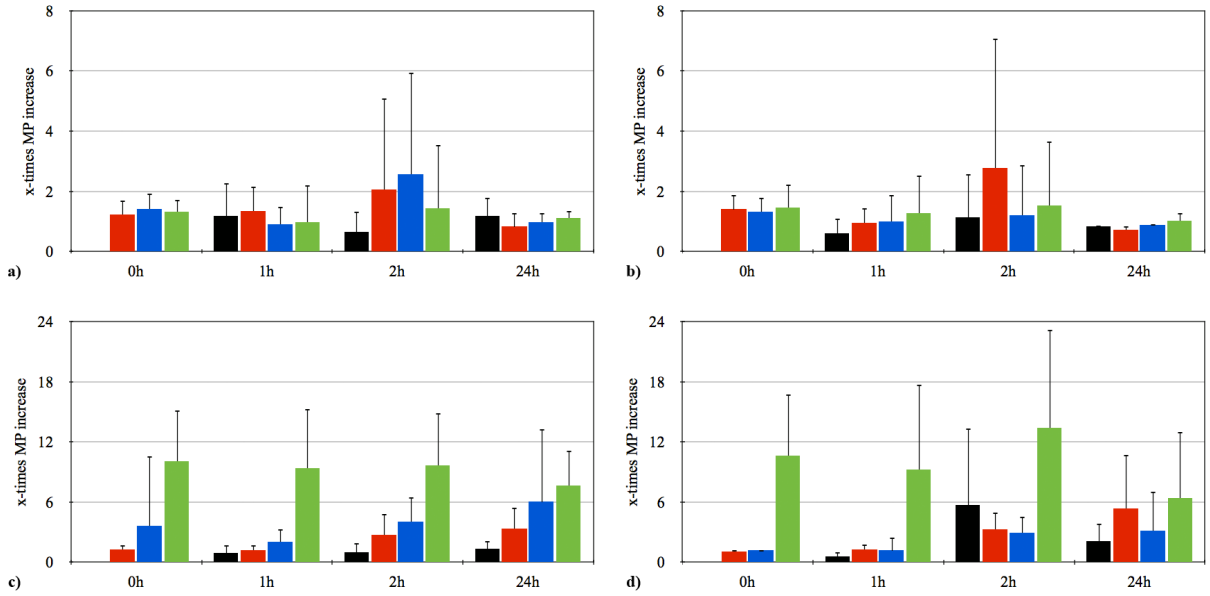

Figure 49: Multiple times increase of the MP amount compared to 0h incubated not mixed solution or for mixed solutions multiple times increase compared to one half of each measured solution. Figure a) shows the MP amount of annexin V label of SCLC cells and b) of MV3 cells. c) depicts the MP amount of CD41 of SCLC cells and d) of MV3 cells. The error bars are calculated by standard deviation.

These results are in parts in line with the literature. A receptor transfer due to incorporation from PMPs to the tumor cells or from tumor cell derived MPs to platelets was measured. Some authors reported that integrins αIIbβ3 and αVβ3 commonly found on platelets were expressed on the surface of tumor cells (Chen et al., 1997; Felding-Habermann et al., 1996; Oleksowicz et al., 1997). Therefore, the binding of tumor cells to platelets would be possible and even the formation of platelet-tumor cell aggregates mediated by adhesive proteins like vWF (McCarty et al., 2000; Karpatkin et al., 1988). Interactions of vWF and tumor cells were reported by involving αIIbβ3 (Floyd et al., 1992) or αVβ3 (Pilch et al., 2002) or GPIb (Oleksowicz et al., 1997). In a flow system the interaction of platelet integrin αIIbβ3 and an unidentified ligand on human colon carcinoma cell line LS174T by vWF was observed

(McCarty et al., 2000). Consequently, the receptor expressing on tumor cells is an important part in the platelet-tumor cell interaction.

Hematogenous tumor cell metastasis is a complex process, which is dependent on various cellular and molecular interactions within the vasculature. In a first step to metastasize successfully, the tumor cells must adhere to the blood vessel walls (Terraube et al., 2006). Most of the groups, who are involved in platelet-tumor cell or tumor cell-PMPs interactions normally used at 4°C stored PRP or PMPs. This might be the basis for the variation in the presented results. A combination of in vivo and in vitro measurements would be a good starting point for further investigations. The correlation of mouse models with human in vitro models is difficult due to various probe types. Comparing the monitoring assays of mouse models and human in vitro models would be the next step for further platelet-tumor cell interaction studies.

Taken together, an ATP dependent aggregation of platelets with tumor cells was observed, although a flow chamber set-up could not monitor the platelet-tumor cell interaction. The receptor transfer from platelet to tumor cells or vice versa was not detectable, but the expression of αIIbβ3 receptors on SCLC and MV3 cells was measured.

11. Summary

A model system was established to study the integrity of the cytoskeleton and especially, the modifications of the adhesion and tether forming process. Variations in the cytoskeleton induce changes in the membrane tension, which generate alterations in the membrane undulations. Disruption of the F-actin reduces the membrane tension and increases the membrane undulation. However, a breakage of the microtubuli acts contradictionary. The membrane-cytoskeleton adhesion was minimal increased by cholesterol loading and depletion. To bridge the gap between the platelet-vWF interaction the vWF site was varied. For patient treatment the physiological concentration of vWF products was crucial, but minimal changes in the multimer size distribution did not influence the platelet recruitment process. In contrast, the vWF lofm strongly influenced the platelet-vWF interplay and led to a significant reduction in the effectiveness of the GPIbα and A1 domain binding. The A1 domain exposure of the vWF multimer, the bond strength and bond lifetime of the GPIbα and the vWFA1 domain as well as the vWF sugar content and the shear rate are the key characteristics for the formation of platelet-vWF aggregates rolling over the surface. To investigate the first step in the blood clotting process, collective phenomena as the variation in the HCT were crucial influence factors. A higher HCT increased the platelet concentration near the wall and thus, the probability to adhere. Increasing the HCT over physiological values flattens the velocity profile and enhances the non-Newtonian behaviour of the blood. The platelet-tumor cell interplay could not be visualized under flow conditions, but the tumor cells induced the platelet ATP secretion leading to aggregation. The receptor distribution on platelets and tumor cells remained constant after interaction of tumor cells and platelets or their MPs with each other, but tumor cells expose the αIIbβ3 receptor. Changes in the shear rate have a minimal impact on the platelet weak adhesion area and the tether length, but massively influence the adhered platelet and tether number.

Taken together, the individual phenomena showed that the mechanism of platelet attachment and adhesion under flow cannot be reduced to specific ligand-receptor interactions, but must include the structural integrity of the cytoskeleton, its interaction with the lipid membrane and the elastic properties of the entire membrane shell. This adhesion process is secured by shear rate activation of vWF leading to reversible platelet aggregate-vWF network formation. These presented results are the first steps towards a complete understanding of the platelet-vWF crosstalk on the basis of physical concepts.

12. References

Aarts PA, van den Broek SA, Prins GW, Kuiken GD, Sixma JJ, Heethaar RM. 1988. Blood platelets are concentrated near the wall and red blood cells, in the center in flowing blood. Arteriosclerosis. 8: 819–824

Abid Hussein MN, Meesters EW,Osmanovic N, Romijn FP, Nieuwland R, Sturk A. 2003. Antigenic characterization of endothelial cell-derived microparticles and their detection ex vivo. J. Thromb. Haemost. 1: 2434-2443

Albersdörfer A, Feder T, Sackmann E. 1997. Adhesion-induced domain formation by interplay of long-range repulsion and short-range attraction force: a model membrane study. Biophys. J. 73: 245-257

Alberts B, Johnson A, Lewis J, Raff M, Roberts K, Walter P. 2003. Molecular biology of the cell. Garland Science. 4th edition

Alexander-Katz A, Netz RR. 2008. Dynamics and instabilities of collapsed polymers in shear flow. Macromolecules. 41: 3363-3374

Alexander-Katz A, Netz RR. 2007. Surface-enhanced unfolding of collapsed polymers in shear flow. EPL. 80: 18001

Alkhamis TM, Beissinger RL, Chediak JR. 1988. Red blood cell effect on platelet adhesion and aggregation in low-stress shear flow. Myth or fact? ASAIO Trans. 34: 868–873

Ammann A, Lipowsky R. 1996. Discontinuous phase transitions of membranes: a Monte Carlo study. J. Phys. II France. 6: 255-270

Andrews RK, Berndt MC. 2008. Platelet adhesion: a game of catch and release. JCI. 118(9): 3009-3011

Andrews RK, Brendt MC. 2004. Platelet physiology and thrombosis. Thrombosis Research. 114: 447-453

Andrews R, Shen Y, Gardiner E, Dong J, Lopez J, & Berndt M. 1999. The glycoprotein Ib-IX-V complex in platelet adhesion and signaling. Thromb Haemost, 82: 357–364

Arya M, Anvari B, Romo GM, Cruz MA, Dong J-F, McIntire LV, Moake JL, López JA. 2002. Ultralarge multimers of von Willebrand factor form spontaneous high-strength bonds with the platelet glycoprotein Ib-IX complex: studies using optical tweezers. Blood. 99: 3971-3977

Back LD, Radbill JR, Crawford DW. 1977. Analysis of pulsatile, viscous blood flow through diseased coronary arteries of man. J Biomech. 10: 339–53

Barkalow KL, Italiano JE Jr, Chou DE, Matsuoka Y, Bennett V, Hartwig JH. 2003. α-Adducin dissociates from F-actin and spectrin during platelet activation. JCB. 161 (3): 557-570

Behnke O. 1970. The morphology of blood platelet membrane systems. Seminars in Haematology. 3: 3-16

Bell GI. 1978. Models for the specific adhesion of cells to cells. Science. 200: 618-627

Bergmeier W, Piffath CL, Georg T, Cifuni SM, Ruggeri ZM, Ware J, Wagner DD. 2006. The role of platelet adhesion receptor GPIbalpha far exceeds that of its main ligand, von Willebrand factor, in arterial thrombosis. Proc Natl Acad Sci USA. 103: 16900-16905

Bernardo A, Bergeron AL, Sun CW, Guchhait P, Cruz MA, Lòpez, Dong J-F. (2004). Von Willebrand factor present in fibrillar collagen enhances platelet adhesion to collagen and collagen-induced platelet aggregation. J Thromb Haemost. 2: 660-9

Bessis M. 1973. Living blood cells and their ultrastructure (pp.767). New York. Springer-Verlag

Bird RB, Stewart WE, Lightfoot EN. 1960. Transport Phenomena. New York, NY: John Wiley and Sons, Inc

Bizzozero J. 1882. Ueber einen neuen formbestandteil des blutes und dessen Rolle bei der Thrombose und der Blutgerinnung. Arch Pathol Anat Physiol. 90. 261-332

Boek ES, Padding JT, den Otter WK, Briels WJ. 2005. Mechanical properties of surfactant bilayer membranes from atomistic and coarse-grained molecular dynamics simulations. J. Phys. Chem. B. 109(42): 19851-19858

Boucharaba A, Serre C-M, Grès S, Saulnier-Blache JS, Bordet J-C, Guglielmi J, Clézardin P, Peyruchaud O. 2004. Platelet-derived lysophosphatidic acid supports the progression of osteolytic bone metastases in breast cancer. J Clin Invest. 114(12): 1714–1725

Brenner SL, Korn ED. 1979. Substoichiometric Concentrations of Cytochalasin D Inhibit Actin Polymerization. The Journal of Biological Chemistry. 254(20): 9982-9985

Brinkley BR. 1985. Microtubule Organizaing Centers. Ann. Rev. Cell Biol. 1: 145-72

Brochard-Wyart F, Borghi N, Cuvelier D, Nassoy P. 2006. Hydrodynamic narrowing of tubes extruded from cells. PNAS. 103(20): 7660-7663

Brown SS, Spudich JA. 1979. Cytochalasin Inhibits the Rate of Elongation of Actin Filaments Fragments. JCB. 83: 657-662

Bruhn, Schambeck, Hach-Wunderle. 2007. Hämostaseologie für die Praxis. Sicher durch den klinischen Alltag. Schattauer. 1. Auflage

Bruinsma R. 1995. Adhesion and rolling of leukocytes: a physical model.Proc. NATO Adv. Inst. Phys. Biomater. NATO ASI Ser. 332:61-75

Boulbitch A, Guttenberg Z, Sackmann E. 2001. Kinetics of membrane adhesion mediated by ligand–receptor interaction studied with a biomimetic system. Biophysical Journal. 81: 2743-2751

Bukman, DJ, Yao JH, Wortis M. 1996. Stability of cylindrical vesicles under axial tension. Phys. Rev. E. 54: 5463–5468

Burridge K, Fath K. 1989. Focal contacts: Transmembrane links between the extracellular matrix and the cytoskeleton. Bioessays.10(4): 104–108

Burridge K, Nuckolls G, Otey C, Pavalko F, Simon K, Turner C. 1990. Actin-membrane interaction in focal adhesions. Cell Differ Dev. 32(3): 337–34

Butenas S, Branda RF, van´t Veer C, Cawthern KM, Mann KG. 2001. Platelets and phospholipids in tissue factor-initiated thrombin generation. Thromb Haemost. 86: 660–7

Butt HJ, Jaschke M. 1995. Thermal noise in atomic force microscopy. Nano technol. 6: 1-7

Carvalho AC, Colman RW, Lees RS. 1974. Platelet function in hyperlipoproteinemia. N Engl J Med. 290: 434–8

Casella JF, Flanagant MD, Lin S. 1981. Cytochalasin D inhibits actin polymerisation and induces depolymerisation of actin filaments formed during platelet shape change. Nature. 293: 302-305

Chen YQ, Trikha M, Gao X, Bazaz R, Porter AT, Timar J, Honn KV. 1997. Ectopic expression of platelet integrin alphaIIb beta3 in tumor cells from various species and histological origin. Int J Cancer. 72: 642–8

Chesterman CN, Berndt MC. 1986. Platelet and vessel wall interactions and the genesis of atherosclerosis. Clin Haematol 15(2): 323-53

Chien S, Usami S, Taylor HM, Lundberg JL, Gregersen MI. 1966. Effects of hematocrit and plasma proteins on human blood rheology at low shear rates. J Appl Physiol. 21: 81– 87

Christian AE, Haynes MP, Phillips MC, Rothblat GH. 1997. Use of cyclodextrins for manipulating cellular cholesterol content. J Lipid Res. 38: 2264–72

Cooper JA. 1987. Effects of cytochalasin and phalloidin on actin. JCB. 105: 1473-1478

Cramer EM, He Lu H, Caen JP, Soria C, Berndt MC, Tenza D. 1991. Differential redistribution of platelet glycoproteins Ib and IIb-IIIa after plasmin stimulation. Blood. 77(4): 694-699

Cramer EM, Breton-Gorius J, Beesley JE, Martin JF. 1988. Ultrastructural demonstration of tubular inclusions coinciding with von Willebrand factor in pig megak- aryocytes. Blood. 71: 1533–8

Crowl LM, Fogelson AL. 2009. Computational model of whole blood exhibiting lateral platelet motion induced by red blood cells. Int. J. Numer. Meth. Biomed. Engng. 26: 471-487

Dardik R, Kaufmann Y, Savion N, Rosenberg N, Shenkman B, Varon D. 1997. Platelets mediate tumor cell adhesion to the subendothelium under flow conditions: involvement of platelet GPIIb-IIIa and tumor cell alpha(v) integrins. Int J Cancer. 70: 201–7

Dashevsky O, Varon D, Brill A. 2009. Platelet-derived microparticles promote invasiveness of prostate cancer cells via upregulation of MMP-2 production. Int. J. Cancer. 124: 1773-1777

Davey Smith G, Pekkanen J. 1992. Should there be a moratorium on the use of cholesterol lowering drugs? BMJ. 304: 431-4

Dawber TR, Kannel WB. 1966. The Framingham study. An epidemiological approach to coronary heart disease. Circulation. 34: 553–5

Del Conde I, Bharwani LD, Dietzen DJ, Pendurthi U, Thiagaraja P, Lopez JA. 2007. Microvesicle-associated tissue factor and Trousseau's syndrome. J. Thromb. Haemost. 5: 70-74

Dong JF, Berndt MC, Schade A, McIntire LV, Andrews RK, López JA. 2001. Ristocetin-dependent, but not botrocetin-dependent, binding of von Willebrand factor to the platelet glycoprotein Ib-IX-V complex correlates with shear- dependent interactions. Blood. 97: 162–168

Donne A. 1842. De porigine des globules du sang, de leur mode de formation et du leur fin. Comptes Render Seances de L'Academia de Sciences. 14: 366-368

Dopheide SM, Maxwell MJ, Jackson SP. 2002. Shear-dependent tether formation during platelet translocation on von Willebrand factor. Blood. 99(1): 159-167

Duke WW. 1910. The relation of blood platelets to hemorrhagic disease. J Am Med Assoc. 55(14): 1185-1192

Eckstein EC, Koleski JF, Waters CM. 1989. Concentration profiles of 1 and 2.5 microns beads during blood flow. Hematocrit effects. ASAIO Trans. 35: 188–190

Eckstein EC, Bilsker DL, Waters CM, Kippenhan JS, Tilles AW. 1987. Transport of platelets in flowing blood. Ann N Y Acad Sci. 516: 442–452

Edelman NH, Kaplan RM, Buist AS, Cohen AB, Hoffman LA, Kleinhenz ME, Snider GL, Speizer FE**.** 1992. Chronic Obstructive Pulmonary Disease. CHEST. 102(3): 243S-256S

Eilers U, Klumperman J, Hauri H-P. 1989. Nocodazole, a microtubule-active drug, interferes with apical protein delivery in cultured intestinal epithelial cells (caco-2). JCB. 108: 13-22

Escolar G, Clemetson K, White JG. 1994. Persistence of mobile receptors on surface- and suspension-activated platelets. J Lab Clin Med. 123: 536–546

Escolar G, Krumwiede M, White JG. 1986. Organization of the actin cytoskeleton of resting and activated platelets in suspension. Am J Pathol. 123: 86–94

Evans EA, Calderwood DA. 2007. Forces and bond dynamics in cell adhesion. Science. 316(5828): 1148-1153
Evans EA. 1995. In The structure and dynamics of membranes. Vol.1 of Handbook of Biological Physics, edited by R. Lipowsky and E. Sackmann (Elsevier Amsterdam)
Evans E,Yeung A. 1994. Hidden dynamics in rapid changes of bilayer shape. Chemistry and Physics of Lipids. 73(1-2): 39-56
Evans E. 1985. Detailed mechanics of membrane-membrane adhesion and separation. I. Continuum of molecular cross-bridges. Biophys. J. 48: 175-183
Fahraeus R, Lindquist T. 1931. The viscosity of the blood in narrow capillary tubes. Am J Physiol. 96: 562–568
Fallah MA, Myles VM, Krüger T, Sritharan K, Wixforth A, Varnik F, Schneider SW, Schneider MF. 2010. Acoustic driven flow and lattice Boltzmann simulations to study cell adhesion in biofunctionalized-fluidic channels with complex geometry. Biomicrofluidics. 4: 1932-1058
Felding-Habermann B, Habermann R, Saldivar E, Ruggeri ZM. 1996. Role of beta3 integrins in melanoma cell adhesion to activated platelets under flow. J Biol Chem. 271: 5892–900
Flanagan MD, Lin S. 1980. Cytochalasins block actin filament elongation by binding to high affinity sites associated with F-actin. JBC. 255(3): 835-838
Fleck C, Netz RR, von Grünberg HH. 2002. Poisson Boltzmann theory for membranes with mobile charged lipids and the pH-dependent interaction of a DNA molecule with a membrane. Biophys. J. 82: 76-92
Florin EL, Rief M, Lehmann H, Ludwig M, Dornmair C, Moy VT, Gaub HE. 1995. Sensing specific molecular interactions with the atomic force microscope. Biosensors Bioelectr. 10: 895-901
Floyd CM, Irani K, Kind PD, Kessler CM. 1992. Von Willebrand factor interacts with malignant hematopoietic cell lines: evidence for the presence of specific binding sites and modification of von Willebrand factor structure and function. J Lab Clin Med. 119: 467–76
Fowler WE, Fretto LJ. 1989. Electron microscopy of von Willebrand factor. In: Zimmerman TS, Ruggeri ZM, eds. Coagulation and Bleeding Disorders. The Role of Factor VIII and von Willebrand Factor. New York: Dekker, 181–93
Fox J, Boyles J, Berndt M, Steffen P, Anderson L. 1988. Identification of a membrane skeleton in platelets. J. Cell Biol. 106: 1525–1538
Fox J, Reynolds C, Morrow J, Phillips D. 1987. Spectrin is associated with membrane-bound actin filaments in platelets and is hydrolyzed by the Ca2+ -dependent protease during platelet activation. Blood. 69: 537–545
Fox JBE, Boyles JK, Reynolds CC, Phillips DR. 1984. Actin filament content and organization in unstimulated platelets. The Journal of Cell Biology. 98: 1985-1991
Frick MH, Elo O, Haapa K, et al. Heinonen OP, Heinsalmi, Helo P, Huttunen JK, Kaitaniemi P, Koskinen P, Manninen V, Mäenpää H, Mälkönen M, Mänttäri M, Norola S, Pasternack A, Pikkarainen J, Romo M, Sjöblom T, Nikkilä EA. 1987. Helsinki Heart Study: primary-prevention trial with gemfibrozil in middle-aged men with dyslipidemia: safety of treat- ment, changes in risk factors, and incidence of coronary heart disease. N Engl J Med. 317: 1237-45
Fritz M, Radmacher M, Gaub HE. 1994. Granula motion and membrane spreading during activation of human platelets imaged by atomic force microscopy. Biophys. J. 66: 1328-1334
Gaffet P, Bettache N, Bienvenüe A. 1995. Phospatidylserine exposure on the platelet plasma membrane during A23187-induced activation is independent of cytoskeleton reorganization. EJCB. 67: 336-345
Geiger B, Spatz J, Bershadsky AD. 2009. Enviromental sensing through focal adhesion. Nature Reviews. 10: 21-33
George JN, Nurden AT, Phillips DR. 1984. Molecular defects in interactions of platelets with vessel wall. N Engl J Med. 311: 1084-1098
Glassinger E, Raphael RM. 2006. Influence of thermally driven surface undulations on tethers formed from bilayer membranes. Biophys J. 91: 619-625
Goddette DW, Frieden C. 1986. The Journal of Biological Chemistry. 261(34): 15974-15980
Gönnenwein S. 2003. Generic and specific cell adhesion: investigations of a model system by micro-interferometry
Golde D.1991. The stem cell. Sci Am. 265: 86-93
Goldmann WH, Ezzell RM, Adamson ED, Niggli V, Isenberg G. 1996. Vinculin, talin and focal adhesion. J. Muscle Res. Cell Motil. 17: 1-5
Goldsmith HL, Skalak R. 1975. Hemodynamics. Annu. Rev. Fluid Mech. 7: 213–247
Goldsmith HL, Turitto VT. 1986. Rheological aspects of thrombosis and haemostasis: basic principles and applications. Thromb Haemost. 55: 415– 435
Goldsmith H. 1971. Red cell motions and wall interactions in tube flow. Federation Proceedings. 30(5): 1578–1588
Gosh A, Li W, Febbraio M, Espinola RG, McCrae KR, Cockrell E, Silverstein RL. 2008. Platelet CD36 mediates interactions with endothelial cell-derived microparticles and contributes to thrombosis in mice. J. Clin. Invest. 118: 1934-1943
Goto S, Salomon DR, Ikeda Y, Ruggeri ZM. 1995. Characterization of the unique mechanism mediating the

shear-dependent binding of soluble von Willebrand factor to platelets. J Biol Chem. 270: 23352-23361
Gousset K,Tsvetkova NM, John H. Crowe JH, Tablin F. 2004. Important role of raft aggregation in the signaling events of cold-induced platelet activation. Biochimica et Biophysica Acta. 1660: 7–15
Grgurevich S, Krishnan R, White MM, Jennings LK. 2002. Role of in vitro cholesterol depletion in mediating human platelet aggregation. Thromb. Haemost. 1: 576-586
Guttenberg Z, Lorz B, Sackmann E, Boulbitch A. 2001. First order transition between adhesion states in a system mimicking cell-tissue interaction. Europhys. Lett. 54: 826-832
Heinrich D, Youssef S, Schroth-Diez B, Engel U, Aydin D, Blümmel J, Spatz JP, Gerisch G. 2008. Actin-cytoskeleton dynamics in non-monotonic cell spreading. Cell Adhesion & Migration. 2(2): 58-68
Haberichter SL, Montgomery RR. 2006. Structure and function of von Willebrand factor. In: Colman RW, Marder VJ, Clowes AW, George JN, Goldhaber SZ, eds. Hemostasis and Thrombosis Basic Principles and Clinical Practice. Philadelphia, PA: Lippincott Wil- liams & Wilkins. 707–22
Harmandaris VA, Deserno M. 2006. A novel method for measuring the bending rigidity of model lipid membranes by simulating tethers. The Journal of Chemical Physics. 125(20): 204905-11
Hartwig JH. 2007. The platelet cytoskeleton. Platelets. Elsevier Science
Hartwig J, DeSisto M. 1991. The cytoskeleton of the resting human blood platelet: Structure of the membrane skeleton and its attachment to actin filaments. J. Cell Biol. 112: 407–425
Haskell WL, Alderman EL, Fair JM, Maron DJ, Mackey SF, Superko HR, Williams PT, Johnstone IM, Champagne MA, Krauss RM, Farquhar JW. 1994. Effects of intensive multiple risk factor reduction on coronary atherosclerosis and clinical cardiac events in men and women with coronary artery disease. The Stanford Coronary Risk Intervention Project (SCRIP). Circulation. 89: 975–90
Hathcock JJ. 2006. Flow effects on coagulation and thrombosis. Arterioscler Thromb Vasc Biol. 26: 1729-1737
Heijnen HFJ, Debili N, Vainchenker W, Breton–Gorius J, Geuze HJ, Sixma J. 1998. Multivesicular bodies are an intermediate stage in the formation of platelet α granules. Blood. 91: 2313–2325
Heinrich D, Youssef S, Schroth-Diez B, Engel U, Aydin D, Blümmel J, Spatz JP, Gerisch G. 2008. Actin-cytoskeleton dynamics in non-monotonic cell spreading. Cell Adhesion & Migration. 2(2): 58-68
Helfrich W. 1995. Tension-induced mutual adhesion and a conjectured superstructure of lipid membranes. Handbook of Biological Physics Volume 1 edited by R. Lipowsky and E. Sackmann
Hochmuth RM, Marcus WD. 2002. Membrane tethers formed from blood cells with available area and determination of their adhesion energy. Biophys. J. 82: 2964-2969
Hochmuth RM, Evans EA. 1982. Extensional flow of erythrocyte membrane from cell body to elastic tether. Biophys. J. 39: 71-81
Hochmuth RM, Shao J-Y, Dai J, Sheetz MP. 1996. Deformation and flow of membrane into tethers extracted from neuronal growth cones. Biophys. J. 70: 358-369
Hochmuth RM, Evans EA, Wiles HC, McCown JT. 1983. Mechanical measurement of red cell membrane thickness. Science. 220: 101–102
Hochmuth RM, Evans EA. 1982. Extensional flow of erythrocyte membrane from cell body to elastic tether: I Analysis. Biophys. J. 39: 71– 81
Holme PA, Orvim U, Hamers MJ, Solum NO, Brosstad FR, Barstad RM, Sakariassen KS. 1997. Shear-induced platelet activation and platelet microparticle formation at blood flow conditions as in arteries with a severe stenosis. Arterioscler Thromb Vasc Biol.17: 646–653
Holmsen H. 1994. Significance of testing platelet functions in vitro. Eur J Clin Invest. 24: 3–8
Hulley SB, Walsh JMB, Newman TB. 1992. Health policy on blood cholesterol: time to change directions. Circulation. 86: 1026-9
Huxley H. 1963. Electron microscopic studies on the structure of natural and synthetic protein filaments from striated muscle. J Mol Biol. 3: 281-308
Jung SM, Yamazaki H, Tetsuka T, Moroi M. 1981. Effect of nocodazole, a new microtubule inhibitor, on platelet aggregation and release. Thrombosis Research. 23: 401-410
Karpatkin S, Pearlstein E, Ambrogio C, Coller BS. 1988. Role of adhesive proteins in platelet tumor interaction in vitro and metastasis formation in vivo. J Clin Invest. 81: 1012–9
Kasirer-Friede A, Cozzi MR, Mazzucato M, De Marco L, Ruggeri ZM, Shattil SJ. 2004. Signalling through GP Ib-IX-V activates alpha IIb beta 3 independently of other receptors. Blood. 103: 3403–11
Kenney DM, Weiss DL, Linck RW. 1988. A novel microtubule protein in the marginal band of human blood platelets. J Biol Chem. 263: 1432-1438
Kenney D, Linck R. 1985. The cytoskeleton of unstimulated blood platelets: structure and composition of the isolated marginal microtuble band. J Cell Sci. 78(1): 22
Kilsdonk EPC, Yancey PG, Stoudt GW, Bangerter FW, Johnson WJ, Phillips MC, Rothblat GH. 1995. Cellular cholesterol efflux mediated bycyclodextrins. J Biol Chem. 270: 17250–6
Kim HK, Song KS, Park YS, Kang YH, Lee YJ, Lee KR, Kim HK, Ryu KW, Bae JM, Kim S. 2003. Elevated levels of circulating platelet microparticles. VEGF, IL-6 and. RANTES in patients with gastric cancer: possible role of metastasis predictor. Eur J Cancer. 39: 184-91
Kim T, Hwang W, Lee H, Kamm RD. 2009. Computational analysis of viscoelastic properties of crosslinked

actin networks. PLoS computational biology. 5(7)
Kimura N, Uchida M, Nishimura S, Yamaguchi H. 1998. Promotion of polypeptide folding by interactions with Asn-Glycans. J Biochem. 124(4): 857-862
Kirszberg C, Rumjanek VM, Monteiro RQ. 2005. Assembly and regulation of prothrombinase complex onB16F10 melanoma cells. Throm Res. 115: 123-129
Kloboucek A, Behrisch A, Faix J, Sackmann E. 1999. Adhesion-Induced Receptor Segregation and Adhesion Plaque Formation: A Model Membrane Study. Biophys. J. 77: 2311–2328
Kodali VK, Roos W, Spatz JP, Curtis JE. 2007. Cell-assisted assembly of colloidal crystallites. Soft Matter. 3: 337-348
Koolman J, Röhm K-H. 2002. Taschenatlas der Biochemie. Thieme. 3. Auflage
Koster G, VanDuijn M, Hofs B, Dogterom M. 2003. Membrane tube formation from giant vesicles by dynamic association of motor proteins. Proc. Natl. Acad. Sci. USA. 100: 15583–15588
Koutts J, Walsh PN, Plow EF, Fenton JW, Bouma BN, Zimmerman TS. 1978. Active release of human platelet factor VIII-related antigen by adenosine diphosphate, collagen, and thrombin. J Clin Invest. 62: 1255–63
Ku DV, Flannery CJ. 2007. Development of a flow-through system to create occluding thrombus. Biorheology. 44(4): 273-284
Kuznetsova TG, Starodubtseva MN, Yegorenkov NI, Chizhik SA, Zhdanov RI. 2007. Atomic force microscopy probing of cell elasticity. Science. 38: 824-833
LaRosa JC, Hunninghake D, Bush D, Criqui MH, Getz GS, Gotto AM, Grundy SM, Rakita L, Robertson RM, Weisfeldt ML. 1990. The cholesterol facts: a sum- mary of the evidence relating dietary fats, serum cholesterol, and coronary heart disease: a joint statement by the American Heart Association and the National Heart, Lung, and Blood Institute. Circulation. 81:1721- 33
Laemmli UK. 1970. Cleavage of structural proteins during the assembly of the head of bacteriophage T4. Nature. 227: 680
Le Goff L, Hallatschek O, Frey E, Amblard F. 2002. Phys. Rev. Lett. 89: 258101
Leckband DE, Muller W, Schmitt FJ, Ringsdorf H. 1995. Molecular mechanism determining the strength of receptor-mediated intermembrane adhesion. Biophys. J. 69: 1162-1169
Lindahl E, Edholm O. 2000. Mesoscopic undulations and thickness fluctuations in lipid bilayers from molecular dynamic simulations. Biophys. J. 79(1): 426-433
Lipowsky R, Seifert U. 1991. Adhesion of vesicles and membranes. Mol. Cryst. Liq. Cryst. 202: 17-25
Lipowsky R. 1995. The morphology of lipid membranes. Curr. Opin. Struct. Biol. 5: 531–540
López JA, Dong J-F. 2005. Shear stress and the role of high molecular weight von Willebrand factor multimers in thrombus formation. Blood Coagulation and Fibrinolysis. 16: 11-16
Mailhac A, Badimon JJ, Fallon JT, Fernandez-ortiz A, Meyer B, Chesebro JH, Fuster V, Badimon L. 1994. Effect of an eccentric severe stenosis on fibrin(ogen) deposition on severely damaged vessel wall in arterial thrombosis. Relative contribution of fibrin(ogen) and platelets. Circulation. 90: 988–96
Malek AM, Izumo S. 1996. Mechanism of endothelial cell shape change and cytoskeletal remodeling in response to fluid shear stress. JCS. 109:13-726
Mancuso DJ, Tuley EA, Westfield LA, Worrall NK, Shelton-Inloes BB, Sorace JM, Alevy YG, Sadler JE. 1989. Structure of the gene for human von Willebrand factor. J Biol Chem. 264: 19514-27
Mannucci PM, Lattuada A, Ruggeri ZM. 1994. Proteolysis of von Willebrand factor in therapeutic plasma concentrates. Blood. 83: 3018-3027
Marrink SJ, Mark AE. 2001. Effect of undulations on surface tension in simulated bilayers. J. Phys. Chem. B. 105(26): 6122-6127
Matsuhita T, Sadler JE. 1995. Identification of amino acid residues essential for von Willebrand factor binding to platelet glycoprotein Ib. J. Biol. Chem. 270: 13406–13414
McCarty OJ, Mousa SA, Bray PF, Konstantopoulos K. 2000. Immobilized platelets support human colon carcinoma cell tethering, rolling, and firm adhesion under dynamic flow conditions. Blood. 96: 1789– 97
McGrath RT, McKinnon TAJ, Byrne B, O'Kenney R, Terraube V, McRae E, Preston RJS, Laffan MA, O'Donnell JS. 2010. Expression of terminal α2-6-linked sialic acid on von Willebrand factor specifically enhances proteolysis by ADAMTS 13. Blood. 115: 2666-2673
Metzner HJ, Hermentin P, Cuesta-Linker T, Langner S, Müller HG, Friedebold J. 1998. Characterization of factor VIII/von Willebrand factor concentrates using a modified method of von Willebrand factor multimer analysis. Haemophilia. 4(suppl): 25-32
Mitra N, Sinha S, Ramya TN, Surolia A. 2006. N-linked oligosaccharides as outfitters for glycoprotein folding, form and function. Trends Biochem Sci. 31(3): 156-163
Moake JL, Rudy CK, Troll JH, Weinstein MJ, Colannino NM, Azocar J, Seder RH, Hong SL, Deykin D. 1982. Unusually large plasma factor VIII:von Willebrand factor multimers in chronic relapsing thrombotic thrombocytopenic pur- pura. N Engl J Med. 307: 1432–5
Mohrdieck C, Dalmas F, Arzt E, Tharmann R, Claessens MMAE, Bausch AR, Roth A, Sackmann E, Schmitz CHJ, Curtis J, Roos W, Schulz S, Uhrig K, Spatz JP. 2007. Biomimetic models of the actin cytoskeleton. Small. 3(6): 1015-1022

Morganti M, Carpi A, Amo-Takyi B, Sagripanti A, Nicolini A, Giardino R, Mittermayer C. 2000. Von Willebrand's factor mediates the adherence of human tumoral cells to human endothelial cells and ticlopidine interferes with this effect. Biomedecine & Pharmacotherapy. 54(8): 431-436

Mouton WJ, Fehr MJ, Bombeli T. 2004. Evaluation of the effect of 6 von Willebrand Factor Concentrates on platelet adhesion to human vein segments under flow conditions. The Japanese Society of Hematology (Int J Hematol.). 80: 383-385

Mouritsen OG, Zuckermann MJ. 2004. What's So Special About Cholesterol? Lipids. 39: 1101–1113

Nachmias V. 1980. Cytoskeleton of human platelets at rest and after spreading. J Cell Biol. 86: 795-802

Narhi LO, Arakawa T, Aoki KH, Elmore R, Rohde MF, Boone T, Strickland TW. 1991. The effect of carbohydrate on the structure and stability of erythropoietin. J Biol Chem. 266(34): 23022-23026

Nash GF, Turner LF, Scully MF, Kakkar AK. 2002. Platelets and cancer. Lancet Oncol. 3: 425–30

Nash GF, Walsh DC, Kakkar AK. 2001. The role of the coagulation system in tumour angiogenesis. The Lancet Oncology. 2(10): 608-613

Needham D, Hochmuth RM. 1992. A sensitive measure of surface stress in the resting neutrophil. Biophys. J. 61: 1664–1670

Nesheim M, Pittman DD, Giles AR, Fass DN, Wang JH, Slonosky D, Kaufman RJ. 1991. The effect of plasma von Willebrand factor on the binding of human factor VIII to thrombin- activated human platelets. J Biol Chem. 266: 17815–20

Nielsen VG, Geary BT, Baird MS. 2000. Evaluation of the contribution of platelets to clot strength by thromboelastography in rabbits: the role of tissue factor and cytochalasin D. Ansth Analg. 91: 35-9

Nieswandt B, Hafner M, Echtenacher B, Mannel DN. 1999. Lysis of tumor cells by natural killer cells in mice is impeded by platelets. Cancer Res. 59: 1295–300

Nishiyama T, Kimura N, Jitsuhara Y, Uchida M, Ochi F, Yamaguchi H. 2000. N-Glycans protect proteins from protease digestion through their binding affinities for aromatic amino acid residues. J Biochem. 127(3): 427-433

Notarbartolo A, Davi G, Averna M, Barbagallo CM, Ganci A, Giammarresi C, La Placa FP, Patrono C. 1995. Inhibition of thromboxane biosynthesis and platelet function by simvastatin in type IIa hypercholesterolemia. Arterioscler Thromb Vasc Biol. 15: 247–51

Ogawa M. 1993. Differentiation and proliferation of hematopoietic stem cells. Blood. 81: 2844-2853

Oleksowicz L, Dutcher JP, Deleon-Fernandez M, Paietta E, Etkind P. 1997. Human breast carcinoma cells synthesize a protein immunorelated to platelet glycoprotein-Ib alpha with different functional properties. J Lab Clin Med. 129: 337–46

Oliver MF. 1991. Might treatment of hypercholesterolaemia increase non-cardiac mortality? Lancet. 337: 1529-31

Olorundare OE, Simmons SR, Albrecht RM.1992. Cytochalasin D and E: Effects on fibrinogen receptor movement and cytoskeletal reorganization in fully spread, surface-activated platelets: a correlative light and electron microscopic investigation. Blood. 79(1): 99-109

Patel SR, Richardson J, Schulze H, Kahle E, Galjart N, Drabek K, Shivdasani RA, Hartwig JH, Italiano JE, Jr. (2005). Differential roles of microtubule assembly and sliding in proplatelet formation by megakaryocytes. Blood. 15: 4076– 4085

Pelletier O, Pokidysheva E, Hirst LS, Bouxsein N, Li Y, Safinya CR. 2003. Structure of Actin Cross-Linked with α-Actinin: a network of bundles. Physical Review Letters. 91 (14)

Pilch J, Habermann R, Felding-Habermann B. 2002. Unique ability of integrin alpha(v)beta 3 to support tumor cell arrest under dynamic flow conditions. J Biol Chem. 277: 21930–8

Pipeleers DG, Pipeleers–Marichal MA, Kipnis DM. 1977. Physiological regulation of total tubulin and polymerized tubulin synthesis. J Cell Biol. 74: 351–35

Pitha J, Irie T, Sklar PB, Nye JS. 1988. Drug solubilizers to aid pharmacol-ogists: amorphous cyclodextrin derivatives. Life Sci. 43: 493–502

Pötzsch, Madlener. 2009. Hämostaseologie. Grundlagen, Diagnostik, Therapie. Springer. 2. Auflage

Raucher D, Sheetz MP. 1999. Characteristics of a membrane reservoir buffering membrane tension. Biophys. J. 77: 1992–2000

Raucher D, Stauffer T, Chen W, Shen K, Guo S, York JD, Sheetz MP, Meyer T. 2000. Phosphatidylinositol 4,5-bisphosphate functions as a second messenger that regulates cytoskeleton-plasma membrane adhesion. Cell. 100: 221–228

Reininger AJ. 2009. Platelet function under high shear conditions. Hämostaseologie. 29: 21-24

Reininger AJ. 2008 a). Function of von Willebrand factor in haemostasis and thrombosis. Haemophilia. 14(5): 11-26

Reininger AJ. 2008 b). VWF attributes-impact on thrombus formation. Thrombosis Research. 122(4): 9-13

Reininger AJ. 2007. Koagulatorische Aktivität der Thrombozyten. Hämostaseologie. 27: 247-250

Reininger AJ, Heijnen HFG, Schumann H, Specht HM, Schramm W, Ruggeri ZM. 2006. Mechanism of platelet adhesion to von Willebrand factor and microparticle formation under high shear stress. Blood. 107(9): 3537-3545

Reininger AJ. 2006. Primary haemostasis and its assessment by laboratory tests. Hämostaseologie. 26: 42-7
Ruggeri ZM, Orje JN, Habermann R, Federici AB, Reininger AJ. 2006. Activation-independent platelet adhesion and aggregation under elevated shear stress. Blood. 108(6): 1903-1910
Ruggeri ZM, Dent JA, Saldivar E. 1999. Contribution of distinct adhesive interactions to platelet aggregation in flowing blood. Blood. 94: 172-178
Ruggeri ZM, De ML, Gatti L, Bader R, Montgomery RR. 1983. Platelets have more than one binding site for von Willebrand factor. J Clin Invest. 72: 1-12
Ruggeri ZM, Zimmerman TS. 1981. The Complex Multimeric Composition of Factor VIII/ von Willebrand Factor. Blood. 57(6)
Ruggeri ZM, Pareti FI, Mannucci PM, Ciavarella N, Zimmerman TS. 1980. Heightened interaction between platelets and factor VIII/von Willebrand factor in a new subtype of von Willebrand's disease. N. Engl. J. Med. 302: 1047–1051
Sackmann E, Merkel R. 2010. Lehrbuch der Biophysik. Wiley. 1. Auflage
Sackmann E. 2004. Mikromechanik der Zelle. Physik Journal. 3(2)
Sackmann E, Bruinsma R. 2002. Cell adhesion as wetting transition? ChemPhys Chem 3(3): 262-269
Sackmann E. 1995. in Handbook of Biological Physics Vol. IA. Elsevier
Sadler JE, Budde U, Eikenboom JCJ, Favaloro EJ, Hill FGH, Holmberg L, Ingerslev J, Lee CA, Lillicrap D, Mannucci PM, Mazurier C, Meyer D, Nichols WL, Nishino M, Peake IR, Rodeghiero F, Schneppenheim R, Ruggeri ZM, Srivstava A, Montgomery RR, Federici AB. The working party on von Willebrand disease classification. 2006. Update on the pathophysiology and classification of von Willebrand disease: a report of the Subcommittee on von Willebrand Factor. Thromb. Haemost. 4(10): 2103–2114
Sadler JE. 2005. New concepts in von Willebrand disease. Annu. Rev. Med. 56:173–191
Sadler JE. 1994. A revised classification of von Willebrand disease. Thromb Haemost. 71: 520-5
Savage B, Sixma JJ, Ruggeri ZM. 2002. Functional self-association of von Willebrand factor during platelet adhesion under flow. Proc. Natl. Acad. Sci. USA. 99(1): 425-430
Savage B, Ginsberg MH, Ruggeri ZM. 1999. Influence of fibrillar collagen structure on the mechanisms of platelet thrombus formation under flow. Blood. 94: 2704–15
Savage B, Saldivar E, Ruggeri ZM. 1996. Initiation of platelet adhesion by arrest onto fibrinogen or translocation on von Willebrand factor. Cell. 84: 289-297
Schliwa M. 1982. Action of cytochalasin D on cytoskeletal networks. JCB. 92: 79-91
Schneider SW, Nuschele S, Wixforth A, Gorzelanny C, Alexander-Katz A, Netz RR, Schneider MF. 2007. Shear-induced unfolding triggers adhesion of von Willebrand factor fibers. Proc Natl Acad Sci USA. 104: 7899–903
Schneppenheim R, Budde U. 2006. Von Willebrand-Syndrom und von Willebrand-Faktor. Aktuelle Aspekte der Diagnostik und Therapie. Uni-Med. 2. Auflage
Schneppenheim R. 2004. Molekulare Genetik des von-Willebrand-Syndroms. Hämostaseologie. 37-43
Schneppenheim R, Budde U. 2004. Klassifikation des von-Willebrand-Syndroms. Hämostaseologie. 24: 27-36
Schultze M. 1865. Ein heizbarer Objecttisch und seine Verwendung bei Untersuchungen des Blutes. Archiv für mikroscopische Anatomie, 1, 1–42
Seifert U. 1995. Self-consistent theory of bound vesicles. Physical Review Letters. 74(25)
Seifert U, Lipowsky R. 1990. Adhesion of vesicles. Phys. Rev. A. 42: 4768-4771
Shastri KM, Carvalho AC, Lees RS. 1980. Platelet function and platelet lipid composition in the dyslipoproteinemias. J Lipid Res. 21: 467–72
Shattil SJ, Bennett JS, Colman RW, Cooper RA. 1977. Abnormalities of cholesterol-phospholipid composition in platelets and low-density lipoproteins of human hyperbetalipoproteinemia. J Lab Clin Med. 89: 341–53
Sheetz MP. 2001. Cell control by membrane-cytoskeleton adhesion. Nat. Rev. Mol. Cell Biol. 2: 392–396
Shrimpton CN, Borthakur G, Larrucea S, Cruz MA, Dong J-F, López JA. 2002. Localization of the adhesion receptor glycoprotein Ib-IX-V complex to lipid rafts is required for platelet adhesion and activation. JEM. 8: 1057-1066
Siediecki CA, Lestini BJ, Kottke-Marchant K, Eppell SJ, Wilson DL, Marchant RE. 1996. Shear-dependent changes in the three-dimensional structure of human von willebrand factor. Blood. 88(8): 2939-2950
Silbernagel S, Despopoulos A. 2007. Taschenatlas der Physiologie. Thieme. 7. Auflage
Simson R, Sackmann E. 1998. Mimicking physics of cell adhesion. Biophysik Skript E22. 4. Verbesserte Auflage
Simson R, Wallraff E, Faix J, Niewöhner J, Gerisch G, Sackmann E. 1998. Membrane Bending modulus and adhesion energy of wild-type and mutant cells of dictyostelium lacking talin or cortexillins. Biophys J. 74: 514–522
Sing CE, Alexander-Katz A. 2010. Globule-stretch transitions of collapsed polymers in elongational flow fields. Macromolecules. 43: 3532-3541
Smith A-S, Sengupta K, Goennenwein S, Seifert U, Sackmann E. 2008. Force-induced growth of adhesion domains is controlled by receptor mobility. PNAS. 105(19)
Smith A-S, Sackmann E, Seifert U. 2004. Pulling tethers from adhered vesicles. Physical Review Letters. 92(20)

Strony J, Beaudoin A, Brands D, Adelman B. 1993. Analysis of shear stress and hemodynamic factors in a model of coronary artery stenosis and thrombosis. Am J Physiol. 265: H1787–96

Sun M, Northup N, Marga F, Huber T, Byfield FJ, Levitan I, Forgacs G. 2007. The effect of cellular cholesterol on membranecytoskeleton adhesion. Journal of Cell Science. 120(13): 2223-2231

Sun M, Graham JS, Hegedüs B, Marga F, Zhang Y, Forgacs G, Grandboisy M. 2005. Multiple membrane tethers probed by atomic force microscopy. Biophys. J. 89: 4320-4329

Swanson DK, Myerowitz PD, Hegge JO, Watson KM. 1986. Arterial blood-flow waveform measurement in intact animals: new digital radiographic technique. Radiology. 161: 323–328

Szanto T, Schlammadinger A, Salles I, Pareyn I, Vauterin S, Harsfalvi J, Vanden Bulcke A-M, Deckmyn H, Vanhoorelbeke K. 2007. Type 2B von Willebrand disease in seven individuals from three different families: phenotypic and genotypic characterization. Thromb. Haemost. 98: 251–254

Tablin F, Castro MD. 1992. Equine platelets contain an anisotropic array of microtubules which reorganise upon activation. Comparative HaematologyInternational. 2: 125-132

Tablin F, Castro M, Leven RM. 1990. Blood platelet formation in vitro: the role of the cytoskeleton in megakaryocyte fragmentation. J Cell Sci. 97: 59-70

Tablin F, Reeber MR, Nachmias VT. 1988. Platelets contain a 210K microtubule-associated protein related to a similar protein in HeLa cells. J Cell Sci. 90: 317-324

Takada Y, Shinkai F, Kondo S, Yanamoto S, Tsuboi H, Korenaga R, Ando J. 1994. Fluid shear stress increases the expression of thrombomodulin by cultured human endothelial cells. Biochem Biophys Res Commun. 205: 1345–1352

Tangelder GJ, Teirlinck HC, Slaaf DW, Reneman RS. 1985. Distribution of blood platelets flowing in arterioles. American Journal of Physiology—Heart and Circulatory Physiology. 248(3): 318–323

Terraube V, Marx I, Denis CV. 2007. Role of von Willebrand factor in tumor metastasis. Thrombosis Research. 120(2): 64-70

Terraube V, Pendu R, Baruch D, Gebbink MFBG, Meyer D, Lenting PJ, Denis CV. 2006. Increased metastatic potential of tumor cells in von Willebrand factor-deficient mice. Thromb. Haemost. 4(3): 519–526

Thomas GM, Panicot-Dubois L, Lacroix R, Dignat-George F, Lombardo D, Dubois C. 2009. Cancer cell-derived microparticles bearing P-selectin glycoprotein ligand 1 accelerate thrombus formation in vivo. JEM. 206(9): 1913-1927

Thurston GB. 1972. Viscoelasticity of human blood. Biophys J. 12: 1205–1217

Tilles AW, Eckstein EC. 1987. The near-wall excess of platelet-sized particles in blood flow: its dependence on hematocrit and wall shear rate. Microvascular Research. 33: 211–223

Tilley RE, Holscher T, Belani R, Nieva J, NMackman N. 2008. Tissue factor activity is increased in a combined platelet microparticle sample from cancer patients. Throm. Res. 122: 604-609

Titani K, Kumar S, Takio K, Ericsson LH, Wade RD, Ashida K, Walsh KA, Chopek MW, Sadler JE, Fujikawa K. 1986. Amino acid sequence of human von Willebrand factor. Biochemistry. 25(11): 3171-3184

Tocantins LM. 1938. The mammalian blood platelet in health and disease. Medicine. 17: 155-260

Tokarev AA, Butlylin AA, Ataullakhanov FI. 2011. Platelet adhesion from shear blood flow is controlled by near-wall rebounding collisions with erythrocytes. Biophys. J. 100: 799-808

Toyoda T, Arakawa T, Yamaguchi H. 2002. N-glycans stabilize human erythropoietin through hydrophobic interactions with the hydrophobic protein surface: studies by surface plasmon resonance analysis. J Biochem. 131(4): 511-515

Tsai HM, Nagel RL, Hatcher VB, Sussman II. 1989. Multimeric composition of endothelial cell-derived von Willebrand factor. Blood. 73: 2074–6

Turitto V, Benis A, Leonard E. 1972. Platelet diffusion in flowing blood. Industrial and Engineering Chemistry Fundamentals. 11(2): 216–223

Van der Kwast TH, Stel HV, Cristen E, Bertina RM, Veerman EC. 1986. Localization of factor VIII-procoagulant antigen: an immunohistological survey of the human body using monoclonal antibodies. Blood. 67: 222–7

Van Lier M, Lee F, Fardale RW, Gorter G, Verhoef S, Ohno-Iwashita Y, Akkerman J-WN, Heijnen HFG. 2005. Adhesive surface determines raft composition in platelets adhered under flow. Journal of Thrombosis and Haemostasis. 3: 2514-25

Verweij CL, Diergaarde PJ, Hart M, Pannekoek H. 1986. Full-length von Willebrand factor (vWF) cDNA encodes a highly repetitive protein considerably larger than the mature vWF subunit. EMBO J. 5: 1839–1847

Wagner DD. 1989. Storage and secretion of von Willebrand Factor. In: Zimmerman TS, Ruggeri ZM, eds. Coagulation and Bleeding Disorders. The Role of FactorVIII and von Willebrand Factor. New York: Dekker. 161–80

Wagner DD, Marder VJ. 1984. Biosynthesis of von Willebrand protein by human endothelial cells: processing steps and their intracellular localization. J Cell Biol. 99: 2123–30

Waheed AA, Shimada Y, Heijnen HF, Nakamura M, Inomata M, Hayashi M, Iwashita S, Slot JW, Ohno-Iwashita Y. 2001. Selective bindingof perfringolysin O derivative to cholesterol-rich membrane microdomains (rafts). Proc Natl Acad Sci USA. 98: 4926–31

Weibel ER, Palade GE. 1964. New cytoplasmic components in arterial endothelia. J Cell Biol. 23: 101–12

White JG. 2007. Platelet structure. Platelets. Elsevier Science

White JG. 1999. Platelet glycosomes. Platelets. 10: 242–246

White MC, Jennings LK. 1999. Platelet protocols: research and clinical laboratory procedures. Academic Press: San Diego, CA

White JG, Rao GH. 1998. Microtubule coils versus the surface membrane cytoskeleton in maintenance and restoration of platelet discoid shape. American Journal of Pathology. 152(2): 597-609

White JG, Krumwiede MD, Cocking–Johnson DJ, Escolar G. 1995 a). Dynamic redistribution of glycoprotein Ib/IX on surface-activated platelets. A second look. Am J Pathol. 147: 1057–1067

White JG, Krumwiede MD, Cocking–Johnson D, Rao GH,Escolar G. 1995 b). Retention of glycoprotein Ib/IX receptors on external surfaces of thrombin-activated platelets in suspension. Blood. 86: 3468–3478

White JG, Krumwiede MD, Cocking–Johnson DK, Escolar G. 1995 c). Redistribution of GPIb/IX and GPIIb/IIIa during spreading of discoid platelets. Br J Haematol. 90: 633–644

White JG, Krumwiede MD, Cocking–Johnson D, Escolar G. 1994. Influence of combined thrombin stimulation, surface activation, and receptor occupancy on organization of GPIb/IX receptors on human platelets. Br J Haematol. 88: 137-148

White JG, Escolar G. 1993. Current concepts of platelet membrane response to surface activation. Platelets. 4: 175-198

White JG, Escolar G. 1990. Fibrinogen receptors do not undergo spontaneous redistribution on surface-activated platelets. Arteriosclerosis. 10. 738–744

White JG. 1987. Platelet structural physiology: The ultrastructure of adhesion, secretion and aggregation in arterial thrombosis. Cardiovasc Clin. 18: 13-33

White JG, Radha E, Krumwiede M. 1986. Isolation of circumferential microtubules and platelets without simultaneous fixation. Blood. 67: 873-877

White JG, Sauk JJ. 1984. The organization of micro- tubules and microtubule coils in giant platelet disorders. Am J Pathol. 116: 514–522

White JG. 1971. Platelet morphology. In S. E. Johnson (Ed.). The circulating platelet (pp.45-121). New York Academic Press

Woldhuis B, Tangelder GJ, Slaaf DW, Reneman RS. 1992. Concentration profile of blood platelets differs in arterioles and venules. American Journal of Physiology—Heart and Circulatory Physiology. 262(4): H1217–H1223

Wootton DM, Ku DN. 1999. Fluid mechanics of vascular systems, diseases, and thrombosis. Annu Rev Biomed Eng. 1: 299 –329

Wormald MR, Dwek RA. 1999. Glycoproteins: glycan presentation and protein-fold stability. Structure. 7(7): R155-R160

Wurzinger LJ. 1990 Histophysiology of the circulating platelet. Adv Anat Embryol Cell Biol. 120: 1–96

Wyss DF, Choi JS, Li J, Knoppers MH, Willis KJ, Arulanandam AR, Smolyar A, Reinherz EL, Wagner G. 1995. Conformation and function of the N-linked glycan in the adhesion domain of human CD2. Science. 269(5228): 1273-1278

Yago T, Lou J, Wu T, Yang J, Miner JJ, Coburn L, López JA, Cruz MA, Dong J-F, McIntire LV, McEver RP, Zhu C. 2008. Platelet glycoprotein Ibα forms catch bonds with human WT vWF but not with type 2B von Willebrand disease vWF. JCI. 118(9): 3195-3207

Yeh C, Eckstein EC. 1994. Transient lateral transport of platelet-sized particles in flowing blood suspensions. Biophys. J. 66: 1706–1716

Zieve GW, Turnbull D, Mullins JM, Mcintosh JR. 1980. Production of large numbers of mitotic mammalian cells by use of reversible microtubule inhibitor nocodazole. 126: 397-405

Zimmerman TS, Ratnoff OD, Powell AE. 1971. Immunologic differentiation of classic hemophilia (factor VIII deficiency) and von Willebrand's disease, with obser- vations on combined deficiencies of antihemophilic factor and proaccelerin (factor V) and on an acquired circulating anticoagulant against antihemophilic factor. J Clin Invest. 50: 244–54

Zwicker IJ, Furie BC, Furie B. 2007. Cancer-associated thrombosis. Crit. Rev. Oncol. Hematol. 62:126-136

Appendix A

Product	Company	Location
ACD	Caridian BCT	Canewood, USA
aggrastat	MSD Sharp & Dohme GmbH	Haar Germany
Alexa Fluor	Invitrogen	Karlsruhe, Deutschland
annexin V	Serotec	
apyrase grade 7	Sigma	
BSA	Sigma	
CD 41	Serotec	
cholesterol	Sigma	
collagen	Horm-Chemie, Nycomed	Munich, Germany
cytochalasin D	Sigma	
DMSO	Sigma	
Fanhdi	Grifols	Langen, Germany
glutaraldehyde	Sigma	
Haemate	CSL Behring GmbH	Wien, Austria
Haemoctin	Biotest	Dreieich, Germany
IgG	Serotec	
Immunate	Baxter	Unterschleißheim, Germany
MβCD	Sigma	
nocodazole	Sigma	
Octanate	Octapharma	Langenfeld, Germany
paraformaldehyde	Sigma	
PPACK	Bachem	Budendorf, Switzerland
rvWF	Baxter	Unterschleißheim, Germany
Wilate	Octapharma	Langenfeld, Germany

Appendix B

Supplement movies on DVD	Discripton
figure 35_I	DA1 coating, blood suspension with recombinant full-length vWF, at 30,000s^{-1}
figure 35_II	DA1 coating, blood suspension with recombinant full-length vWF, at 30,000s^{-1} to 10,000s^{-1}
figure 36 a)	DA1 coating, whole blood suspension, at 20,000s^{-1} to 10,000s^{-1}
figure 36 b)	DA1 coating, blood suspension with E250, at 20,000s^{-1}
figure 36 c)	DA1 coating, blood suspension with Haemate, at 20,000s^{-1} to 10,000s^{-1}
figure 37 a)	DA1 coating, blood suspension with recombinant full-length vWF, at 20,000s^{-1}
figure 37 b)	DA1 coating, blood suspension with vWF containing sugar, at 40,000s^{-1}
figure 40 a) and b)	collagen coating, blood suspension with recombinant full-length vWF, at 2,000s^{-1}
figure 40 c) and d)	collagen coating, blood suspension with recombinant full-length vWF, at 40,000s^{-1}
figure 41	collagen coating, blood suspension with vWF mutant type 2B, at 1,500s^{-1}

Curriculum vitae

Name	Angerer
Surname	Jennifer Ivonne
Date & Place of Birth	07. June 1983, Augsburg
Profession	Physicist
Nationality	German

Education

01/2008-06/2011	PhD at the University of Augsburg and the University Clinic of the Ludwig Maximilians University Munich: „Blood platelet behaviour and platelet-von Willebrand factor interaction under force" funded by a Scholarship of the German Israeli Foundation for Scientific Research and Development
10/2002-10/2007	Academic studies of physics at the University of Augsburg Diploma thesis: „Rasterkraftspektroskopische Untersuchung von Protein-Substrat-Wechselwirkungen" Minor field of study: Buisness economics with focus on: organisation, personal and marketing Degree: Diploma physicist
1993-2002	Grammar school Stettensches Institut in Augsburg
1989-1993	Primary school in Langweid

International scientific conferences

03/2011	NIM Winter Meeting in Munich Posterpresentation: "Platelet adhesion and tether formation under stress"
10/2010	Minerva School: Frontiers in Vascular Biology in Jerusalem Chairman and talk: "Platelet adhesion and tether formation under shear stress"
07/2009	International Biophysical Conference in Genoa Bursary of the German Biophysical Society, Berlin Posterpresentation: "Platelet Adhesion and Tether Formation under Force "
09/2008	German Biophysical Society Meeting 2008 in Berlin Posterpresentation: "von Willebrand Factor (vWF) membrane interaction" Poster price award

07/2007	International Biophysical Conference in London
	Bursary of the German Biophysical Society, Berlin
	Posterpresentation: “von Willebrand Factor (vWF) membrane interaction“
09/2006	German Biophysical Conference in Mainz
	Posterpresentation: “New insight into Wound Healing by AFM Force Spectroscopy“

Study period abroad

06/2010-10/2010	Boston University and Massachusetts Institut of Technology (USA)
	funded by a Scholarship of the DAAD
09/2004-05/2005	University of St Andrews (GB)
	5. and 6. semester studies in the degree course of physics

Course integrated practical experience

08/2005-10/2005	Training at the BMW Group Munich

Soft Skills

Foreign language	English fluent in spoken and written
Computer applications	Microsoft Office, basic knowledge in C and in Origin
Soft skills	LMU Entrepreneurship Seminar
	Führungskompentenz entwickeln
	Scientific Writing in English

Publications

(1) D.M. Steppich, J.I. Angerer, K. Sritharan, S.W. Schneider, S. Thalhammer, A. Wixforth, A. Alexander-Katz, M.F. Schneider (2008): Relaxation of ultralarge VWF bundles in a microfluidic - AFM hybrid reactor. Biochemical and Biophysical Research Communications 369(2): 507-512

(2) D.M. Steppich, J.I. Angerer, S. Bössinger, S.W. Schneider, A. Wixforth, M.F. Schneider: pH regulates the shear-driven activation of von Willebrand factor (in preparation)

(3) D.M. Steppich, J.I. Angerer, S. Bössinger, S.W. Schneider, A. Wixforth, M.F. Schneider: Structural aging and entropic driven membrane adhesion controlled by mechanical shear stress (in preparation)

(4) J. I. Angerer, M. Napoleone, H. F. G. Heijnen, A. Wixforth, A. J. Reininger, M. F. Schneider: Platelet adhesion and tether formation under stress (in preparation)

(5) J. I. Angerer, M. Napoleone, A. Wixforth, M. F. Schneider, A. J. Reininger: Importance of multimer size for von Willebrand factor function under blood flow-Comparison of commercially available products (in preparation)

(6) A. J. Reininger, J. I. Angerer, M. Napoleone, M. A. Fallah, A. Wixforth, R. Schneppenheim, M. F. Schneider: Reversible shear-induced platelet-von Willebrand factor self assembly- a new mechanism of leak sealing and thrombosis (in preparation, authorlist not complete)

(7) J. I. Angerer, M. Napoleone, A. Wixforth, R. Schneppenheim, M. F. Schneider, A. J. Reininger: Improved classification of von Willebrand disease- the von Willebrand factor Miami mutant as an example (in preparation)

(8) J. I. Angerer, H. Chen, M. Napoleone, A. Wixforth, M. F. Schneider, A. Alexander-Katz, A. J. Reininger: Theoretical and experimental investigations on the haematocrit impact on the platelet-von Willebrand factor interaction under blood flow conditions (in preparation)

(9) J. I. Angerer, C. Leonhardt, M. Benoit, A. Wixforth, M. F. Schneider, A. J. Reininger: Influence of cytoskeleton disrupting drugs on tether extraction of a blood platelet by an atomic force microscope tip (in preparation)

(10) A. Kern, J. I. Angerer, M. Napoleone, A. Wixforth, M. F. Schneider, A. J. Reininger: Effect of membrane cholesterol on platelet adhesion and tether formation (in preparation)

(11) J. I. Angerer, M. Napoleone, S. Dwivedi, A. Wixforth, M. F. Schneider, W. Siess, A. J. Reininger: The interaction of platelets and small lung carinoma cells or maligne melanoma cells (in preparation)